Modeling Mismatch Repair Deficiency in Small Cell Lung Cancer

Inaugural Dissertation

zur

Erlangung des Doktorgrades

Dr. nat. med.

der Medizinischen Fakultät

und

der Mathematisch-Naturwissenschaftlichen Fakultät

der Universität zu Köln

vorgelegt von

Olta Ibruli

aus Tirana

Köln

2025

Betreuer*in: PD Dr. Grit Sophie Herter-Sprie

Referenten: Prof. Dr. Björn Schumacher

Prof. Dr. Mirka Uhlirova

Datum der mündlichen Prüfung: 03.11.2025

Disclaimer:

Some figures and illustrations presented in this thesis have previously appeared in the publication Ibruli et al. 2024 (Journal of Cancer Research and Clinical Oncology), in which the author is the first author.

Table of Contents

Zusammenfassung

Das kleinzellige Lungenkarzinom (SCLC) ist eine hochaggressive Malignität mit rascher Progression, früher Metastasierung und sehr schlechter Prognose. Obwohl die Einführung von Immun-Checkpoint-Inhibitoren (ICIs) in die Erstlinientherapie die Überlebensraten moderat verbessert hat, sprechen die meisten Patienten nicht an, und prädiktive Biomarker fehlen. Ein molekulares Kennzeichen von SCLC ist die hohe Tumormutationslast (TMB), hauptsächlich verursacht durch tabakinduzierte Mutagenese. Jüngste proteogenomische Studien haben eine Patientensubgruppe (~15 %) mit Mismatch-Reparatur-Defizienz (MMRd) identifiziert, darunter Veränderungen in zentralen MMR-Genen wie *MSH2*. Diese Subgruppe weist einzigartige Mutationssignaturen und schlechte klinische Ansprechraten auf, ist jedoch weitgehend unerforscht – bedingt durch seltene Biopsien und fehlende präklinische Modelle. Diese Arbeit beschreibt die Entwicklung eines neuartigen genetisch veränderten Mausmodells (GEMM) für SCLC durch konditionale *Msh2*-Deletion im *Rb1/Trp53*-defizienten (RP) Hintergrund, wodurch das RPM-Modell (*Rb1*$^{fl/fl}$*;Trp53*$^{fl/fl}$*;Msh2*$^{fl/fl}$) entsteht. Mithilfe von Whole-Exome-Sequencing (WES) zeigten wir, dass RPM-Tumoren mit biallelischem *Msh2*-Verlust erfolgreich die für MMRd typische genomische Landschaft nachbilden – mit erhöhter TMB, Frameshift-Mutationen und dominanten MMRd-Mutationssignaturen (SBS15/SBS21). Diese Veränderungen führten zu einer höheren Neoantigenlast im Vergleich zu RP-Tumoren. Funktionell zeigten RPM-Tumore eine erhöhte Sensitivität gegenüber PD-1-Blockade. Zudem wiesen mit einem Treg-Suppressor (CDK4/6-Inhibitor) kombinierte Behandlungen mit platinbasierter Standardchemotherapie und ICI auf ein verbessertes Überleben hin. Immunprofiling mittels Durchflusszytometrie und Imaging Mass Cytometry (IMC) zeigte unterschiedliche Muster der T-Zell-Aktivierung und stromalen Umgestaltung im Vergleich zu RP-Kontrollen. Diese Arbeit liefert das erste physiologisch relevante SCLC-GEMM zur Untersuchung von MMRd und beleuchtet die Auswirkungen des *Msh2*-Verlusts auf Tumorentwicklung, Immunogenität und Therapieansprechen. Die Erkenntnisse unterstützen die Entwicklung neuer, auf DNA-Reparatur-defiziente SCLC-Tumoren zugeschnittener Behandlungsstrategien.

Abstract

Small cell lung cancer (SCLC) is a highly aggressive malignancy characterized by rapid progression, early dissemination of metastases, and very poor prognosis. Although the introduction of immune checkpoint inhibitors (ICIs) into first-line therapy has shown modest improvement in survival outcomes, most patients remain unresponsive, and predictive biomarkers are lacking. One molecular hallmark of SCLC is its high tumor mutational burden (TMB), attributed mainly to tobacco-induced mutagenesis. However, recent proteogenomic studies have identified a subset of patients (~15%) harboring mismatch repair deficiency (MMRd), including alterations in key MMR genes such as *MSH2*. This subgroup exhibits unique mutational signatures and poor clinical outcomes. However, it remains largely understudied due to sparse tumor biopsies and a lack of representative preclinical models. To address this gap, this thesis presents the development of a novel genetically engineered mouse model (GEMM) of SCLC by introducing conditional *Msh2* deletion into the *Rb1/Trp53*-deficient (RP) background, generating the RPM model (*Rb1*$^{fl/fl}$;*Trp53*$^{fl/fl}$;*Msh2*$^{fl/fl}$). Using whole-exome sequencing (WES), we demonstrate that RPM tumors with bi-allelic loss of *Msh2* successfully recapitulate the genomic landscape associated with MMRd, including a significant increase in TMB, frameshift mutations, and dominant MMRd-associated mutational signatures (SBS15/SBS21). These alterations resulted in a higher load of neoantigens compared to RP tumors. Functionally, RPM tumors displayed significantly increased sensitivity to PD-1 blockade. Furthermore, the RPM mouse model showed improved survival when treated with a Treg suppressor (CDK4/6 inhibitor) in combination with standard-of-care platinum-based chemotherapy and ICI. Additionally, immune profiling via flow cytometry and imaging mass cytometry (IMC) indicates distinct patterns of T cell activation and stromal remodeling in the RPM model compared to RP controls. This thesis provides the first GEMM of SCLC that serves as a physiologically relevant platform to study MMRd in SCLC and highlights the effects of *Msh2* loss on tumorigenesis, immunogenicity, and treatment response. These findings have direct implications for developing therapeutic stratification strategies and designing novel treatment regimens tailored to DNA repair-deficient SCLC tumors.

1. Introduction

1.1 Lung cancer

Lung cancer is the most common cause of cancer mortality worldwide. It accounts for approximately 18% of all cancer deaths and results in around 1.8 million fatalities yearly (World Health Organization, 2023). It is also the second most commonly diagnosed cancer, with 2.2 million new cases annually (Hoang and Landi 2022). Although there have been significant treatment advancements recently, the overall 5-year survival rate remains low at 19%. This is primarily due to late diagnosis and the aggressive nature of tumor progression (Hiddinga et al. 2021a).

Lung cancer is categorized into non-small cell lung cancer (NSCLC) and small cell lung cancer (SCLC), comprising approximately 85-90% and 10-15% of all diagnoses, respectively **(Figure 1.1)** (Hoang and Landi 2022; Inamura 2017) . NSCLC is the most common form of lung cancer and it includes three histological types: adenocarcinoma, squamous cell carcinoma, and large cell carcinoma. Compared to SCLC, NSCLC exhibits slower tumor progression and spread, resulting in a better prognosis and improved response to treatment (American Cancer Society, 2023).

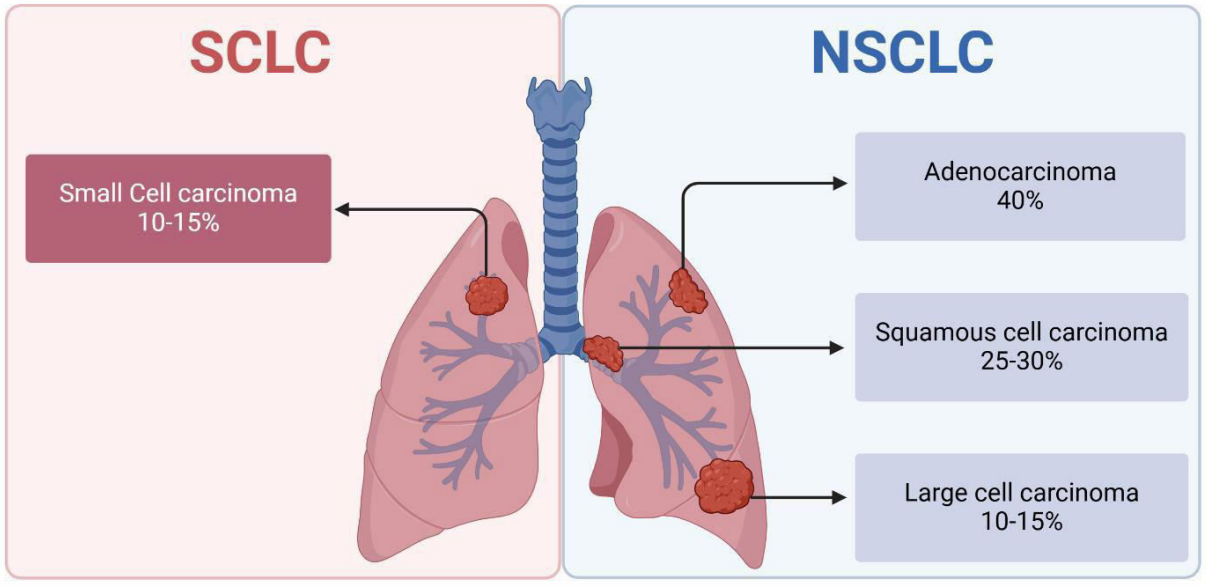

Figure 1.1 Schematic representation of lung cancer classification.
Lung cancer is broadly categorized into small cell lung cancer (SCLC) and non-small cell lung cancer (NSCLC) based on histological and clinical characteristics. SCLC accounts for 10-15% of lung cancer cases. NSCLC represents 85-90% of lung cancer cases and is further divided into three major subtypes: adenocarcinoma (40%), squamous cell carcinoma (25-30%), and large cell carcinoma (10-15%). Created with Biorender.com.

1.2 Overview of small cell lung cancer

1.2.1 Epidemiology and risk factors

SCLC is the most aggressive form of lung cancer, characterized by rapid proliferation and early dissemination of metastases (Gazdar et al., 2017; Rudin et al., 2021; Sabari et al., 2017). There are over 300.000 new cases annually worldwide. Around two-thirds of these are diagnosed at a late stage, at which point the disease is characterized by extensive metastatic spread. This results in extremely poor survival outcomes (Wang et al. 2023). Extensive-stage SCLC (ES-SCLC) has a median overall survival (OS) of only 2-4 months and a 5-year survival rate of less than 7% (Hiddinga et al. 2021; Zhou et al. 2020).

Unlike NSCLC, which has various risk factors, SCLC is strongly associated with tobacco exposure, with around 95% of cases occurring in long-term smokers and former smokers. Additionally, second-hand tobacco smoke also increases the likelihood of an SCLC diagnosis (Johnston-Early et al. 1980; Videtic et al. 2003). Other risk factors contributing to SCLC include occupational exposure to several other carcinogens, such as asbestos, arsenic, and industrial chemicals like benzene. Individuals who have received radiation therapy in the chest are also at greater risk for developing SCLC. Although family history and genetic predispositions may play a role, the genetic factors of SCLC are not yet well understood (Raso, Bota-Rabassedas, and Wistuba 2021a).

1.2.2 Histopathological characteristics

SCLC has several histopathological features that contribute to its aggressiveness. Histologically, SCLC tissue appears very densely packed with small, round to spindle-shaped tumor cells that contain scant cytoplasm and dense nuclear chromatin **(Figure 1.2a)** (Raso et al., 2021). Typically, SCLC cells have exceptionally high mitotic rates, estimated as >10 mitoses per mm^2 (Dumoulin, Bironzo, and Passiglia 2023). SCLC has limited architectural organization, and in combination with the small cell size, early detection becomes difficult. The tumors grow in diffuse sheet patterns, facilitating their infiltration into the surrounding tissues. Necrosis, because of rapid

outgrowth of the tumor's blood supply, is very common and reflects its aggressive behavior **(Figure 1.2b)** (Raso et al. 2021).

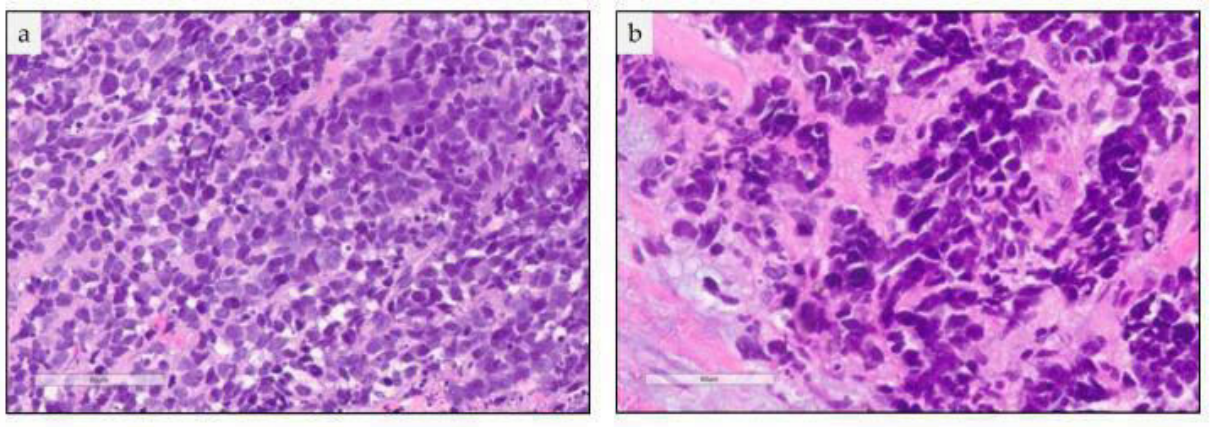

Figure 1.2 SCLC histological features (adapted from Raso et al. 2021**).**
Representative H&E images of formalin-fixed paraffin-embedded (FFPE) SCLC tissues showing **a)** small cells with scant cytoplasm and **b)** densely packed tissue with intratumoral necrosis.

In addition, SCLC tumors are highly vascularized with small vessels and lymphatic channels, which promote early dissemination of tumor cells. Metastases are a hallmark of malignancy, and they tend to invade the liver, brain, adrenal glands, and bones (Ganti et al. 2021).

At the cellular level, SCLC has a neuroendocrine (NE) origin, and its cells of origin are thought to be pulmonary neuroendocrine cells (PNECs) in the lung epithelium. Therefore, SCLC can be differentiated from other lung tumor entities because it expresses neuroendocrine markers such as CD56/ neural adhesion molecule (NCAM), synaptophysin, chromogranin A, and neuron-specific enolase (NSE). CD56 is the most common marker as it stains >90% of all SCLC samples. However, SCLC often exhibits a mixed phenotype and co-expresses markers typical for epithelial cells, including cytokeratins (Raso et al., 2021). The mixed cellular composition contributes to the complexity of the disease as it makes the tumor more adaptable and resistant to treatments.

1.3 Current treatment strategies for SCLC

SCLC is a very challenging disease to manage clinically. Despite continuous research efforts to advance the therapeutic strategies that would be successful in eradicating or controlling this aggressive malignancy, classic chemotherapy and radiation therapy remain the primary treatment modalities. The therapeutic algorithm for SCLC is depicted in **Figure 1.3**.

For limited-stage SCLC (LS-SCLC), defined as a confined lesion to one hemithorax and regional lymph nodes, the standard of care consists of chemotherapy (cisplatin-etoposide or carboplatin-etoposide) and radiotherapy (thoracic and nodal irradiation) (Dingemans et al. 2021). Moreover, prophylactic cranial radiotherapy (PCI) is advised based on numerous studies demonstrating its effect in reducing the risks of brain metastases (Nne et al., 1999). Surgical treatment with lobectomy and mediastinal lymph node resection (lymphadenectomy) is an option only in cases where localized disease is confirmed, where the tumor is present in only a single lung without extensive nodal spread. Such surgical interventions yield a five-year survival rate of 45-65%. Adjuvant chemotherapy is still recommended, even when pathological tests detect no evidence of cancer spread to the lymph nodes (Dingemans et al., 2021). Additionally, thoracic and nodal irradiation may be used based on clinical staging and resection status. For ES-SCLC, where the tumors have spread to distant organs such as the brain, liver, or bone, platinum-based chemotherapy has remained the first-line treatment for over 30 years, providing a median OS of 7-11 months. In recent years, the addition of immune checkpoint inhibitors (ICI), atezolizumab and durvalumab, to standard chemotherapy has been approved because it achieved a moderate increase in median OS by approximately 2 months (Horn et al. 2018; Paz-Ares et al. 2019). Additionally, radiotherapy continues to play a key role in ES-SCLC, including thoracic and nodal irradiation, palliative radiation to control symptoms, and prophylactic cranial irradiation in selected patients.

However, despite the established treatment protocols, achieving durable responses and improving long-term survival remains significantly challenging. Chemotherapy and radiotherapy outperform any novel treatment agents due to SCLC's aggressive and rapid-growing nature (Hiddinga et al., 2021). However, SCLC is a very

chemo-sensitive cancer with a response rate of 70-90%; thus, rapid relapses are almost unavoidable (Zhang et al., 2023). As a result, long-term survival is extremely low, and new complementary strategies are urgently needed.

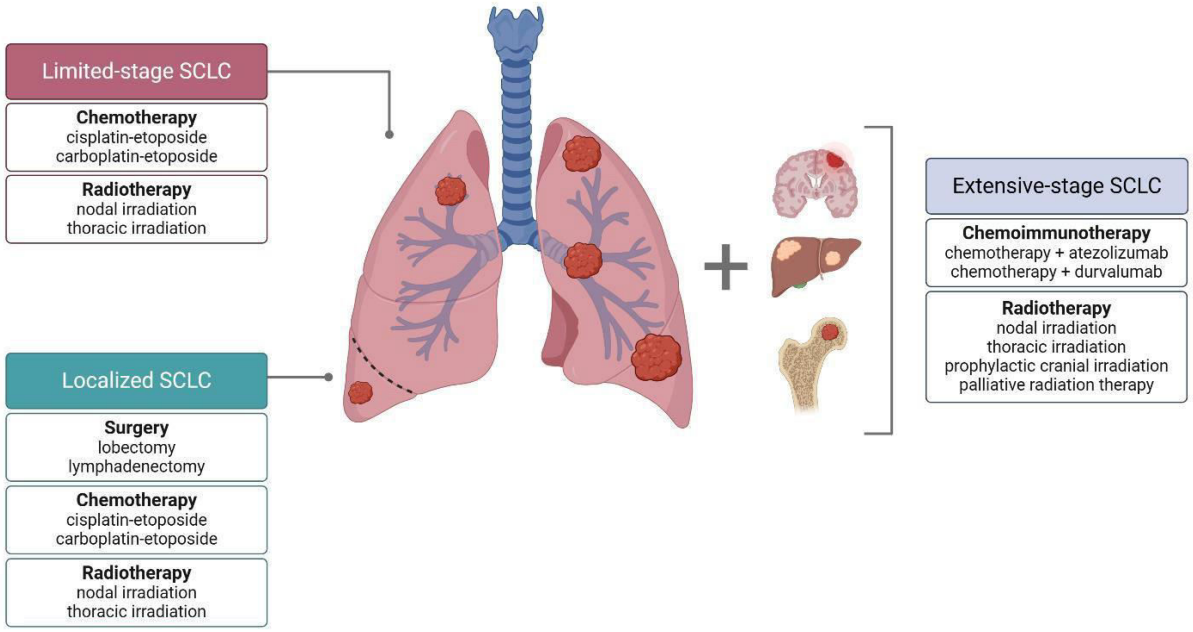

Figure 1.3 Treatment strategies for different stages of SCLC.
The illustration displays treatment approaches for SCLC according to different stages of the disease. In limited-stage SCLC, the tumor is confined to one hemithorax and regional lymph nodes and is treated with platinum-based chemotherapy (cisplatin/carboplatin + etoposide) and radiotherapy (nodal and thoracic irradiation). Localized SCLC, where the tumor is present in only a single lung without extensive nodal spread, is managed with surgical resection (lobectomy and lymphadenectomy), followed by chemotherapy and nodal/thoracic irradiation. Extensive disease, characterized by distant metastases to organs such as the brain, liver, and bone, is treated with a combination of chemotherapy and ICIs (atezolizumab or durvalumab) and radiotherapy mainly for symptoms management, prophylactic cranial irradiation, and thoracic/nodal irradiation in selective cases. Created with Biorender.com

1.3.1 Standard chemotherapy

Chemotherapy has been the standard of care and the cornerstone of SCLC treatment for decades. Even today, the first-line regimen in clinical practice is a combination of platinum-based chemotherapy (cisplatin or carboplatin) and etoposide, a DNA topoisomerase II inhibitor (Jiang et al. 2021; Mascaux et al. 2000). Mechanistically, cisplatin and carboplatin induce DNA crosslinks and, thus, prevent DNA replication and proliferation of cancer cells (Dilruba and Kalayda 2016). Etoposide augments this effect by further disrupting the repair and replication of DNA and not allowing the tumor cells to divide and grow (Montecucco, Zanetta, and Biamonti 2015; Nguyen et al.

2023). This therapy remains the most efficient in both limited-stage and extensive-stage SCLC, with objective response rates (ORR) of 60-80% and 50-60%, respectively (Roth et al. 1992). However, almost all patients experience chemoresistance shortly after the start of therapy, with extensive-stage disease patients relapsing within 6-12 months (Farid and Liu 2020; Socinski et al. 2009). The second-line treatment in such cases is topotecan, another topoisomerase inhibitor. However, topotecan exhibits only a minor efficacy with a median survival of less than 6 months and is associated with very high toxicity levels (Horita et al. 2015).

1.3.2 Standard radiation therapy

Radiation therapy remains an important part in the management of SCLC, particularly for patients with limited-stage disease. In these cases, the standard treatment approach involves concurrent chemoradiation, which includes a combination of chemotherapy and thoracic radiation. This treatment strategy aims to achieve a curative outcome as it targets both the primary lung tumors and adjacent lymph nodes. On the other hand, the use of radiation for extensive disease is more limited and is primarily recommended for palliative reasons since the body is infested by metastases in different organs (Glatzer et al. 2017). In such cases, radiation helps in controlling symptoms like pain or bleeding from metastases. In addition to thoracic radiotherapy, PCI is suggested for patients who responded to chemotherapy to prevent brain metastases, which commonly follow metastases in other parts of the body. Although it improves overall survival moderately, it presents a high risk of multiple neurocognitive side effects, making it a difficult decision on whether it should be used (Tang, Tian, and Li 2024).

1.3.3 Immunotherapy

After decades of no significant advancements in SCLC treatment strategies and minimal survival outcome improvements, the introduction of ICI revolutionized the clinical management of ES-SCLC (Horn et al. 2018; Paz-Ares et al. 2019). Targeting the immune system to fight cancer has become an important focus of novel treatment strategies, especially in tumors such as SCLC with high mutation rates and DNA instability. ICIs disrupt the regulatory pathways of the immune system that suppress immune responses and prevent autoimmunity. These pathways are often utilized by

cancer cells to evade the immune system.

Specifically, ICIs block proteins like programmed death-1 (PD-1), programmed death-ligand 1 (PD-L1), or cytotoxic T-lymphocyte-associated protein 4 (CTLA-4) immune checkpoints that are expressed on the surface of immune cells and tumor cells. Under physiological conditions, the engagement of these checkpoints results in T-cell inactivation and tumor immune escape. Anti-CTLA-4 antibodies block the binding of CTLA-4 to CD80/CD86 on antigen-presenting cells (APCs), restoring the activation of T cells **(Figure 1.4a)**. Similarly, inhibiting the PD-1/PD-L1 interaction with respective checkpoint inhibitors prevents the suppression of T cell activity, reactivating the anti-tumor immune responses **(Figure 1.4b)** (Soularue et al. 2018). Thus, immune checkpoint inhibition restores the ability of the immune system to recognize and kill tumor cells (Kong et al. 2024).

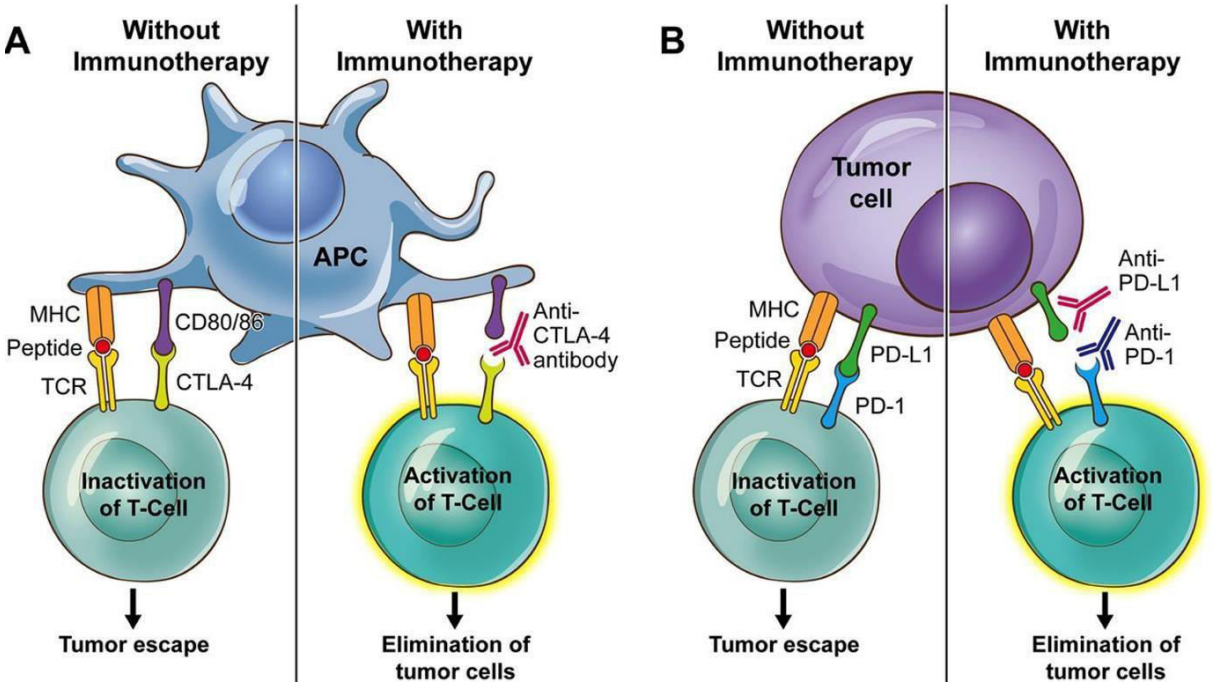

Figure 1.4 Mechanisms of immune checkpoint inhibition in cancer therapy (adapted from Soularue et al. 2018).
a) Under normal conditions, antigen-presenting cells (APCs) activate T cells through the interaction of the T-cell receptor (TCR) with MHC-peptide complexes. However, CTLA-4 on the surface of T cells binds to the CD80/CD86 on APCs, leading to T cell inactivation and tumor escape. When anti-CTLA-4 antibodies are used, this inhibitory reaction is blocked, and the T cell activation is restored, resulting in tumor cell elimination. **b)** Similarly, tumor cells can express PD-L1, which binds to the PD-1 receptor on the T cell surface and leads to its inactivity, enabling tumor escape. Anti-PD-1 and anti-PD-L1 antibodies prevent this interaction, restoring T-cell activation and eliminating tumor cells.

In 2019, the U.S. Food and Drug Administration (FDA) approved atezolizumab and durvalumab, PD-L1 inhibitors, for administration alongside chemotherapy as a first-line treatment for ES-SCLC (FDA 2019, 2020). The Impower133 trial demonstrated that the addition of atezolizumab to first-line chemotherapy improved the median overall survival by 2 months in patients with extensive disease (12.3 months in the combination group vs 10.3 months in the chemotherapy alone group) (Horn et al. 2018). Similarly, the CASPIAN trial showed that the combination of durvalumab with standard chemotherapy enhanced survival rates up to 13 months compared to 10.3 months in ES-SCLC patients treated with chemotherapy alone (Paz-Ares et al. 2019).

Even though ICIs have revolutionized SCLC clinical management and initiated a new treatment era, major challenges remain. The response rates to ICI in SCLC are lower than in other cancer types, such as NSCLC. Furthermore, there is a profound variability in responsiveness among patients and only a small subset of patients is sensitive to ICI (Hamilton and Rath 2019; Rossi et al. 2023). Therefore, new biomarkers and predictive models for ICI response as well as stratification of patients who likely will benefit from immunotherapy are urgently required.

1.3.4 Emerging treatments and their limitations

Emerging therapies in various cancers focus on targeting specific molecular pathways, which might overcome some conventional therapy limitations, such as resistance to treatment and recurrence of disease. However, these novel therapies have their own challenges and have not made significant improvements in SCLC to date. Targeted therapies are among the most researched treatment approaches, as they have made substantial progress in treating many cancers with identifiable driver mutations, such as in NSCLC (McLaughlin et al., 2023). However, this is not the case for SCLC, which is characterized by rapid genetic evolution and a lack of consistent and actionable mutations (Denninghoff et al. 2021). Nevertheless, inhibitors of *the phosphoinositide 3-kinase/protein kinase B/mammalian target of rapamycin* (*PI3K/AKT/mTOR)* pathway and *fibroblast growth factor receptor 1* (*FGFR1)* are actively investigated in clinical trials and have shown only modest results (Hung, Wang, and Chi 2022; Weeden, Solomon, and Asselin-Labat 2015).

Another group of drugs currently being studied in SCLC is antibody-drug conjugates (ADCs). ADCs allow for selective delivery of chemotherapy into the tumor cells since they include cytotoxic drugs that are conjugated to antibodies that target a specific tumor antigen. For instance, an ADC targeting delta-like 3 (DLL3), a protein expressed in SCLC cells, showed initial promise in clinical trials, however, it quickly developed significant toxicity and was discontinued (Ding and Yeong 2024).

Another emerging treatment for SCLC is the administration of poly (ADP-ribose) polymerase (PARP) inhibitors. PARP is an enzyme involved in DNA repair, and its inhibition in SCLC cells, which generally have impaired DNA repair mechanisms, leads to cell death. Olaparib, a PARP inhibitor, has demonstrated promising results when combined with chemotherapy or immunotherapy in preclinical studies, and its efficacy is still under investigation. Like other drugs, the PARP inhibitors´ efficacy in SCLC is limited due to the cancer´s ability to develop resistance (Barayan, Ran, and Lok 2020).

Furthermore, in addition to PD-1/PD-L1 inhibitors currently being used in the clinical management of SCLC, other immunotherapeutic components are being explored. For instance, ipilimumab, a CTLA-4 inhibitor, is currently undergoing testing in combination with PD-1/PD-L1 inhibitors to achieve broader immune stimulation and to overcome the potential resistance that cancer can create against monotherapy (Cheng et al. 2024).

Despite showing great potential, these novel therapies yield only low response rates in SCLC and can have immune-related toxicities. All in all, emerging treatments in SCLC are promising, especially in the late stages of the disease, where conventional therapies are not generally effective. However, their clinical application remains challenging due to heterogeneous patient responses, high toxicity, and the development of treatment resistance.

1.4 Genetic and molecular landscape of SCLC

1.4.1 High tumor mutational burden and genetic instability

SCLC is characterized by a highly complex and heterogeneous genomic profile harboring a high load of mutations, contributing to its aggressive phenotype. Unlike NSCLC, which generally harbors actionable driver mutations, SCLC displays genomic instability without distinct oncogenic drivers (Rudin et al. 2021). Additionally, SCLC has one of the highest tumor mutational burdens (TMB) among cancers, primarily associated with chronic exposure to carcinogens in cigarette smoke. The elevated TMB leads to pronounced genomic instability and a rapid accumulation of somatic mutations, including new mutations emerging during treatment cycles (Hellmann et al. 2018). These mutations contribute to tumor heterogeneity and treatment resistance.

The increased TMB also forms neoantigens, which are tumor-specific antigens generated by somatic mutations. Neoantigens can produce abnormal proteins presented on the tumor cell surface by major histocompatibility complex (MHC) molecules. Unlike normal self-antigens, neoantigens are not recognized by the immune system. This makes them highly immunogenic and potential targets of anti-tumor immune responses (Zhang et al. 2021). Although there is great potential in utilizing neoantigens in clinical settings to elicit strong immune responses, their effectiveness in SCLC is limited due to the typical immunosuppressive tumor microenvironment in SCLC tumors.

High TMB has also been proposed as a surrogate marker for ICI response in patients, as tumors with elevated TMB may be more prone to immune attack after ICI exposure. Notably, the FDA has approved the administration of pembrolizumab, an anti-PD-1 agent, for all tumor types presenting with a TMB of more than 10 mutations per megabase, underscoring the role of TMB in predicting ICI outcomes (Strickler, Hanks, and Khasraw 2021). In the CheckMate 032 clinical trial of SCLC, patients with high TMB, defined as having more than 248 somatic missense mutations, exhibited an improved ORR, OS, and progression-free survival (PFS) when exposed to nivolumab (a PD-1 blocker) alone or in combination with ipilimumab (a CTLA-4 blocker) (Hellmann et al. 2018). However, although a high TMB is often linked to a better ICI

response in some tumor entities, its predictive role in SCLC remains unclear. Most patients with high TMB do not durably respond to immunotherapy; thus, TMB alone cannot stratify patients into responders and non-responders (Le et al. 2017; Westcott et al. 2023a). Some studies have demonstrated that TMB alone does not consistently predict ICI response and, therefore, is not a reliable biomarker (Gurjao et al. 2020). This highlights the importance of understanding other factors that mediate ICI sensitivity alongside TMB.

1.4.2 Tumor suppressor gene alterations

The genes responsible for cancer development are commonly categorized into two major groups: oncogenes and tumor suppressor genes. Oncogenes are modifications of proto-oncogenes, the first regulatory factors of biological processes, including cell differentiation and growth. An oncogene is created when a proto-oncogene is activated excessively, leading to uncontrolled cell proliferation. In contrast, tumor suppressor genes regulate cell division under normal conditions, and their inactivation leads to unchecked cell growth and tumor formation (Dakal et al. 2024; Kontomanolis et al. 2020).

Even though the genetic landscape of SCLC is not fully understood to date, comprehensive studies have identified a near-universal alteration in two key tumor suppressor genes: *tumor protein p53 (TP53*) and *retinoblastoma 1 (RB1*). Mutations in these genes are present in approximately 90% and 50-90% of clinical cases, respectively, and are considered the main drivers of tumorigenesis (George et al. 2015, 2024; Sivakumar et al. 2023). These genetic features are strikingly different in NSCLC, where oncogenic drivers such as *epidermal growth factor receptor* (*EGFR*) and *anaplastic lymphoma kinase* (*ALK*) mutations are prominent (Rudin et al. 2021).
The *TP53* gene encodes the p53 protein, which functions as a tumor suppressor by initiating cell cycle arrest or apoptosis upon DNA damage. In SCLC, *TP53* mutation results in loss of function, allowing accumulation of DNA errors. As a result, mutated cells continue to proliferate excessively, leading to genomic instability and tumor progression (Jeong et al., 2025). Similarly, the *RB1* gene encodes the retinoblastoma protein (Rb) that regulates the cell cycle progression by controlling the G1/S transition. Inactivation of *RB1* disrupts this process and allows rapid tumor progression and early metastases (Dyson et al., 2016).

1.4.3 DNA repair deficiencies and mismatch repair defects in SCLC

Although SCLC is predominantly associated with smoking (Wang et al. 2023), approximately 15% of cases in a recent cohort exhibited a distinct DNA mismatch repair (MMR) mutational signature (Liu et al., 2024). MMR deficiency (MMRd) leads to genomic instability, which is a hallmark of SCLC that largely contributes to its high TMB and rapid disease progression (Dietlein et al., 2014). This instability is linked to impaired DNA damage repair (DDR) pathways, which are responsible for maintaining genomic integrity. Among DDR mechanisms, the MMR system plays a fundamental role in identifying and correcting replication errors, including base mismatches and small insertions/deletions (indels). MMR is performed by key proteins, such as MutS homolog 2 (MSH2), MutS homolog 6 (MSH6), MutL homolog 1 (MLH1), and post-meiotic segregation increased 1/2 (PMS1/PMS2). These proteins work as heterodimers, where MSH2/MSH6 creates the MutSα complex and recognizes replication errors and MLH1/PMS2 forms the MutLα complex and mediates downstream repair processes (Friker et al. 2025). Loss or inactivation of these components leads to the accumulation of mutations across the genome (Li 2008). Failure of MMR function results in the accumulation of replication errors and, subsequently, elevated mutation rate, microsatellite instability (MSI), and increased tumor heterogeneity (Schöniger and Rüschoff 2022).

At the genetic level, MMRd causes the buildup of single nucleotide variants (SNVs) and frameshift mutations, the latter arising from indels (Germano et al. 2018). Frameshift alterations generate longer, highly immunogenic peptides, which increase the probability of producing strong neoantigens, eliciting a stronger immune response and improving the ICI sensitivity. Consequently, MMR-deficient and high MSI tumors exhibit greater sensitivity to ICIs. Supporting these results, studies have demonstrated a positive correlation between neoantigenic load and immune infiltration, as well as better survival in MSI cancers, such as colorectal tumors (Sahin et al. 2019). Notably, the clinical relevance of a positive MMRd status has been recognized by the FDA, which authorized pembrolizumab, a PD-I inhibitor, for MMR-deficient cancers, highlighting its role as a predictive biomarker (FDA., 2017; Marcus et al. 2019).

However, the impact of MMR loss on prognosis and therapy responses is different

across cancer types. For instance, MMRd and MSI are associated with favorable prognosis and OS and high infiltration with immune cells in colorectal cancer (Batur et al. 2016; Gatalica et al. 2016). However, similar outcomes are not observed for endometrial cancers (McMeekin et al. 2016). Additionally, some studies have shown that MMRd tumors exhibit heightened resistance to cytotoxic drugs such as cisplatin and carboplatin (L. P. Martin, Hamilton, and Schilder 2008). At the same time, no significant effect has been noted on the response to oxaliplatin (Seetharam, Sood, and Goel 2009). These inconsistencies highlight the necessity for further comprehensive research to better understand the role of MMRd across various tumor types, including SCLC.

1.4.4 *MSH2* loss and its role in SCLC

MSH2 is a crucial component of the MMR system and helps maintain genomic stability by detecting mismatched DNA bases and indel errors during DNA replication. *MSH2* can complete this function by forming heterodimers with *MSH6* (MutSα complex) to detect replication errors and with *MSH3* (MutSβ complex) to repair longer insertions or deletions. *MSH2* recruits MLH1/PMS2 to begin the repair when a mismatch is identified (Edelbrock, Kaliyaperumal, and Williams 2013). Unlike other MMR deficiencies where partial activity remains, *MSH2* loss results in a complete disruption of the MMR system since it is involved in the initial mismatch detection process, making it one of the most important components of the MMR machinery. Consequently, *MSH2* inactivation allows for replication errors to happen undetected, resulting in MSI, increased accumulation of frameshift mutations, and intratumoral heterogeneity (Li et al. 2023).

In addition to its role in controlling genomic integrity, *MSH2* inactivation has been associated with tumor development, modulation of immune responses, and treatment resistance across various cancer types (He et al. 2022). In colorectal and endometrial cancers, *MSH2* alterations are a hallmark of Lynch syndrome and make patients more prone to early-onset and highly immunogenic tumors. In sporadic cancers, *MSH2* is often inactivated not by direct mutation, but via allelic loss, promotor hypermethylation, or other forms of genetic silencing (Peltomäki et al. 2023). *MSH2*-deficient tumors have higher resistance to platinum-based chemotherapy in prostate and ovarian

cancers, likely because of reduced DNA damage recognition. Additionally, defective *MSH2* has been correlated with incorrect apoptotic signaling via the p53 pathway since p53 depends on MMR-mediated DNA damage detection to initiate cell death. This suggests that *MSH2* inactivation causes genetic instability and is an indicator of increased tumor survival during chemotherapy exposure (Dong et al. 2023).

In SCLC, *MSH2* loss remains largely unexplored, as no studies to date have specifically examined its isolated role in this tumor type. However, based on the broader evidence from MMR-deficient tumors, *MSH2* inactivation may have important implications for tumor development and therapy resistance. For instance, its loss has been linked in other tumor types with increased genetic instability, increased frameshift load, and intratumoral heterogeneity, which are also hallmarks of SCLC. These effects may lead to pronounced evolution and plasticity in SCLC, which can contribute to therapy resistance (George et al. 2015; Ireland et al. 2020). However, whether *MSH2* alone can drive these features of SCLC has not been explored, representing a significant gap in understanding the molecular players of therapy resistance and immune evasion in MMRd-SCLC. Therefore, characterizing the function of *MSH2* in SCLC remains an important area of future research.

1.4.5 Other genetic alterations

Several other genetic alterations have been identified in SCLC as drivers of tumorigenesis, in addition to *TP53* and *RB1* mutations. Some alterations belong to the myelocytomatosis (*MYC)* family of oncogenes, especially *MYC* amplifications. *MYC* mutations are detected in approximately 20% of SCLC cases. *MYC* genes promote cell growth and proliferation, and their amplification leads to heightened disease aggressiveness and poor prognosis (Umemura 2014). Moreover, mutations in genes involved in the *PI3K/AKT/mTOR* pathway are found in about 36% of SCLC patients. Such alterations result in the disruption of optimal cellular growth, metabolism, and survival (Umemura 2014).

Besides genetic dysregulation, SCLC is also affected significantly by epigenetic changes, particularly changes in DNA methylation and histone modifications. For instance, mutations in *CREBBP* and *EP300* histone modifiers are frequently observed

in SCLC, occurring in approximately 15-17% and 5-13% of cases, respectively (Jia et al. 2018). Such mutations promote tumor progression by inducing alterations in the chromatin structure and gene expression (Zhu et al. 2023).

Another hallmark of SCLC, which makes it highly challenging to treat, is its intrinsic tumor heterogeneity, referring to the presence of different tumor cell subpopulations within a single tumor. SCLC exhibits heterogeneity at both genetic and phenotypic levels. Genetically, the excessive accumulation of mutations, copy number alterations (CNAs), and chromosomal rearrangements result in distinct subclones that respond differently to therapeutic interventions and make the tumor more adaptable and resistant (George et al. 2015; Peifer et al. 2012). Additionally, SCLC displays phenotypic heterogeneity, with the tumor cells showing different expression levels of neuroendocrine proteins, such as achaete-scute homolog 1 (ASCL1), neurogenic differentiation factor 1 (NEUROD1), synaptophysin (SYP), and chromogranin A (CHGA) (Augustyn et al. 2014; Rudin et al. 2019). Recent studies have identified different molecular subtypes of SCLC based on the expression of these markers, each with distinct transcriptional profiles. For example, ASCL1-high tumors have a typical neuroendocrine phenotype, while NEUROD1-high subtype exhibits neuronal-like behavior. The increased heterogeneity in SCLC makes standard treatments like chemotherapy and immunotherapy unsuitable for long-term therapeutic strategies (Rudin et al. 2019, 2021).

1.4.6 Emerging SCLC subtypes

Although genomic profiling in SCLC has not revealed mutationally defined subtypes, a recent classification based on the expression of transcription factors has been proposed **(Figure 1.5)**. This poses an essential step towards the establishment of new therapeutic targets. The novel classification strategy identifies four distinct molecular subtypes of SCLC: SCLC-A (expressing ASCL1), SCLC-N (expressing NEUROD1), SCLC-P (expressing POU class 2 homeobox 3), and SCLC-I (representing tumors with an inflammatory phenotype) (Gay et al. 2021; Rudin et al. 2019).

SCLC-A and SCLC-N are NE tumors expressing typical NE markers such as CHGA and SYP. In contrast, SCLC-P and SCLC-I exhibit a non-NE phenotype (Gay et al.

2021). SCLC-P is associated with POU2F3, normally expressed in tuft cells, which are chemosensory cells in the pulmonary epithelium, suggesting a different cell of origin from the two NE subtypes (Huang et al. 2018). Some non-NE tumors express yes-associated protein 1 (YAP1), which does not exclusively define a new subtype (Baine et al. 2020). In 2021, Gay et al. proposed the new SCLC-I subtype to classify tumors with epithelial-mesenchymal transition (EMT) and immune-related gene expression, including human leukocyte antigens, interferon-γ (IFNγ), and immune checkpoint molecules.

This classification system for SCLC is being actively investigated for treatment stratification purposes. Notably, a retrospective analysis of the IMpower 133 trial, the first randomized trial to determine the OS and PFS of SCLC patients exposed to ICI, revealed that SCLC-I derives the greatest benefit from the combination of ICI with chemotherapy, followed by SCLC-A, SCLC-N, and SCLC-P **(Figure 1.5, Right).** The figure also illustrates that under treatment, the subtype SCLC-A can undergo subtype switching and turn chemoresistant, highlighting the dynamics of the plasticity of SCLC (Gay et al. 2021; Saida, Watanabe, and Kikuchi 2023).

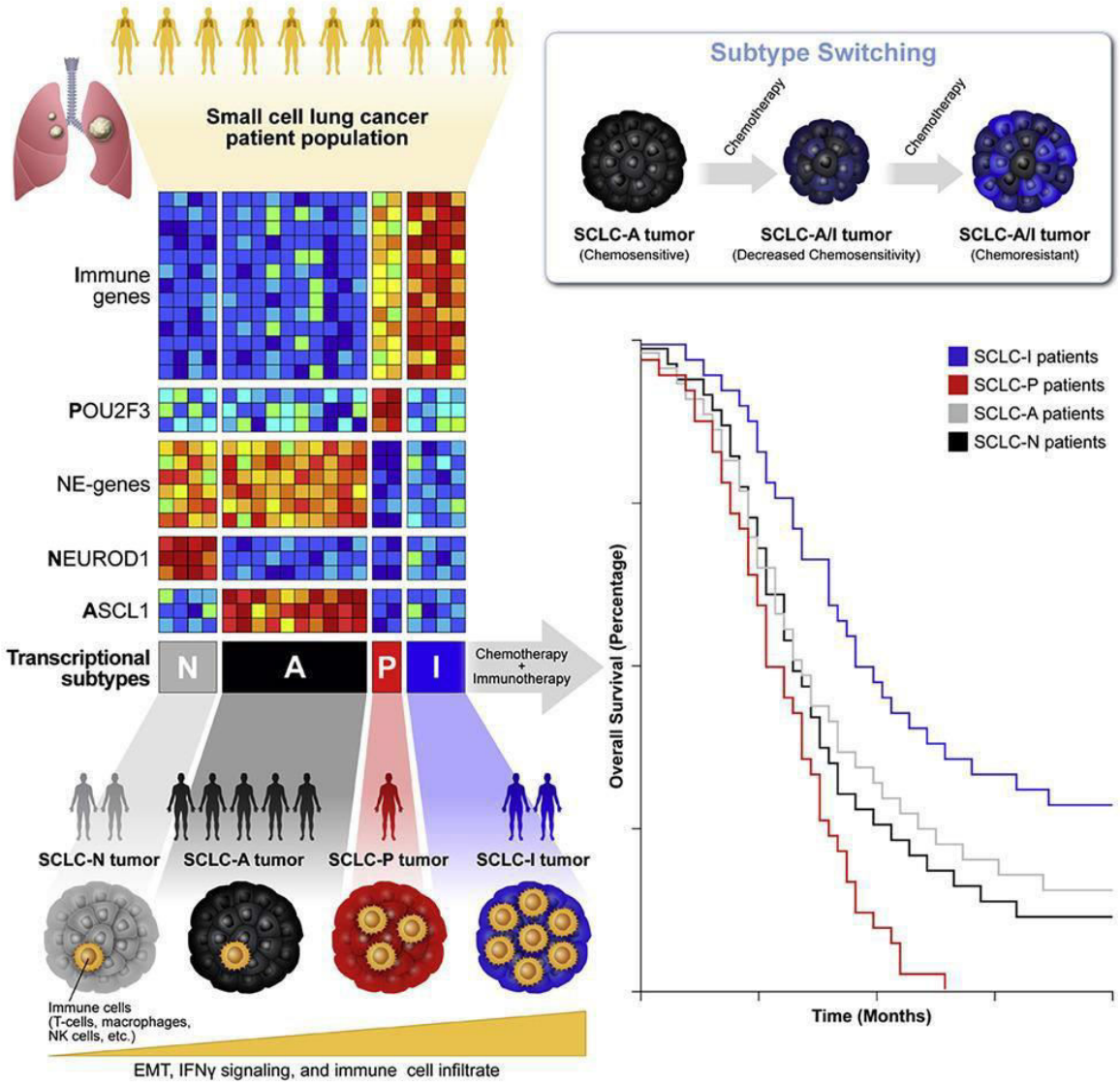

Figure 1.5 Transcriptional subtypes of SCLC and their association with immune-related properties and therapeutic outcomes (adapted from Gay et al. 2021).
Heatmaps depict the differential expression of immune-related genes, POU2F3, NE-genes, NEUROD1, and ASCL1 across the four SCLC subtypes: SCLC-N, SCLC-A, SCLC-P, and SCLC-I. The SCLC-I exhibits high EMT, IFNγ signaling, and immune infiltration. The right panel shows the survival outcomes of all subtypes, with SCLC-I having the greatest benefit from combining chemotherapy and immunotherapy. The inset illustrates the subtype plasticity, with the potential of SCLC-A tumors to transition to a chemoresistant type.

1.5 Emerging role of the tumor microenvironment

The tumor microenvironment (TME) is a complex and dynamic network of non-cancerous cells and extracellular structures that surround and interact with tumor cells. It consists of various components, such as immune cells, stromal cells, blood vessels, mesenchymal stem cells, and the extracellular matrix (ECM). These structures can affect the behavior of the tumor as well as impact important processes like tumor growth, proliferation, invasion, formation of metastasis, and response to therapies (Dai et al. 2020; Zhao et al. 2023).

1.5.1 Overview of the TME

There are different mechanisms for how TME influences tumor growth. For instance, the TME contributes to cancer progression by releasing signaling molecules that promote angiogenesis, which is the formation of new blood vessels that deliver nutrients and oxygen to the tumor (Z. Li et al. 2024; Yang, Lee, and Fan 2024). Additionally, the TME can lead to immune suppression, allowing cancer cells to evade the body´s immune defense and, thus, spread to other organs (W. Liu et al. 2024). Furthermore, the TME makes a favorable environment to support cancer stem cells, which are often resistant to conventional treatment strategies (Borlongan, Saha, and Wang 2024).

Both the innate and adaptive immune systems are part of the TME. The innate immune system is the first line of defense against pathogens and tumors. It elicits rapid and non-specific responses with the help of macrophages, natural killer (NK), and dendritic cells (Marshall et al. 2018). In contrast, adaptive immune responses generated by T and B cells are slower to initiate but highly specific. The adaptive immune system is characterized by immunological memory, enabling quicker reaction upon a repeated encounter with the same antigen (Vesely et al. 2011). However, tumors develop mechanisms to suppress or evade both innate and adaptive immune responses, leading to immune escape and disease progression (Vinay et al. 2015). Given its critical role in shaping tumor dynamics, TME has become a major focus in cancer research. Discovering ways to suppress its tumor-promoting properties and modulate it to support drug efficacies holds great potential to improve treatment outcomes.

1.5.2 Key cellular components of the TME

Effector immune cells

CD8⁺ T cells (Cytotoxic T Lymphocytes): These cells are key players in anti-tumor immunity. They directly kill cancer cells using mechanisms like perforin- and granzyme-mediated apoptosis (Lin, Zou, and Wen 2023). However, some tumors can evade $CD8^+$ T cell activity by upregulating immune checkpoints (e.g., PD-1, PD-L1) and producing immunosuppressive cytokines (Lin et al. 2024a).

NK cells: NK cells detect and destroy tumor cells that escape the adaptive immune system by recognizing stress-induced signals or the lack of MHC molecules. They can release perforin and granzyme to induce tumor cell death (Paul and Lal 2017).

Regulatory and suppressive immune cells

CD4⁺ T cells (Helper T cells): These cells support the anti-tumor activity by orchestrating adaptive immune responses. They can activate macrophages and $CD8^+$ T cell-mediated cytotoxicity via IFN-γ release and support macrophages by producing interleukin-4 (IL-4), IL-5, and IL-3 cytokines. Besides the primary function in anti-tumor immunity, some $CD4^+$ T cell subsets (e.g., T helper 2 (Th2), T helper 17 (Th17) contribute to tumor progression under chronic inflammation (Kim and Cantor 2014).

Regulatory T Cells (Tregs): Tregs are a subset of $CD4^+$ T cells that exhibit suppressive abilities to anti-tumor immune responses by inhibiting effector T cells and dendritic cells. They achieve this by the secretion of IL-10 and transforming growth factor beta (TGF-β). Tumors often utilize Tregs to escape from the immune system (Josefowicz, Lu, and Rudensky 2012; Tanaka and Sakaguchi 2017).

Other key cells

Tumor-Associated Macrophages (TAMs): TAMs include the pro-inflammatory M1 and pro-tumorigenic M2 macrophages. Briefly, M1 macrophages promote anti-tumor activity by enhancing T-cell cytotoxicity, while M2 macrophages support tumor growth via angiogenesis and immune suppression (Pan et al. 2020).

Dendritic cells (DCs): DCs are antigen-presenting cells that play a critical role in initiating immune responses. They provide a link between the innate and adaptive immune systems by recognizing, capturing, and presenting antigens to T cells (Del Prete et al. 2023).

Cancer-Associated Fibroblasts (CAFs): CAFs are known to remodel the ECM, promote angiogenesis, and secrete growth factors that contribute to tumor cell thriving (Popova and Jücker 2022).

1.5.3 Non-cellular components of the TME

Extracellular Matrix (ECM): The ECM is a network of proteins and polysaccharides that provide structural support, facilitate the exchange of chemical signaling between tissues, and impact cell behavior. Tumors often remodel the ECM to support their survival and invasion (Popova and Jücker 2022).

Cytokines and chemokines: These are signaling molecules produced by various cells to regulate immune cell recruitment and activate anti-tumor immune responses. However, tumors can use the cytokine network to create an immunosuppressive microenvironment (Yeo et al. 2021).

Exosomes and extracellular vesicles: Tumors can secrete vesicles to transport pro-tumorigenic molecules like microRNAs (miRNAs) or proteins to neighboring cells, enhancing tumor progression (Aseervatham 2023).

1.5.4 Immune microenvironment in SCLC

SCLC is generally considered an immune “cold” tumor as it exhibits low infiltration with immune cells, especially effector T cells, which are critical for anti-tumor responses. In addition, despite the high TMB in SCLC, which is commonly associated with elevated immunogenicity, the immune microenvironment in these tumors is characterized as predominantly immunosuppressive and thereby favors tumor growth (Rudin et al. 2021).

As depicted in **Figure 1.6**, the cancer-immunity cycle in SCLC is disrupted at several levels. First, the antigen presentation is impaired due to a low or total lack of MHC class I and II expression on the surface of tumor cells and dendritic cells. As a result, the priming of $CD8^+$ and $CD4^+$ T cells is compromised. Additionally, the lack of costimulatory proteins worsens the priming further (Chen et al., 2023). The main features of SCLC, including rapid proliferation, high genomic instability, and expression of a high number of neoantigens, would theoretically make this tumor entity highly immunogenic. However, SCLC surprisingly often evades and suppresses the immune system, which is one of the hallmarks of cancer progression. Immune evasion allows cancer cells to escape immune detection and destruction and, thus, enables them to survive and thrive without being targeted by the body´s immune system (Hanahan and Weinberg 2011). The mechanisms used by cancer cells for immune evasion impact both innate and adaptive responses. One key strategy that SCLC cells use to evade immune responses is the upregulation of immune checkpoint molecules on tumor cells, such as PD-L1 (Rudin et al. 2019). PD-L1 normally interacts with the respective inhibitory receptor PD-1, which is expressed on the surface of T cells, leading to the inhibition of effector T cell-mediated cytotoxicity (Soularue et al. 2018). Other similar inhibitory molecules that contribute to effector T cell suppression include CTLA-4, T cell immunoreceptor with Ig and ITIM domains (TIGIT), and B7 homolog 3 (B7-H3). SCLC cells also secrete immunosuppressive cytokines, including TGF-β and IL-10, which suppress the activity of effector cells and promote the recruitment of Tregs (Chen, Li, and Fan 2023b).

Additionally, the SCLC microenvironment recruits immunosuppressive cells, such as Tregs and myeloid-derived suppressor cells (MDSCs), which repress the effector T cell and NK cell activity (Iclozan et al. 2013). TAMs exhibit predominantly a pro-tumorigenic M2-like phenotype that supports angiogenesis, ECM remodeling, as well as immune suppression (Dora et al. 2021). Moreover, NK cells frequently become ineffective due to tumor-derived signals reducing their activator ligands and inhibiting their cytotoxic activity (Chen et al. 2023). The combined effect of these suppressive mechanisms disrupts all major steps of anti-tumor immunity, rendering immunotherapy less effective and making it difficult to reverse immune resistance in SCLC.

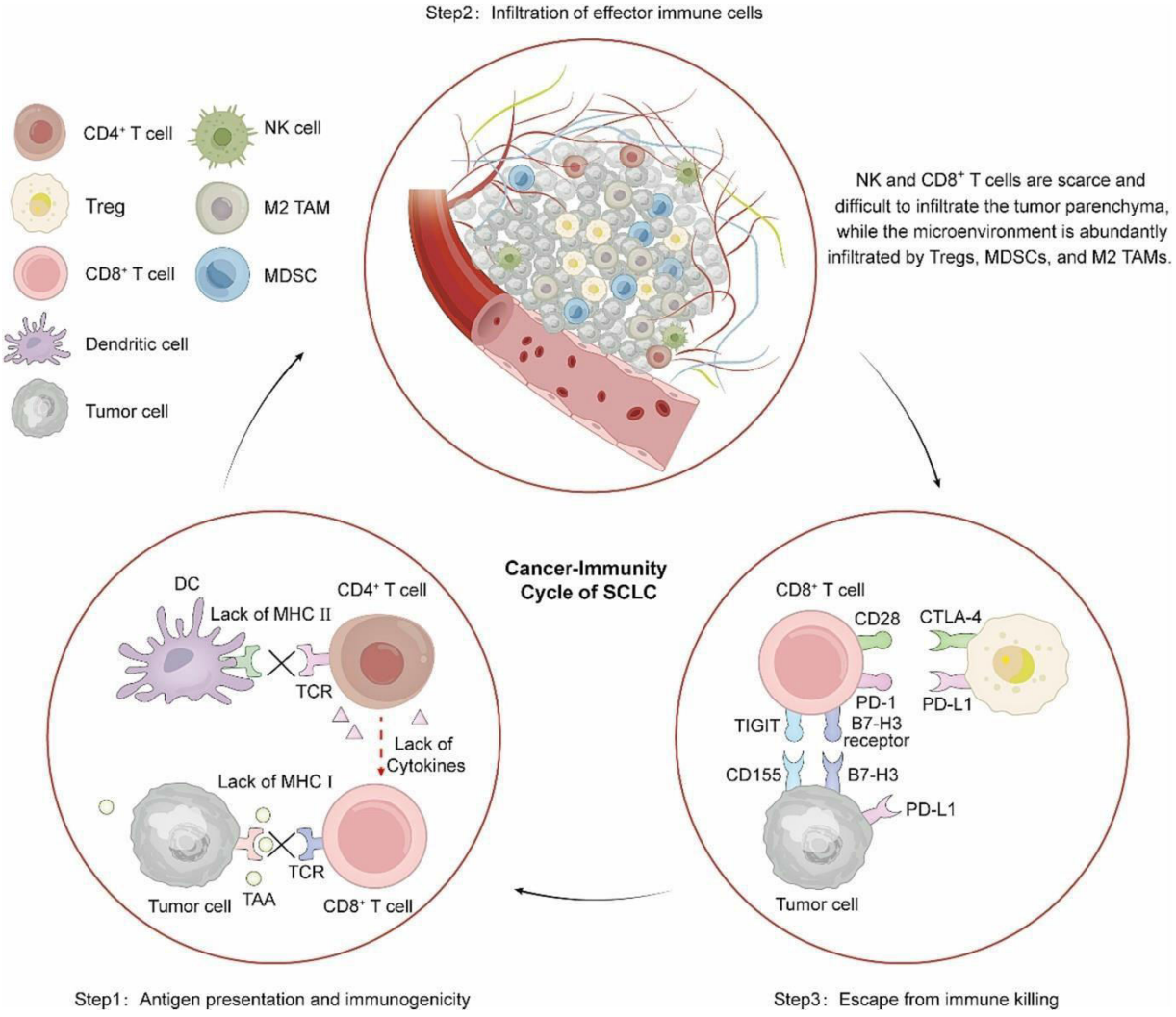

Figure 1.6 Schematic overview of the cancer-immunity cycle in SCLC (adapted from Chen et al., 2023).
This schematic illustrates the key mechanisms enabling immune evasion in SCLC. **Step 1: Antigen presentation and immunogenicity**. SCLC cells downregulate the expression of MHC class I and II, disrupting effective antigen presentation by DCs and reducing T cell priming. $CD4^+$ and $CD8^+$ T cells cannot be activated due to the lack of antigen presentation and costimulatory cytokines. **Step 2: Infiltration of effector immune cells**. NK cells and $CD8^+$ T cells are not abundant and do not penetrate the tumor parenchyma. At the same time, the TME is heavily infiltrated by immunosuppressive immune cells such as Tregs, MDSCs, and TAMs. **Step 3: Escape from immune killing**. SCLC tumors express immune checkpoints like PD-L1 and B7-H3, which bind to respective inhibitory receptors (PD-1, TIGIT, and CTLA-4) on T cells, leading to T cell inactivation.

1.6 Mouse models of SCLC

1.6.1 The need for preclinical mouse models

Historically, SCLC has been challenging to investigate as human tumor samples are extremely scarce. Despite its high incidence, SCLC is typically diagnosed at advanced stages when metastases are already present, and surgical resection is no longer an option (Byers et al. 2015). Additionally, the rapid progression of the disease makes it difficult to collect longitudinal biopsy specimens. As a result, little progress has been made in understanding how SCLC evolves and acquires therapeutic resistance and what role immune interactions play. Due to these limitations, patient-derived xenografts (PDXs) and genetically engineered mouse models (GEMMs) have become essential tools in SCLC research (Oser et al. 2024). PDXs are generated by implanting immunocompromised mice with patient tumor samples, which allows the study of tumor heterogeneity and treatment responses in a setting that closely mirrors the human scenario (Liu and Yang 2025). Meanwhile, GEMMs are generated by altering the mouse genome and obtaining controlled genetic modifications. GEMMs provide another physiologically relevant platform, enabling research into the role of key mutations and a fully competent immune system in the development and progression of malignancy (Oser et al. 2024).

1.6.2 Existing mouse models of SCLC and their limitations

The first and most important GEMM of SCLC was developed in 2003 by Meuwissen et al. This model incorporates the inactivation of two key genetic drivers, *Rb1* and *Trp53*, in lung epithelial cells, particularly in PNECs. In this model, mice have floxed (fl) alleles of *Rb1* and *Trp53* (*Rb1*$^{fl/fl}$*;Trp53*$^{fl/fl}$), and the conditional deletion of the genes is achieved exclusively in lungs by infecting the animals via intratracheal injection with an adenoviral vector containing Cre recombinase (Ad-CMV-Cre) **(Figure 1.7)**. The *Rb1/Trp53* (RP) model effectively recapitulates SCLC's histopathological and metastatic patterns, including neuroendocrine differentiation, rapid progression, and therapy resistance (Meuwissen et al. 2003). However, a major limitation of the RP mouse is the development of only a few lung lesions (1-5 tumors per animal) with a long latency period of approximately 210 days (Oser et al. 2024). Several other mouse lines have been developed based on the RP model to overcome this limitation and

achieve faster-growing tumors. For instance, the RPR2 (*Rb1;Trp53;Rbl2*) model was created considering findings that p130*/RBL2* expression is low in human SCLC, and it develops 10-20 times more tumors in half the time compared to the RP model (McFadden et al. 2014; Schaffer et al. 2010). The RPM (*Rb1/Trp53/MycT58A*) model also includes inducible *MYCT58A* expression, a key oncogene of SCLC, leading to a significantly shorter tumor onset (4-10 weeks) (Mollaoglu et al. 2017). Tumors in both RP and RPR2 mouse systems mainly express *Ascl1*, while RPM tumors are *Neurod1*-high, representing different molecular subtypes of SCLC (Oser et al. 2024).

However, significant limitations of the existing GEMMs of SCLC include low TMB and low rate of acquiring new mutations. Since one of the most important hallmarks of human SCLC is high TMB and genomic instability, the current mouse models fail to capture the mutational complexity of the disease. In human SCLC, the main driver of genomic instability is chronic exposure to carcinogens in cigarette smoke, which creates a mutational signature harboring mainly C>A conversions (Rudin et al. 2021; Wang et al. 2023). Therefore, an ideal GEMM to study SCLC would carry tobacco-induced mutations in its genome. This preclinical model is very challenging to replicate and non-existent to date. In addition to the smoking signature, a subset of SCLC cases exhibits MMRd mutational signature, containing excessive indels and MSI. These patients also present with elevated TMB and neoantigenic load (Q. Liu et al. 2024). Therefore, establishing SCLC models with high TMB and MMRd patterns would provide a more suitable system for investigating SCLC biology and testing novel therapeutic strategies.

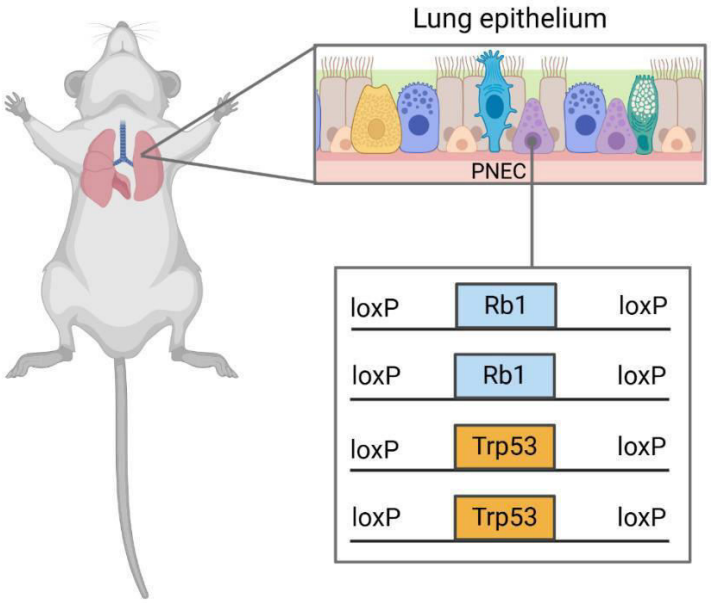

Figure 1.7 Schematic representation of the RP (*Rb1*$^{fl/fl}$;*Trp53*$^{fl/fl}$) mouse model of SCLC. This model incorporates the conditional deletion of the *Rb1* and *Trp53* tumor suppressor genes in lung epithelial cells, especially in PNECs, which are believed to be the cells of origin for SCLC. These cells contain floxed *Rb1* and *Trp53* alleles, flanked by *loxP* sites, which are excised by Cre recombinase delivered via an adenoviral vector. Once the genes are inactivated, lung lesions are developed. This model closely mirrors the histopathological features of human SCLC. Created with Biorender.com

1.6.3 The novel RPM model: Introducing MMR deficiency into SCLC

Despite the development of several GEMMs of SCLC, existing mouse models do not fully capture genetic instability and the high TMB. Although the RP mouse model and its derivatives can mimic the neuroendocrine differentiation and tumor progression in humans, they lack the high rate of spontaneous mutations driven by smoking carcinogens or defective DNA repair mechanisms (Ibruli et al. 2024). The subset of patients who harbor MMRd, including *MSH2* loss, will also present with MSI, increased indel alterations, heightened neoantigenic load, and excessive TMB. MMRd in solid tumors has also been linked to increased sensitivity toward immunotherapy, especially ICI (Dietlein and Reinhardt 2014; Le et al. 2017; Samstein et al. 2019). Therefore, generating an MMR-deficient platform to study SCLC would provide a more physiologically relevant system to represent a subset of clinical cases and examine the impact of this genetic landscape on tumor development, evolution, and treatment response.

To address this gap, we generated a novel *Rb1*$^{fl/fl}$;*Trp53*$^{fl/fl}$;*Msh2* $^{fl/fl}$ (RPM) mouse model containing *Msh2* loss (Ibruli et al. 2024). This model recapitulates the

Msh2 loss-induced MMRd mutational signature of SCLC and allows the investigation of MMRd's impact on tumorigenesis, immune microenvironment, and behavior towards various therapies. Importantly, this RPM model is different from the RPM-*Myc* model, which incorporates overexpression of the *Myc* oncogene. Our model does not include *Myc* activation but serves as a system to investigate the impact of MMRd and high-TMB in SCLC.

1.7 Aim of the thesis

SCLC is a highly aggressive cancer entity with extremely poor prognosis, rapid development of metastases, and limited treatment options (Rudin et al. 2021). For the advanced disease stage, the first-line treatment strategy includes a combination of platinum-based chemotherapy and ICIs. Although the incorporation of ICIs in clinical practice revolutionized the SCLC treatment and improved survival outcomes, the benefit remains modest and heterogeneous across patients, underscoring the urgent need for novel treatment strategies (Dingemans et al. 2021). A hallmark of SCLC is its high TMB, predominantly linked to chronic exposure to tobacco carcinogens (George et al. 2015, 2024; Peifer et al. 2012). However, a subset of SCLC tumors harbors MMRd-associated genetic instability, characterized by indel mutations, MSI, and a high load of neoantigens (Q. Liu et al. 2024). Although MMRd has been widely recognized as a crucial factor in modulating tumor immune microenvironment and response to immunotherapy in various cancer types, its specific role in SCLC remains largely unknown.

The main aim of this thesis is to investigate the influence of MMRd and particularly *MSH2* loss in SCLC tumor development, survival outcome, treatment sensitivity, and immune landscape. To address this, a novel GEMM of SCLC exhibiting MMRd has been developed. We introduced *Msh2* inactivation in the epithelial lung cells of the well-established $Rb1^{fl/fl};Trp53^{fl/fl}$ (RP) model of SCLC, generating the $Rb1^{fl/fl};Trp53^{fl/fl};Msh2^{fl/fl}$ (RPM) model (Ibruli et al. 2024). The RPM mice offer a physiologically relevant platform to study the impact of *Msh2* loss on TMB, neoantigenic load, and response to immunotherapy. The first objective of this study was to generate and validate the RPM mouse line by conditionally deleting *Msh2* in

RP animals. The tumor onset, progression, and histological features were further assessed to understand any potential impacts of MMRd in tumorigenesis.

Furthermore, this study investigates the genomic and mutational landscape of the RPM model by evaluating the TMB and mutational signatures through whole-exome sequencing (WES). Given that MMRd and high TMB are associated with increased neoantigenic presentation in solid tumors (Q. Liu et al. 2024; Zhang et al. 2021), the neoantigen levels were examined in the RPM system to determine if MMRd correlates with enhanced immune recognition. In addition to characterizing the RPM model at the genomic level, this thesis explores how *Msh2* loss influences therapeutic vulnerabilities to platinum-based chemotherapy and ICIs. The research also investigates whether targeting Treg-mediated immunosuppression can promote antitumor immunity. Lastly, this thesis examines the immune microenvironment under the presence of MMRd in preclinical SCLC. Immune cell infiltration in RPM tumors is analyzed using flow cytometry and imaging mass cytometry (IMC) and compared to RP tumors. Both immune activation and suppression are investigated, particularly focusing on T cells and Tregs, to determine any immune-related tendencies influenced by MMRd. By addressing these objectives, this thesis introduces a unique GEMM of SCLC with high TMB that accurately resembles a subset of human cases and provides novel insights into the role of *Msh2* loss and MMRd in SCLC. These findings can pave the way for improved patient stratification for immunotherapy and offer new avenues for therapeutic strategies targeting DNA repair defects in SCLC.

2. Material and methods

2.1 Materials

2.1.1 Devices

Equipment	Company
Achieva 3.0T clinical system	Philips Healthcare, Best, Netherlands
BD FACS Aria	BD
Cell Culture Centrifuge	HERMLE Labortechnik GmbH
Cryostat Leica CM3050 S	Leica Microsystems
Cytoflex S	Beckman Coulter
Gel chamber	Bio-Rad
Heated Paraffin embedding module Leica EG1150 H	Leica Microsystems
Hyperion Imaging System	Standard BioTools
Incubator	Axon Labortechnik GmbH
Laminar airflow cabinet (Biowizard Golden Line)	LMS
Light microscope CKX41SF	Olympus
Microtome Leica RM2	Leica Microsystems
NanoDrop	Thermo Scientific
BX53 bright field microscope	Olympus
Stellaris 5 confocal microscope	Leica Microsystems
T100 Thermal Cycler	Bio-Rad
Tabletop Centrifuge	LMS

2.1.2 Laboratory and cell culture materials

Material	Company
1, 2, 5 and 10 ml syringe	BD
1.5, 2 ml microcentrifuge tube	VWR
1.5 mm biopsy punch	Kai sterile dermal
5, 10, 25 ml serological pipette	Sarstedt
40 µm cell strainer	VWR
Introcan safety-W 24G catheter	Braun
Neubauer chamber	Glaswarenfabrik Karl Hecht
Pipette 0.2-2 µl	Gilson
Pipette 0.5-10 µl	Gilson
Pipette 100-1000 µl	Gilson
Pipette 10-100 µl	Gilson
Pipette tips	VWR
Pipette tips	Sarstedt
Reusable oral gavage needle	PetSurgical
SuperFrost Plus™ Adhesion slide	Thermo Fisher Scientific
Sterile filter pipette tips	Sarstedt
T-Sue microarray mold6	Simport
Tissue-Tek cryomold	Sakura

2.1.3 Buffers

Buffer	Content
1x TAE	40 mM Tris base 20 mM Acetic acid 1 mM EDTA
Flow cytometry buffer	1x PBS 2% FBS 0.5 M EDTA

Lysis buffer	0.2 M NaCl 1.1 1 M Tris HCl pH: 8.5 5 µM EDTA 1.2 % SDS in ddH_2O 5 µl Proteinase K (20mg/ml) *added before use for each 200 ul of Lysis buffer*

2.1.4 Chemicals and solutions

Chemical/Solution	**Company**
4`,6-Diamidin-2-phenylindol (DAPI)	Sigma-Aldrich, Germany
ACK LYSING BUFFER	LONZA or Gibco
Agarose	Sigma-Aldrich, Germany
Anti-mouse CTLA-4 (UC10-4F10-11)	BioXCell
Anti-mouse PD-1 (RMP1-14)	BioXCell
Bovine Serum Albumin (BSA)	Sigma-Aldrich, Germany
Cell-ID™ Intercalator-Ir	Standard BioTools
Cisplatin	Accord
DMSO	ITW
DNase I	Roche, Germany
D-PBS, Dulbecco's Phosphate Buffered Saline	Life Technologies
Eosin	AppliChem, Germany
Ethanol	Roth, Germany
Etoposide	Hexal
Hematoxylin	Merck, Germany
GelRed nucleic acid gel stain 10 000x in water	Sigma
GeneRuler 100bp Plus	Thermo Fisher Scientific
Image-iT™ Fixative Solution	Thermo Fisher Scientific
Intercalator-Ir	Standard BioTools
Isoflurane	Piramal, USA
Isopentane (2-methylbutane)	VWR
Isopropanol	Roth, Germany
Ketavet (ketamine hydrochloride)	Zoetis

Liberase	Sigma-Aldrich
Methanol	Roth, Germany
Mowiol	Merck, Germany
Normal donkey serum (NDS)	Sigma-Aldrich, Germany
Normal goat serum (NGS)	Sigma-Aldrich, Germany
OneTaq Quick-Load 2X Master Mix (NEB)	New England Biolabs
Palbociclib	LC Laboratories
Paraformaldehyde (PFA)	Merck, Germany
Phosphate buffered saline (PBS)	Merck, Germany
Proteinase K	Sigma-Aldrich, Germany
RNase A	Thermo Fisher Scientific
Rompun (xylazine)	Bayer Animal Health
SDS	Carl Roth
Sucrose	VWR
Tissue-Tek O.C.T. compound	Sakura
Trypan Blue	Sigma
Tween-20	AppliChem, Germany
Xylol	Roth, Germany

2.1.5 Flow cytometry murine antibodies

Target	Clone	Fluorophore	Company
CD11b	M1/70	FITC	Biolegend
CD11c	N418	BV605	Biolegend
CD19	6D5	BV510	Biolegend
CD3	17A2	Alexa700	Biolegend
CD4	GK1.5	FITC	Biolegend
CD45	30-F11	PerCP-Cy5.5	Biolegend
CD8	53-6.7	BV510	Biolegend
CTLA-4 (CD152)	UC10-4B9	APC	Biolegend
F4/80	BM8	APC	Biolegend
FoxP3	150D	PE	Biolegend
Ki-67	11F6	BV421	Biolegend
Lag-3 (CD223)	C9B7W	BV650	Biolegend
Ly-6C	HK1.4	PE/Dazzle594	Biolegend
Ly-6G	1A8	BV421	Biolegend
MHC-I	AF6-88.5.5.3	PE/Cyanine7	Thermo Fisher Scientific
Nkp46 (CD335)	29A1.4	PE/Cyanine5	Biolegend
OX-40 (CD134)	OX-86	PE	Biolegend
PD-1 (CD279)	RMP1-30	PE/Dazzle594	Biolegend
PD-L1 (CD274)	10F.9G2	PE/Dazzle594	Biolegend
PD-L2 (CD273)	TY25	PE	Biolegend
Tim-3 (CD366)	RMT3-23	BV605	Biolegend
Zombie violet		BV421	Biolegend

2.1.6 Imaging mass cytometry murine antibodies

Metal	Target	Clone	Source
141Pr	α-SMA	1A4	Standard Bio Tools
142Nd	CD11c	N418	Standard Bio Tools
143Nd	MHC-II	M5/114.15.2	Biolegend
144Nd	MHC-I	28148	Standard Bio Tools
145Nd	CD56/NCAM	123C3	Thermo Fischer Scientific
146Nd	MASH1/ASCL1	24B72D11	Thermo Fischer Scientific
147Sm	CD45	30F11	Standard Bio Tools
148Nd	CD11b/Mac-1	M1/70	Standard Bio Tools
149Sm	CD31	390	Biolegend
150Nd	CD44	IM7	Standard Bio Tools
151Eu	Ly-6G	1A8	Standard Bio Tools
152Sm	CD73	TY/11.8	Biolegend
153Eu	CD274/PD-L1	10F.9G2	Standard Bio Tools
154Sm	CD152/CTLA-4	UC104B9	Standard Bio Tools
155Gd	FasL	MFL3	Biolegend
156Gd	PD-L2	polyclonal	R&D Systems
158Gd	Foxp3	FJK16s	Standard Bio Tools
159Tb	F4/80	BM8	Standard Bio Tools
160Gd	IFNy	EPR21704	Abcam
161Dy	TIM-3	RMT3-23	Biolegend
162Dy	Ly-6C	HK1.4	Standard Bio Tools
163Dy	TCRgd	GL3	BD Biosciences
164Dy	CD134/OX40	OX-86	Thermo Fischer Scientific
165Ho	PD-1	polyclonal	R&D Systems
166Er	CD19	6D5	Standard Bio Tools
167Er	Nk1.1	PK136	Biolegend
168Er	CD8	53-6.7	Biolegend
169Tm	CD206/MMR	C068C2	Standard Bio Tools
170Er	Hif-1a	polyclonal	Novus
171Yb	CD4	RM4-5	Biolegend
172Yb	Cleaved caspase 3	5A1E	standard Bio Tools
173Yb	Ki-67	16A8	Biolegend
174Yb	Lag-3	C9B7W	Standard Bio Tools
175Lu	Perforin	CB5.4	Novus
176Yb	Granzyme B	polyclonal	R&D Systems

2.1.7 Kits

Product	Company
DNeasy blood & tissue kit	Qiagen
MaxPar antibody labeling kits	Standard Biotools
OneTaq Quick-Load 2X Master Mix	NEB
True Nuclear Transcription Factor Buffer Set	Biolegend

2.1.8 Softwares

BWA (v0.7.17)
Cytexpert
Fiji Image J
GATK (v4.2.1.0)
Graph Pad Prism 10
IGV (Integrative Genomics Viewer)
Illustrator
Horos
MCD viewer
Microsoft Office
NetMHCpan (v4.1)
Picard (v2.26)
Python (v3.x)
samtools (v1.13)
SigProfilerAssignment (v0.0.24)
VEP (v104)

2.2 Experimental mice

2.2.1 Animal ethical compliance

All animal experiments in this study were conducted under license number 81-02.04.2019-A491 and were approved by the local Ethics Committee of Animal Experiments authorities (LANUV, North-Rhine-Westphalia, Germany). The care and housing of mice were carried out in accordance with FELASA recommendations and the guidelines from the European Union and Germany (Ibruli et al. 2024).

2.2.2 Mouse models

This study was performed with genetically engineered mice carrying *Rb1*$^{fl/fl}$, in which sections of exons 18 and 19 are flanked by *loxP* sites, and *Trp53*$^{fl/fl}$, in which sections of exons 2 to 10 are flanked by *loxP* sites. This model, named the RP model, is the standard preclinical platform used for replicating the key features of SCLC (Meuwissen et al., 2003).

To generate an MMR-deficient SCLC mouse model, a conditional *Msh2* gene was introduced in the RP background, resulting in the RPM model (Ibruli et al. 2024). For this, the RP mice were crossed with *Msh2*$^{LoxP/LoxP}$ mice, which carry an *Msh2* genomic fragment with a flanked exon 12 and were developed to study *Msh2*-deficient intestinal cancer (Kucherlapati et al. 2010). Both RP and *Msh2*$^{LoxP/LoxP}$ mice were of a C57BL/6 background, and all animals were backcrossed to this background for at least six generations to ensure genetic consistency. Following successful breeding, the mice were intercrossed to obtain the *Rb1*$^{fl/fl}$;*Trp53*$^{fl/fl}$;*Msh2*$^{fl/fl}$ genetic background.

Mice were bred and housed in groups of five animals per cage in individually ventilated cages (IVC) under a controlled environment with a 12-hour light/dark cycle, 20-22°C room temperature (RT), and standard humidity conditions. Standard pellet food and water were available *ad libitum,* and the animals were monitored daily for well-being and general health.

2.2.3 Genotyping

To confirm the deletion of floxed genes in RPM and RP mice, ear biopsies were collected three weeks after birth and stored at -20°C until DNA extraction. The biopsies were subjected to overnight digestion in 200 µl SDS-Lysis buffer supplemented with Proteinase K (0.5 mg/ml) at 55°C with constant agitation at 800 rpm. After centrifugation at maximum speed for 15 minutes, the resulting supernatant (approximately 200 µl) was carefully collected and transferred to a new Eppendorf tube. Genomic DNA was then precipitated by thoroughly mixing samples with 200 µl of 100% isopropanol, followed by centrifugation at maximum speed for 1 minute at RT, and washing the pellet with 600 µl of 70% ethanol, with subsequent centrifugation at maximum speed for 1 minute at RT. The supernatant was discarded, and the genomic DNA precipitate was allowed to dry at 27°C for approximately 30 minutes. The dried precipitates were then resuspended in 60 µl of ddH_2O, and the DNA content was measured using a NanoDrop. The samples were then stored at 4°C until polymerase chain reaction (PCR) analysis. Genotyping PCR assays for *Rb1, Trp53*, and *Msh2* were performed using standard forward and reverse primers (from Sigma) to obtain PCR products of different sizes **(Table 2.1)**.

Table 2.1 List of primers for genotyping PCR.

Gene	Primer	Sequence	Amplicon (bp)
Rb1	Forward 1	5'-ACT CAT GGA CTA GGT TAA GT-3'	201 (flox) 163 (wt)
	Forward 2	5'-GAA GCC ATT GAA ATC TAC CTC CCT TGC CCT GT-3'	
	Reverse 1	5'-TGC CAT CAA TGC CCG GTT TAA CCC CTG T-3'	
	Reverse 2	5'-AGC ATT TTA TAT GCA TTT AAT TGT C-3'	
Trp53	Forward	5'-CAC AAA AAC AGG TTA AAC CCA G-3'	370 (flox) 288 (wt)
	Reverse	5'-AGC ACA TAG GAG GCA GAG AC-3'	
Msh2	Forward	5'-AAC CAG AGC CTC AAC TAG C-3'	340 (flox) 210 (wt)
	Reverse	5'-TAC TGA TGC GGG TTG AAG G-3'	

PCR reactions were performed with OneTaq Quick-Load 2X Master Mix (NEB) according to the manufacturers' recommendations as in **Table 2.2**.

Table 2.2 List of components for genotyping PCR mix.

Component	**25 µl reaction**
10 µM Forward Primer	0.5 µl
10 µM Reverse Primer	0.5 µl
Template DNA	1 µl
One*Taq* Quick-Load 2x Master Mix	12.5 µl
Nuclease-free water	to 25 µl

The thermal cycles shown in **Table 2.3** were used to amplify specific DNA fragments. Samples and a low-range DNA ladder were loaded onto a 1.5% Agarose gel supplemented with GelRed nucleic acid gel stain in a 1:10.000 dilution. Samples were run in 1x TAE Buffer at 100-120 V for about 30 minutes for optimal separation of DNA fragments of interest.

Table 2.3 Genotyping PCR thermal cycles.

Step	**Temperature/Time**		
	Rb1	***Trp53***	***Msh2***
1. Initial denaturation	94°C/ 2 min	94°C/ 2 min	94°C/ 2 min
2. Cyclic denaturation	94°C/ 20 sec	94°C/ 30 sec	94°C/ 1 min
3. Cyclic extension	72°C/ 20 sec		
4. Cyclic denaturation	94°C/ 20 sec		
5. Cyclic annealing	57°C/ 30 sec	60.5°C/ 30 sec	59°C/ 45 sec
6. Cyclic extension	72°C/ 1 min	72°C/ 30 sec	72°C/ 20 sec
7. Final extension		72°C/ 2 min	72°C/ 2 min
Number of cycles	15 (step 2-3), 25 (step 5-6)	40	35

2.2.4 Tumor induction

To initiate lung tumor formation, mice aged between eight and twelve weeks were exposed to an adenovirus. The animals were first anesthetized through intraperitoneal injection of Ketavet (ketamine hydrochloride) (100 mg/kg) and Rompun (xylazine) (20 mg/kg). Anesthesia success was confirmed by pinching the toes of the animals and observing no response. Subsequently, the mice received an intratracheal instillation of replication-deficient adenovirus expressing Cre-recombinase (Ad5-CMV-Cre, 2.5 x 107 PFU). The intratracheal administration was conducted using Introcan safety-W 24G catheters (Braun) to ensure precise delivery of viral particles in the lungs. Mice were carefully positioned in a vertical plane for better exposure to the airways. The upper teeth were fixed, and the tongue was gently placed to the side. An external light source was directed at the throat to assist visualization of the airway and facilitate catheter insertion. Special care was taken to avoid damage to the trachea during the procedure. After inhalation, the animals were kept on a heating pad for observation until they became conscious again. They were monitored for 48 hours for signs of complications or distress, such as difficulty breathing. Viral vectors were provided by the Viral Vector Core at the University of Iowa (http://www.medicine.uiowa.edu/vectorcore).

2.2.5 MRI scans and tumor volume estimation

Five months after tumor induction, the progression of lung lesions was assessed bi-weekly using magnetic resonance imaging (MRI). Imaging was performed using an Achieva 3.0T clinical MRI system (Philips Healthcare, Best, the Netherlands) equipped with a mouse solenoid coil (Philips Healthcare, Hamburg, Germany). Prior to imaging, animals were anesthetized using 2,5% isoflurane (Piramal Critical Care, #30372.00.00) for 5 to 10 minutes. The mice were then placed inside the imaging coil. Axial T2-weighted MRI images were generated with a turbo-spin echo (TSE) sequence (with the following parameters: repetition time [TR] = 3819 ms, echo time [TE] = 60 ms, field of view [FOV] = 40 × 40 × 20 mm^3, voxel resolution = 0.13 × 0.13 × 1.0 mm^3, and a number of averages =1. The images were exported as DICOM files and analyzed to identify and measure regions of interest (ROIs) using Horos™ software (Horos Project, New York, USA).

Tumors were segmented manually in sequential scans to ensure an accurate definition of the tumor borders. The tumor volume was computed by integrating the segmented areas of all slices. Tumor volume progression was displayed as a fold change to correct for tumor size variance at the start of the experiment.

2.2.6 Histology

To confirm typical SCLC histological features of RPM tumors, paraffin-embedded tumor tissue sections were generated. Tumor-bearing lungs were harvested, and tumors were further dissected, ensuring that adjacent normal lung tissue in the surroundings was intact. The tumor samples were fixed in 4% PFA/PBS overnight at 4ºC. Afterward, the tissues were placed in a tissue processor and dehydrated overnight. The following day, tissues were embedded in paraffin and stored at room temperature until further processing. Five-micron tissue slices were collected using a microtome at room temperature. Tissue slices were deparaffinized following the protocol in **Table 2.4**.

Table 2.4 Deparaffinization of paraffin sections steps.

Reagent	Incubation time
Xylol	10 minutes
100% EtOH	5 minutes (x2)
90% EtOH	3 minutes
70% EtOH	3 minutes
50% EtOH and dH_2O	1 minute

In sequence, Hematoxylin-Eosin (H&E) staining was conducted according to the protocol depicted in **Table 2.5**. Imaging of H&E stained tissue sections was performed with an Olympus bright field BX53 microscope with 4x and 40x air objectives.

Table 2.5 Hematoxylin & Eosin staining.

Reagent	Incubation time
Hematoxylin	3 minutes
ddH_2O	1 minute

37% HCl	1 minute
Tap water	5 minutes
Eosin	1 minute
70% - 90% - 100% EtOH	1 minute each dilution
100% Isopropanol	2 minutes (x2)
Xylol	2 minutes (x2)

2.3 Whole exome sequencing and genomic analysis

2.3.1 Sample preparation

For WES analysis, tumor specimens were collected from tumor-bearing RP and RPM animals. Tumor progression in mice was tracked via bi-weekly MRI, and animals were euthanized when sufficient tumor burden was reached. Following euthanasia, mice were perfused with 10 ml of sterile PBS to remove excess erythrocytes from the lungs, which could interfere with the quality of the analysis results. The lungs were then excised under sterile conditions. Tumors were immediately dissected and separated from normal lung tissue, taking care that no lung tissue contaminated the tumor specimen. Dissected tumor tissues were rapidly snap-frozen in liquid nitrogen to preserve DNA and RNA and stored at -80°C.

To proceed with DNA extraction, frozen tumor samples were allowed to thaw on ice. DNA extraction was performed using the DNeasy blood & tissue kit (Qiagen), following manufacturer´s instructions. Approximately 25 mg of tissue was finely minced using sterile scalpels and transferred to a 1.5 mL microcentrifuge tube pre-filled with 590 µl cell lysis solution and 10 µl Proteinase K. The samples were incubated at 55°C overnight in a thermoshaker to ensure complete tissue lysis. The lysed samples were allowed to cool at room temperature before further processing. RNA was removed by adding 3 µl of RNAse A solution, followed by inverting the tubes approximately 15 times for thorough mixing. The samples were then incubated at 37°C for 30 min in a thermoshaker. Protein precipitation was performed by adding 200 µl of Protein Precipitation Solution and vortexing at high speed for 20 seconds. The samples were placed in the freezer for 8 minutes and then centrifuged at 13,000 rpm for 3 minutes. The process was repeated in case a protein pellet did not form. The supernatant was

carefully collected and transferred to new tubes and mixed with 600 µl isopropanol. The tubes were inverted several times to mix, allowing DNA to precipitate, and centrifuged at 13,000 rpm for 1 minute. The DNA pellet was washed with 300 µl of 70% ethanol. The DNA pellets were dried by placing the tubes with their lids open at 45°C for a few minutes, taking care that the pellet does not over dry. Finally, the DNA pellets were rehydrated by adding 25-60 µL DNA Hydration Solution, depending on the size of the pellet. The tubes were incubated at 65°C for an hour, followed by overnight incubation at room temperature to ensure complete hydration.

The concentration and purity of the extracted DNA were assessed using a NanoDrop spectrophotometer. Only samples with high purity (A260/A280 ratio between 1.8-2.0) and sufficient concentration were submitted to sequencing for library preparation. Sequencing was performed in cooperation with the Cologne Center for Genomics (CCG) NGS platform (Cologne).

2.3.2 Sequencing data processing

The extracted DNA from RP and RPM tumor samples were subjected to WES to analyze the genomic landscape and determine the mutational load. Sequencing libraries were obtained using standard protocols optimized for exome regions, and sequencing was conducted on an Illumina platform to generate paired-end reads. First, the sequencing reads were mapped to the Ensembl GRCm39 mouse reference genome utilizing Burrows-Wheeler Aligner (BWA) (version 0.7.17), which is a well-established alignment tool (Li and Durbin 2009). To avoid potential biases during variant calling, PCR duplicates were detected and removed with PICARD (v2.26) and samtools (v1.13). Detection of somatic variants was performed with Mutect2, a component of the Genome Analysis Toolkit (GATK v4.2.1.0) used to detect tumor-specific mutations (McKenna et al. 2010). During this process, a panel of normals was generated using 14 healthy control samples to identify and filter out germline variants and technical artifacts (Depristo et al. 2011). Following variant calling, the list of detected variants was refined using some filtering criteria. Several variants were excluded from the analysis, such as those in more than one sample or in public databases like the database of single nucleotide polymorphisms (dbSNP). In addition, to ensure the accuracy of variant calling, loci with a coverage depth of less

than 30 reads were removed. The resulting list of variants was further improved by applying the GATK FilterMutectCalls tool but without the filter for slippage to allow for the selection of variants with minor allele frequency shifts.

2.3.3 Estimation of *Msh2* recombination efficiency

The *Msh2* recombination has a crucial influence on the degree of MMR deficiency, TMB, and tumorigenesis in the RPM mouse model. Thus, we estimated the *Msh2* recombination efficiency in the WES data generated. For this, the read counts for every exon within the *Msh2* gene were calculated using the GATK CollectReadCounts tool (McKenna et al. 2010). This analysis focused on the exons included in the GENCODE vM27 reference, a comprehensive mouse gene reference database (Frankish et al. 2021). Furthermore, we particularly focused on the floxed *Msh2* exon 12, which is the exon targeted and deleted by our Cre recombinase system. The read counts of exon 12 were first normalized to the counts of the other *Msh2* exons in each sample to control for variations in sequencing depth across different exons and ensure that our data reflected a true recombination event as opposed to technical noise. Subsequently, exon 12 read counts were normalized to the read counts of RP control mice. RP mice were used as the control group because they do not have a floxed *Msh2* allele and recombination does not occur, exhibiting the copy number of 2 of exon 12. A complete reduction of the copy number in the RPM mice indicated successful recombination of the floxed *Msh2* exon 12.

For visualization, the single-base coverage of *Msh2* was obtained via GATK pileup v4.2.10 and visualized as a detailed view of the sequencing coverage across the whole *Msh2* gene, enabling the detection of regions with reduced coverage where the exon was deleted (McKenna et al. 2010). To assess the coverage profile of exon 12 when recombination was not present, data from RP mice was utilized. The coverage of every base in exon 12 was divided by the median coverage of bases from other exons. This ratio was subsequently adjusted for each sample by multiplying it with the median coverage of non-floxed exons within that sample.

2.3.4 TMB estimation and mutation type analysis

To estimate the mutational load in every tumor sample, TMB was determined by counting the number of mutations per million bases within a coverage of at least 30x. Somatic variants were annotated and classified by type using the Ensembl Variant Effect Predictor (VEP, v104) against the GRCm39 mouse genome (McLaren et al. 2016). To study the mutation types associated with *Msh2* loss, the filtered variants were grouped into categories, such as frameshift deletions, insertions, substitutions, intronic, intergenic, splice site, and regulatory mutations. The relative abundance of each of these mutation types in RPM *Msh2*$^{fl/fl}$ was calculated and compared to RP and RPM *Msh2*$^{fl/wt}$ samples. Fold-change values were visualized using heatmaps via GraphPad Prism. Group-wise comparisons were performed via the Kruskal-Wallis test.

2.3.5 Mutational signature analysis

To assess the mutational processes driving tumorigenesis in the RPM mouse system, we conducted a mutational signature analysis using the WES data. First, an in-house Python script and the Mus_musculus.GRCm39 reference genome were used to identify SNVs and their surrounding nucleotides (triplets or trinucleotides). The SNVs were then assigned to known mutational signatures using SigProfilerAssignment (v0.0.24) and the catalog of somatic mutations in cancer (COSMIC)_v3 reference panel, a collection of mutational signatures from various cancer types (Alexandrov et al. 2020). This allowed for the separation of mutational profiles into contributions from different signatures and quantification of their activity levels. All mutational signatures displaying activities above zero were included in the analysis. Given that the main focus of this study is to evaluate MMRd, the single base substitution (SBS) signatures SBS15 and SBS21 were considered.

2.3.6 Neoantigen prediction and HLA-I binding

To investigate the potential immunogenicity of the mutations present in the tumors of RPM mice, we conducted a comprehensive neoantigen prediction and human leukocyte antigen class I (HLA-I) binding analysis. For this, we predicted potential neoantigens, which are mutant peptides that could be recognized by the immune system when presented by MHC class I molecules, including HLA-I. An in-house

bioinformatics pipeline was used to generate a library of mutant coding regions from the WES data. This pipeline allows for the detection of different mutation types, such as missense, in-frame, and frameshift alterations. The mutant sequences in the missense and in-frame mutations were excised in such a way that the mutation was positioned in the center and was flanked by 13 base pairs on both the 3` and 5` ends. On the other hand, the mutant sequences in the frameshift mutations were trimmed only at the 3` end to maintain the novel peptide sequences by protecting the complete frameshift in the 5´ end. By applying this trimming approach, all possible HLA-I binders of 8 to 14 amino acids (8mers-14mers) could be identified, which represent the typical size needed to bind to the HLA-I molecules.

After obtaining trimmed peptide sequences, they were analyzed using the immune epitope database (IEDB) resource, which uses the NetMHCpan (ver. 4.1) tool to predict peptide-MHC interactions (Reynisson et al. 2021). For this study, predictions were focused on the murine H2kb allele, the most common MHC-I allele in mice. Furthermore, for simplicity, the analysis was narrowed down to 9mers, the most common binder size that generates the strongest binding affinities.

The predicted HLA-I binders were categorized based on their binding affinities and presented as a percentage rank relative to the reference dataset. Only candidates with a binding rank less than 2% were further analyzed and divided into strong binders (rank less than 0.5%) and weak binders (rank between 0.5% and 2%).

2.4 Immunoprofiling via flow cytometry

Flow cytometry was used to characterize the immune composition of the RPM TME and compare it to the RP. Flow cytometry examines the physical and chemical properties of individual cells in a single-cell suspension. It utilizes laser beams to detect antibodies previously conjugated with specific fluorescent dyes that bind to the surface or intracellular antigens. To prepare the cells for analysis, we initially disrupted micro-dissected tumors by mincing with scissors, followed by enzymatic digestion with 0.2 mg/ml Liberase^{TM} supplemented with 0.1 mg/ml DNAse I at 37°C for 1 hour with constant agitation. The digested tissues were filtered through a 40 µm cell strainer to remove debris and clumps, and the harvested cells were washed and resuspended in

a flow cytometry buffer. To identify viable cells and exclude dead cells from the analysis, Zombie Violet™ viability dye (1:500, Biolegend) was used. Subsequently, surface staining was performed with antibodies targeting membrane markers at a 1:200 dilution and incubating for 20 minutes at 4°C in the dark **(section 2.1.5)**. Intracellular staining was carried out using the True Nuclear Transcription Factor Buffer Set (Biolegend). After fixing the cells in True Nuclear Fix Buffer overnight at 4°C in the dark, they were washed with 1x Perm Buffer and stained intracellularly with antibodies (1:50 dilution in 1x Perm Buffer) for 45 minutes at RT. We measured protein expression using CytoFLEX S (Beckman Coulter) and processed the data using CytExpert software (Version 2.3, Beckman Coulter).

2.5 Preclinical treatment regimens

To assess the effect of various treatment strategies in the MMR-deficient RPM model, we implemented a structured preclinical therapy design. After verifying tumor appearance via MRI and confirming that the tumor volumes fell within a range of 5-20 mm^3, different therapy regimens were designed, and RPM and RP mice were randomly included.

2.5.1 First-line therapeutic regimens

To reflect the first-line treatments used in the clinical management of SCLC, we treated RPM and RP mice with either platinum-based chemotherapy or ICI, as well as a combination of both. Compound solutions were administered as follows:

Chemotherapy: Etoposide (Hexal), a topoisomerase II inhibitor, was administered intraperitoneally (i.p.) at a dose of 8 mg/kg and injected on days 1, 2, and 3 of a 14-day cycle. Cisplatin (Accord), a platinum-based chemotherapeutic agent that leads to apoptosis of fast-dividing cells (Florea and Büsselberg 2011), was administered i.p. at 4 mg/kg on day 1 of a 14-day cycle.

Immunotherapy: The anti-PD-1 antibody RMP1-14 (BioXCell) was selected for its role in inhibiting the PD-1/PD-L1 immune checkpoint pathway, which is known to be upregulated in SCLC (Lin et al. 2024). Every mouse received 200 mg of antibody, i.p. To evaluate the role of dosing frequency in survival outcomes, two dosing schedules

were applied: twice a week for three weeks and three times per week until study endpoints were reached, such as significant tumor reduction or pronounced disease progression.

For control purposes, phosphate-buffered saline (PBS) was used for comparison, ensuring that any survival outcome differences were attributed to the active compounds only.

2.5.2 Treg suppression treatment

In addition to the standard first-line therapy regimens, we included two additional mouse cohorts treated with a Treg-suppressing agent as a monotherapy or in combination with chemotherapy and anti-PD-1 antibody. Treg suppression was considered in this study based on the emerging evidence of the therapeutic benefits it has shown across various tumor entities, including SCLC, with clinical trials currently ongoing (Daniel et al. 2021).

2.5.2.1 Determination of a Treg suppression agent

First, to identify an agent that suppresses Tregs *in vivo* in our setting, we treated RPM mice with either 200 mg of anti-CTLA-4 antibody, i.p., or palbociclib (a cyclin-dependent kinase 4 and 6, CDK4/6 inhibitor) at a concentration of 100mg/kg via oral gavage. The mice were sacrificed two days after the last dose and the spleens were collected and further processed to isolate single cells, as in section 2.4. The isolated single cells were stained with CD45, CD3, CD4, and Foxp3 antibodies for one hour at 4°C. Cells were counted via Cytoflex S (Beckman coulter) and Treg subsets were defined via sequential gating and adequate channel compensation.

2.5.2.2 Treatment with CDK4/6 inhibition

After determining that palbociclib successfully suppresses Tregs in RPM mouse spleens, tumor-bearing animals were treated with either palbociclib alone or in combination with chemotherapy and ICI. Palbociclib was administered via oral gavage on days 1-7 of a 14-day cycle. It was dissolved in DMSO for aliquoting and long-term storage at -80ºC and further diluted in PBS for injection at a concentration of 100 mg/kg.

2.5.3 Treatment monitoring and criteria

Following tumor initiation, the mice were monitored via MRI imaging for tumor formation. After confirming the tumor appearance and determining a minimum volume of 5 mm^3, the mice were randomly allocated to therapy regimens. Throughout the treatment duration, mice were closely inspected for signs of drug toxicity, administration complications, and general health. Monitoring included daily assessments of physical appearance, body weight, and any breathing difficulties. In addition, tumor progression was tracked via bi-weekly MRI imaging.

2.5.4 Survival analysis and termination criteria

To determine the efficacy of therapeutic agents in the lifespan or remission of tumors, we assessed the OS of the RPM mice and compared that to RP mice. Survival analysis included only those animals that died as a result of the disease or that reached the predefined endpoints, such as weight loss exceeding 20% of initial body weight, severe tumor ulceration, or breathing difficulties. Animals that were terminated for other reasons, such as pronounced weight loss not attributed to the disease, were excluded from the analysis.

2.6 Immune profiling via imaging mass cytometry

To assess the immune infiltration in RPM and RP tumors under different treatment cohorts, we performed imaging mass cytometry (IMC) analysis, including mice from all treatment groups. IMC is used for multiplex spatial analysis of tissue sections as it detects up to 40 metal-labeled antibodies simultaneously, allowing for immune cell profiling in the tumor microenvironment (Giesen et al. 2014).

2.6.1 Tumor collection and preservation

Tumor-bearing lungs were harvested, and tumors were further dissected, ensuring that adjacent normal lung tissue in the surroundings was intact. Dissected tumors were immersed in 20% ice-cold sucrose for 30 minutes to prevent tissue damage during subsequent freezing steps. The tumors were then embedded in Tissue-Tek O.C.T. Compound (Sakura) and frozen in an isopentane liquid nitrogen bath to preserve cellular and structural integrity. The resulting frozen blocks were stored at -80ºC until further processing.

2.6.2 Tissue microarray construction

After collecting all tumor samples, a tissue microarray (TMA) was established to facilitate high-throughput analysis. From every treatment group, tumors from 10 mice per genotype (RPM and RP) were selected, and one tumor per mouse was used in the TMA. To generate the TMA frozen block, the Tissue-Tek O.C.T compound was added to a plastic mold, removing any bubbles that might form, and allowed to freeze at -25ºC for approximately one hour. Once the block had solidified, the plastic mold was removed, revealing the tissue cores. The frozen tumor blocks were processed inside a cryostat at -25ºC. Using single-use 1.5 mm biopsy punches, tissue cores were collected from within the tumor tissue and from the tumor-normal lung interface, enabling the representation of both the central and peripheral tumor areas. These cores were then immediately loaded into a frozen TMA block. Once all cores of the TMA block had been filled with tissue, 5 µm sections were sliced and mounted onto microscope slides for staining.

2.6.3 IMC antibody panel development and validation

For IMC staining and analysis, we established a 30-marker antibody panel **(section 2.1.6)**. This panel includes markers for major immune cell types (pan-leukocytes, T cells, B cells, macrophages, dendritic cells, and Tregs), SCLC tumor cells, and stroma compartments (endothelial cells and fibroblasts). In addition, functional markers were incorporated to assess the functional state of cells, such as activation or exhaustion status, cell death, or proliferation. Each antibody was either pre-conjugated with metal isotopes or conjugated in-house using MaxPar antibody labeling kits (Standard Biotools) following the manufacturer's instructions. We carefully selected metal isotopes to avoid spectral overlaps and improve the signal of weak antibodies. We validated the sensitivity and specificity of all antibodies by staining murine spleen tissue as control tissue.

2.6.4 IMC staining procedure

TMA blocks were cut into 5 µm thick sections using a cryostat and mounted onto SuperFrost Plus™ Adhesion slides (Thermo Fisher Scientific). The slides were stored at -80°C for up to two weeks until staining. Longer storage was not applied to ensure optimal staining quality. The staining procedure began by thawing the slides for

30 minutes at RT, followed by a 10-minute fixation with Image-iT™ Fixative Solution (Thermo Fisher Scientific) to preserve tissue morphology and antigen sites. After fixation, the slides underwent a series of washes in D-PBS and D-PBS/0.05% Tween-20 to remove residual fixatives and prepare the tissues for blocking. To minimize nonspecific binding, the tissue sections were blocked for one hour with Superblock blocking buffer in D-PBS at room temperature. Primary antibody staining was performed overnight at 4°C in a mix of D-PBS/0.05% Tween-20/1% BSA, which helped maintain tissue integrity while ensuring effective antibody penetration. The following morning, the slides were washed twice in D-PBS/0.05% Tween-20, and nuclear staining was performed using a mixture of Cell-ID™ Intercalator-Ir (Standard BioTools) containing iridium at 1:200 and 4`,6-Diamidin-2-phenylindol (DAPI) 1:5000 in D-PBS for 30 minutes in RT. The Iridium and DAPI stains were utilized to allow dual imaging of the slides in the Hyperion system (IMC) and confocal microscope, respectively. After staining, the slides were rinsed in D-PBS and MilliQ water and then air-dried before IMC analysis.

2.6.5 Confocal microscopy for DAPI imaging

Prior to IMC analysis, to facilitate nuclear segmentation of the IMC images, we acquired DAPI images of all tissues using a confocal laser scanning microscope (Stellaris 5, Leica Microsystems). This step was added to achieve a more accurate nuclear segmentation since SCLC tissue is densely packed with tumor cells, and a clear distinction of individual cells is challenging. The Stellaris 5 microscope has an advanced super-resolution mode and can capture images at a resolution of 120 nm, much higher than the resolution of approximately 1 µm of the Hyperion Imaging system used for IMC.

First, we acquired a panoramic image of the whole TMA slice with a low magnification (10x objective) to localize the cores and select ROIs. For each ROI, high-resolution images were generated with 40x magnification and an average of five focal planes per core. For visualization, DAPI images were processed using Fiji ImageJ software.

2.6.6 IMC image acquisition

For each TMA core, one ROI of approximately 500 × 500 µm (~0.25 mm²) was ablated, ensuring we obtained one ROI in the central tumor region and one in the tumor-normal

lung border for each tissue. The IMC data was analyzed using MCD viewer software (Standard Biotools) to select specific channels and generate composite images. Images were pre-processed by image filtering and spillover correction before proceeding with quantitative analysis.

2.6.7 DAPI and IMC images registration

As DAPI and IMC images were produced by different imaging instruments, a step of registration, i.e. cropping and alignment of the two images, was needed. We adopted a semi-automated method using the Fiji plugin bUnwarpJ and a custom-made Python script. With the Fiji plugin bUnwarpJ, we visually compared the DAPI image with the IMC DNA image and marked on both images corresponding landmark points. Around 5 to 10 landmark points were marked for each pair of images and then used by the Python script to compute the best matching affine transform to align the two images. We used linalg.lstsq from the numpy package, returning the least square solution from the linear matrix equation. While the IMC image is left untouched, the cropped and registered DAPI image is saved as a tiff file for further use.

2.6.8 DAPI and single-cell segmentation

Since DAPI images are of higher resolution than IMC images, they were used as input to the pretrained segmentation deep learning network "Mesmer" (https://github.com/vanvalenlab/deepcell-tf/tree/master/deepcell/applications). The Mesmer model outputs nuclear masks, outlining every detected nucleus as a separate object. Several tests were performed with additional channels marking cell membranes, such as NCAM, without giving satisfactory results. Upon manual inspection, even with the resolution achieved by the microscope, most tumors displayed very dense clusters of cells with frequent overlap. In these regions, even careful inspection by experts could not draw with confidence boundaries between overlapping nuclei. Hence, this segmentation was not used in the rest of the analysis because of the impossible performance validation.

2.6.9 Tumor detection

To compare the immune profile between tumor cores and the tumor-normal lung interface (referred to as the tumor border), we manually outlined the tumor boundaries for each image. This was done using the Fiji ImageJ software, based on the DNA and NCAM markers signal. For each IMC image, we created a binary mask where pixels within the tumor were assigned a value of 255, and pixels outside the tumor were assigned a value of 0. These masks were then used for downstream analysis.

2.6.10 Marker detection

As mentioned previously, a nucleus-based single-cell segmentation could not be achieved due to the high density of cells inside the SCLC tumors. To overcome this problem, we used a pixel-based approach. For this, each marker channel was binarized to detect pixels with positive signals. Subsequently, immune cell types were identified based on the co-localization of specific markers within the same pixels. Our analysis focused on key immune and stroma populations, including leukocytes, T cells, B cells, and stroma cells. Pixels positive for CD45 were classified as leukocytes, co-expression of CD45 and CD4 was defined as $CD4^+$ T cells, CD54 and CD8 identified $CD8^+$ T cells, CD45 and CD19 defined B cells, and CD31 and α-SMA were used to mark stroma cells. Therefore, without detecting the nuclear or cellular boundaries, this conservative approach ensured specificity by only counting pixels with positive signals. Following this approach, we quantified and reported the proportion of pixels corresponding to each category.

2.7 Statistical analysis

In this thesis, the data were analyzed with GraphPad Prism 10 software, using unpaired student *t*-test, Mann-Whitney test, Kruskal-Wallis test, and Log-rank (Mantel-Cox) test. The data were presented as mean ± SD and significance of *p*-values was denoted as $*p < 0.5$; $**p < 0.01$; $***p < 0.001$ and $****p < 0.0001$.

3. Results

3.1 Development of the RPM mouse model

The current preclinical models used to study SCLC are primarily based on the RP system, which involves targeted deletion of *Rb1* and *Trp53* (Meuwissen et al. 2003; Oser et al. 2024). However, these models fail to capture the genetic instability and high mutational load that is typically observed in clinical cases. Furthermore, emerging studies are shedding light on distinct mutational and transcriptomic subtypes of the disease with potentially significant impacts on survival and therapy outcomes. For instance, a large-scale gene expression analysis of clinical tumors revealed that 85% of the subjects had smoking-related mutations, 15% had MMR-related mutations, and 5% had APOBEC-associated mutations (Q. Liu et al. 2024). In addition, Rudin et al. (2019) proposed that SCLC can be categorized into four molecular subtypes characterized by the expression of *ASCL1, NEUROD1, POUF2F3*, or *YAP1.*

In this study, we aimed to model tumors with a high TMB associated with deficient MMR. We generated a novel GEMM by breeding into the conventional RP mouse a conditional *Msh2* knockout gene from the $Msh2^{LoxP/LoxP}$ mice (Kucherlapati et al. 2010), resulting in the $Rb1^{fl/fl};Trp53^{fl/fl};Msh2^{fl/fl}$ (RPM) mice **(Figure 3.1a, b)** (Ibruli et al. 2024). *Msh2* is a critical component to the maintenance of the optimal activity of MMR pathways, and its deletion leads to MSI (Dietlein, Thelen, and Reinhardt 2014; De Wind et al. 1995). An Ad-CMV-Cre virus was delivered intratracheally in the lungs to result in the simultaneous inactivation of *Rb1*, *Trp53*, and *Msh2* in pulmonary cells. Tumor manifestation was observed approximately six months post-exposure to the adenovirus **(Figure 3.1c)**.

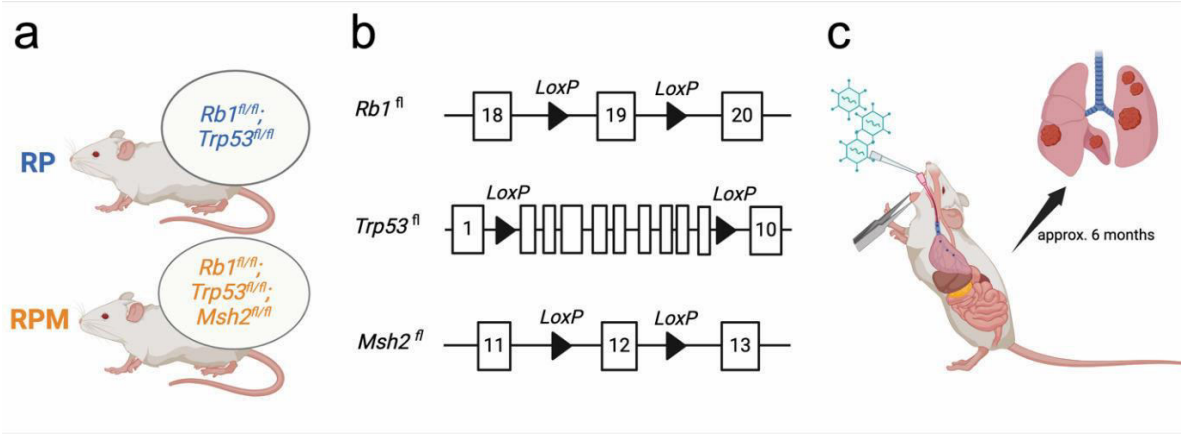

Figure 3.1 Generation of the RPM mouse model.
a) Illustration of the genetic backgrounds of RP and RPM mice. **b)** Representation of the floxed alleles *Rb1*, *Trp53*, and *Msh2*. **c)** Overview of lung tumor induction using intratracheal administration of Ad-CMV-Cre virus. Created with Biorender.com. *Figure originally created by the author and published in Ibruli et al. 2024.*

3.2 Characterization of the primary and secondary RPM lesions

To characterize the SCLC tumors in RPM animals, we aimed to validate the *Msh2* loss and assess corresponding histological features. We conducted WES analysis on micro-dissected lung lesions from mice of the RP, RPM with homozygous loss of *Msh2* (*Msh2*$^{fl/fl}$), and RPM with heterozygous loss of *Msh2* (*Msh2*$^{fl/wt}$) backgrounds. The recombination efficiency of *Msh2* was determined by generating coverage plots of the exon 12 in the *Msh2* gene. As shown in the exemplary plots in **Figure 3.2**, the analysis demonstrated successful Cre-mediated recombination of *Msh2* in RPM carrying *Msh2*$^{fl/fl}$, displayed as a complete loss of coverage in exon 12. As expected, the RPM animals with *Msh2*$^{fl/wt}$ had only a partial recombination, while no recombination was observed in RP mice.

Additionally, histological staining of RPM lesions revealed typical histopathological characteristics of human disease. The tumors displayed dense tissue with small round to fusiform cells containing granular chromatin and scant cytoplasm **(Figure 3.3a)**. These features are similarly observed in RP tumors. (Raso, Bota-Rabassedas, and Wistuba 2021). Furthermore, both models are generally not prone to metastases, but when they occur, they are primarily restricted to the liver **(Figure 3.3b)**.

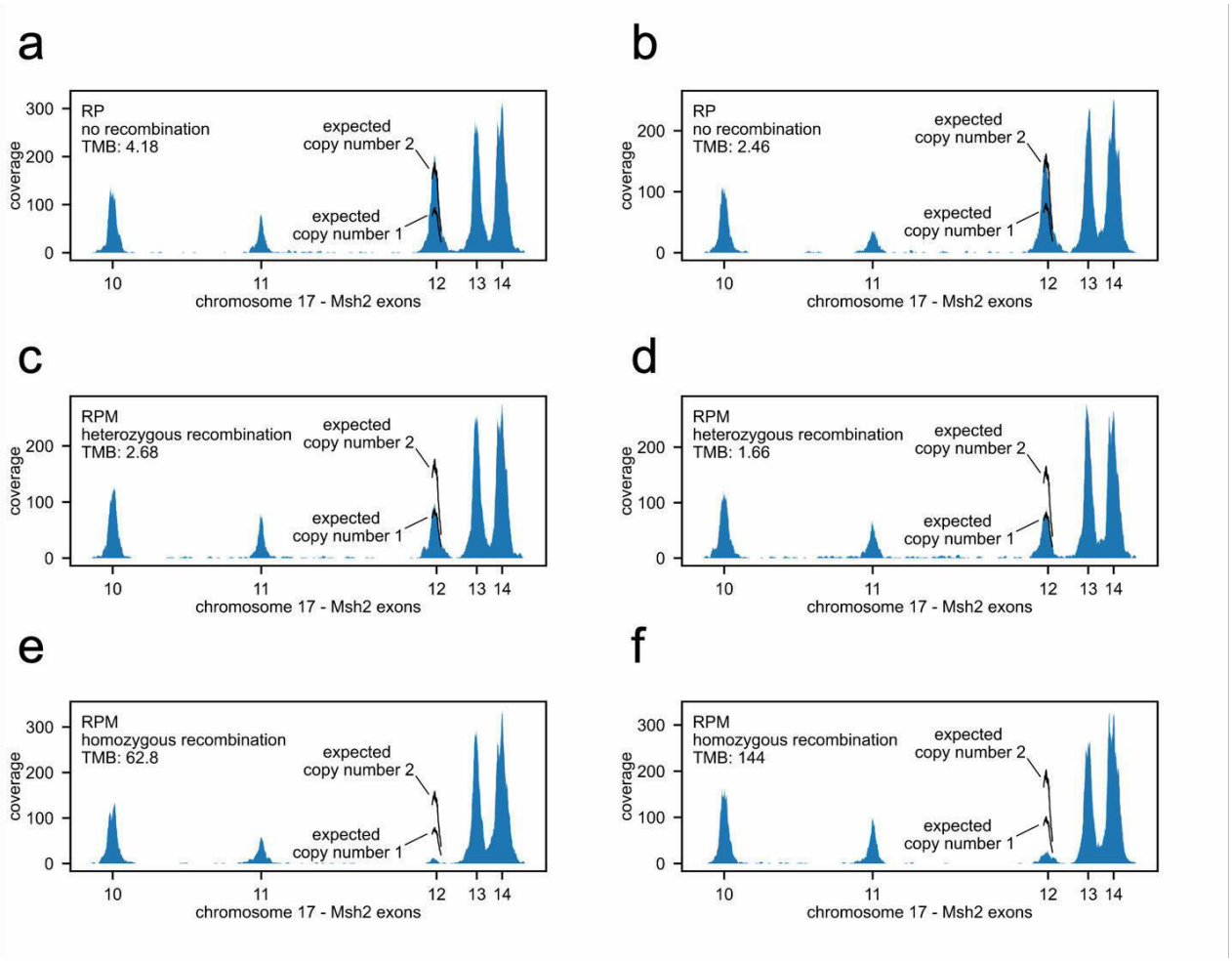

Figure 3.2 Confirmation of the *Msh2* loss in RPM tumors.
WES-based coverage profiles of tumor samples from RP and RPM genotypes. The black lines represent exon 12 coverage profile assuming no recombination (copy number = 2) or heterozygous recombination (copy number = 1). **a, b)** The coverage profile of *Msh2* exon 12 in two exemplary mice of the RP genotype fits the predicted coverage in the absence of recombination. **c, d)** The coverage profile of *Msh2* exon 12 in two mice of the RPM genotype fits the predicted coverage in the presence of heterozygous recombination. **e, f)** The coverage profile of *Msh2* exon 12 in two exemplary mice of the RPM genotype shows full recombination. Residual coverage within exon 12 is likely derived from low-level contamination from healthy lung cells. *Figure originally created by the author and published in Ibruli et al. 2024.*

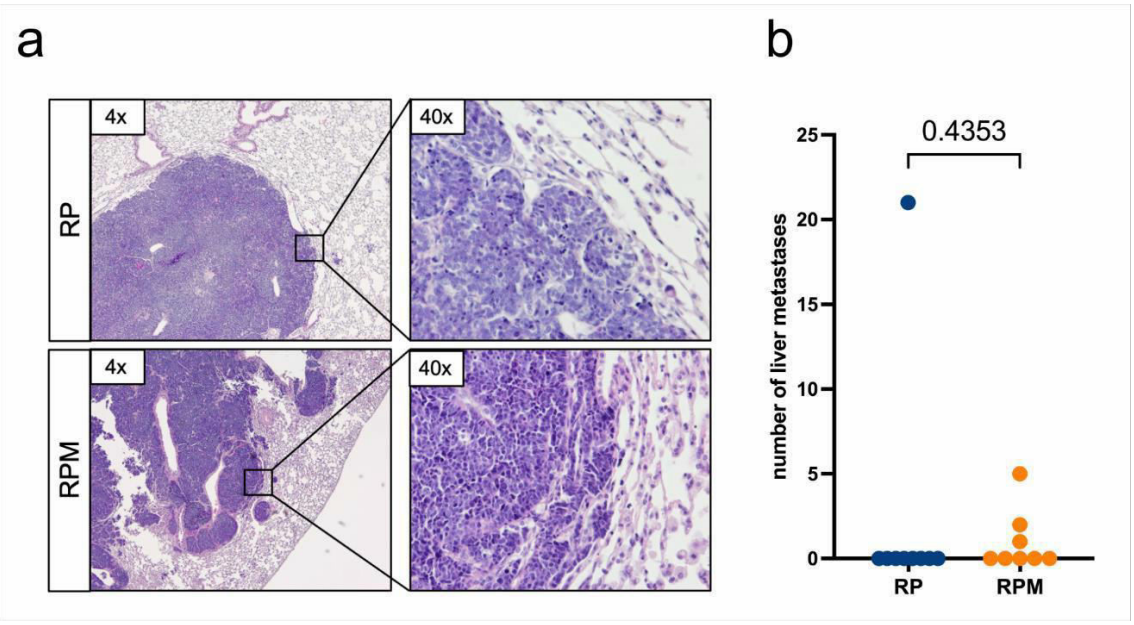

Figure 3.3 Impact of *Msh2* loss in primary and secondary tumors.
a) Histological staining of lung tumors confirms that RPM tumors, similar to RP lesions, display morphological features that are typically observed in clinical cases. Exemplary H&E staining images are obtained using 4x and 40x magnification objectives. **b)** The count of liver metastases identified post-mortem in *n*=8 RPM and *n*=9 RP mice. Statistical significance was assessed using statistical *t*-test *Figure originally created by the author and published in Ibruli et al. 2024.*

3.3 Tumor onset and development in RPM animals

RPM and RP mice were compared to assess how MMR deficiency, particularly *Msh2* loss, influences survival and tumor growth. For this, six months after the Ad-CMV-Cre administration, tumor manifestation and development were tracked bi-weekly via MRI. We observed no survival differences from birth to mortality **(Figure 3.4a)** of RPM animals (median age = 48 weeks) compared to the RP parental strain (median age = 48 weeks). However, RPM mice displayed delayed tumor onset relative to RP animals (median: 285 days vs. 258.5 days; p=0.0233) **(Figure 3.4b)**. Notably, RPM animals survived significantly less from the initial tumor detection compared to RP animals (median survival: 46.5 days vs. 55 days; p=0.018) **(Figure 3.4c)**. Additionally, MRI imaging revealed no significant differences in tumor volume. However, RPM animals tend to have larger lesions than RP at any point in time **(Figure 3.5a-c)**. These results suggest that an *Msh2 loss* in the RP setting promotes a more aggressive SCLC phenotype.

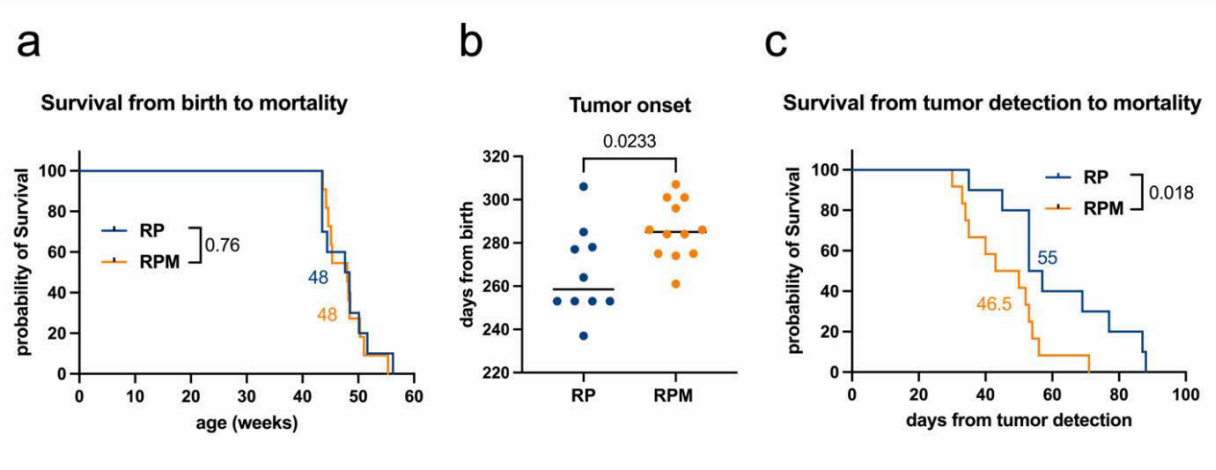

Figure 3.4 Survival and tumor onset analysis in RPM and RP animals.
a) Survival curves from birth of RP (*n*=10, median 48 weeks) and RPM mice (*n*=11, median 48 weeks). **b)** Tumor onset in RP (*n*=10, median 258.5 days) and RPM mice (*n*=12, median 285 days). **c)** Overall survival determined from the timepoint of tumor onset of RP (*n*=10, median 55 weeks) and RPM mice (*n*=12, median 46.5 weeks). The figure was generated with licensed Biorender.com. Log-rank (Mantel-Cox) statistical test **(a,c)** and Mann-Whitney statistical *t*-test (**b**). *Figure originally created by the author and published in Ibruli et al. 2024.*

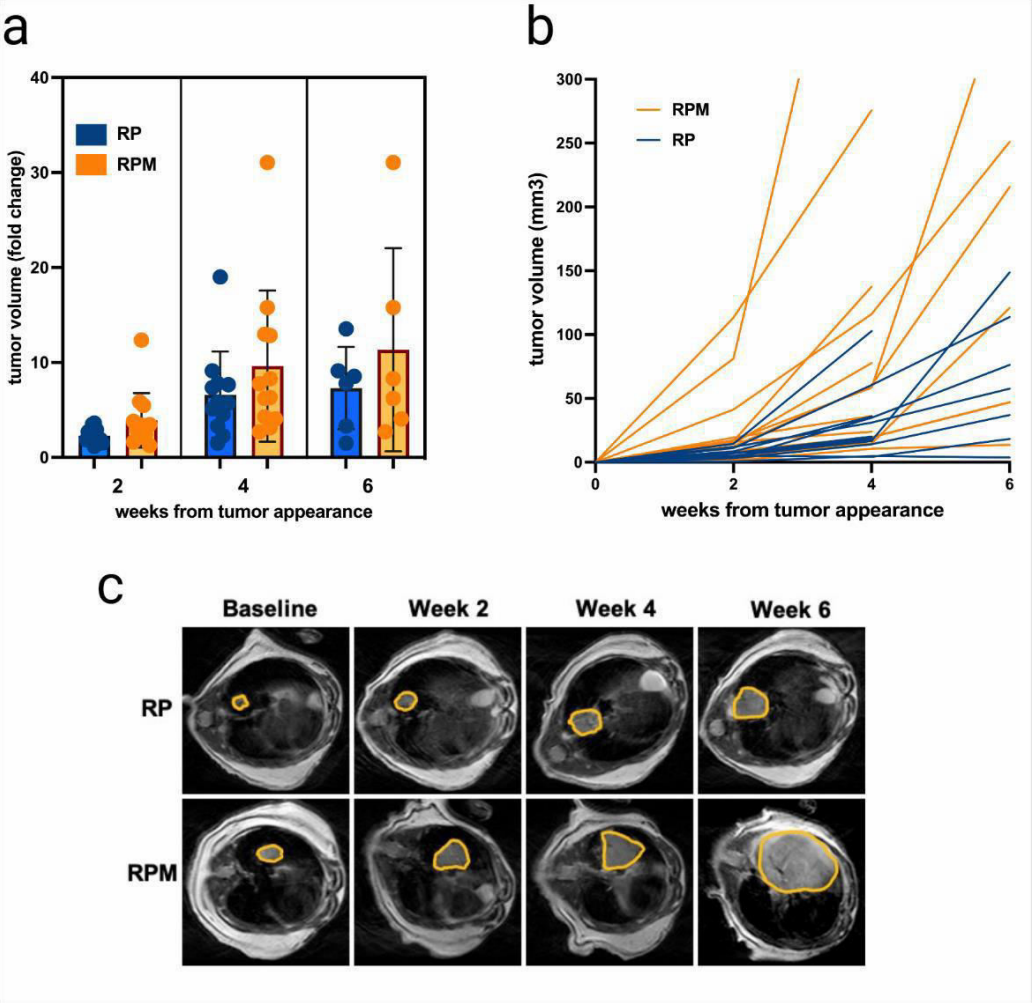

Figure 3.5 Tumor volume and growth trajectories in RP and RPM models.
a) Quantification of tumor volume fold changes based on MRI segmentation after 2 weeks (*n*=12 RP, *n*=13 RPM), 4 weeks (*n*=12 RP, *n*=12 RPM), and 6 weeks (*n*=6 RP, *n*=6 RPM) after first tumor appearance. **b)** Longitudinal analysis of individual tumor growth from the time of detection, obtained by measuring tumor volumes from serial MRI scans (RP *n*=12, RPM *n*=13). **c)** Selected MRI images illustrating lung tumors in RP and RPM mice corresponding to the data in panel **a**. Statistical significance was assessed using Mann-Whitney statistical *t*-test **(a)**. Figure created with a licensed version of Biorender.com. *Figure originally created by the author and published in Ibruli et al. 2024.*

3.4 TMB analysis

To characterize the genomic profile and determine the mutational load of the RPM tumors, WES was performed on micro-dissected lung lesions in cooperation with the Cologne Center for Genomics (CCG) NGS platform (Cologne). We submitted 11 RPM subjects and 5 RP samples as control and verified, using copy number analysis, that 9 RPM subjects had a homozygous loss of *Msh2* (*Msh2*$^{fl/fl}$), while the other 2 had a

mono-allelic loss of *Msh2* (*Msh2*$^{fl/wt}$) **(Figure 3.6a)**. First, TMB was quantified as the mutation count per million base pairs within tumor samples. As previously reported (Ibruli et al. 2024), we observed that the RPM animals with *Msh2*$^{fl/fl}$ exhibited a median TMB of 62.78 mutations/Mb compared to 3.45 mutations/Mb in RP, indicating an 18-fold increase (p=0.0134). Interestingly, the RPM subjects with *Msh2*$^{fl/wt}$ had a median TMB of 2.17 mutations/Mb, similar to RP and, hence, significantly lower than that of *the Msh2*$^{fl/fl}$ RPM group (p=0.0144) **(Figure 3.6b)**. This observation indicates that a mono-allelic deletion of *Msh2* is insufficient to trigger genomic instability and that when both alleles are compromised, the mutational load increases drastically.

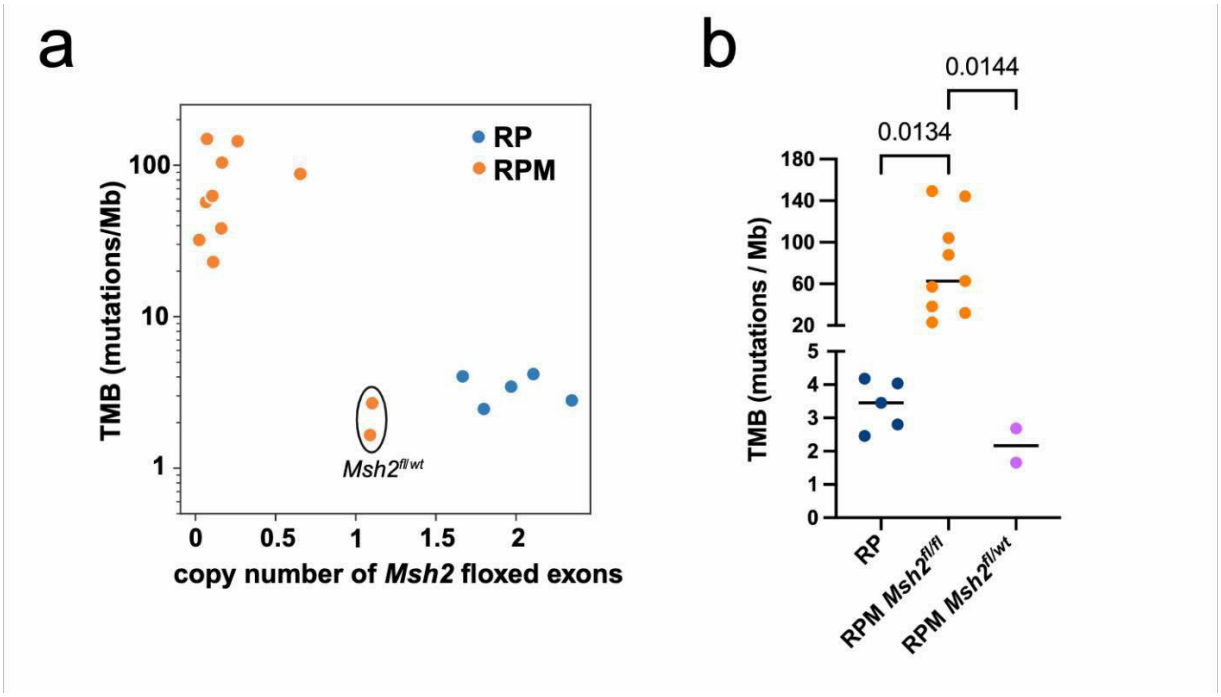

Figure 3.6 TMB in RPM tumors based on WES analysis.
a) Copy number analysis of *Msh2* floxed exons demonstrates homozygous and heterozygous loss in n=9 and n=2 RPM subjects, respectively, as well as no alteration in n=5 RP mice. **b)** Analysis of the TMB extent based on WES data. Kruskal-Wallis statistical test **(b)**. *Figure originally created by the author and published in Ibruli et al. 2024.*

3.5 Mutation type analysis

To further characterize the mutation profile induced by *Msh2* loss, we identified key mutation types present in RPM tumors with *Msh2*$^{fl/fl}$ and compared them to RP and RPM *Msh2*$^{fl/wt}$ subjects. Using WES data, we classified mutations into non-coding/regulatory and coding categories **(Table 3.1)** and visualized their enrichment in RPM *Msh2*$^{fl/fl}$ vs RP using fold-change heatmaps **(Figure 3.7a)**.

The RPM *Msh2*$^{fl/fl}$ tumors showed a substantial increase of silent, intronic, and untranslated region (UTR) mutations in the non-coding and regulatory mutation group. Silent mutations in RPM *Msh2*$^{fl/fl}$ exhibited a 21-fold increase with 514.33 mutations per tumor vs 24.6 in RP. Similarly, intronic mutations were increased 27-fold, from 26 in RP to 377.56 in RPM *Msh2*$^{fl/fl}$. In the coding region, the most dominant mutation types identified were frameshift deletions (267.56/ tumor), frameshift substitutions (3677.50/ tumor), and missense mutations (1972.11/ tumor). The expression of each of these mutation types was significantly increased compared to RP tumors, which showed counts of 2.6, 154, and 75.4, respectively. A strong enrichment was also observed in frameshift indels (165.89/ tumor in RPM *Msh2*$^{fl/fl}$ vs 2.2 in RP) and insertions (32.56/ tumor in RPM *Msh2*$^{fl/fl}$ vs 12.4 in RP). These elevated values were not observed in RPM *Msh2*$^{fl/wt}$, which exhibited counts similar to those of RP in both regulatory and coding regions **(Figure 3.7b-d)**. This further highlights the importance of bi-allelic *Msh2* loss to induce hypermutation. Overall, these findings confirm the role of *Msh2* in maintaining genomic instability and indicate that the *Msh2* deletion disrupts both coding and non-coding regions, particularly inducing frameshift events, which are associated with increased neoantigen load.

Table 3.1 List of mutation types and the corresponding mutation counts obtained by WES. A complete list of mutation type definitions is provided in Appendix.

Mutation type	RP	RPM homozygous	RPM heterozygous	Fold change (RPM hom/RP)
Non-coding/ regulatory mutations				
UTR3	8.2	221.11	5.5	26.95
UTR5	6	93.89	2	15.65
UTR5; UTR3	0.2	1.22	0	6.11
Downstream	0.6	6.56	1	10.93
Exonic; splicing	0	1.89	0	0
Intronic	16	377.56	9	23.6
ncR0_exonic	22.4	400.33	10	17.87
ncR0_intronic	2.4	27.67	1	11.53
Silent	24.6	514.33	17.5	20.91
Splice	4.2	62.89	4	14.97
Stop	1.4	22.22	1	15.87
Upstream	1.4	5.33	0	3.81
Upstream; downstream	0.2	0.89	0	4.44
Intergenic	0.8	0.56	0.5	0.69
Startloss	0.2	0.33	0	1.67
Coding mutations				
Frameshift deletion	2.6	267.56	1.5	102.91
Frameshift insertion	12.4	32.56	8	2.63
Frameshift substitutions	154	3677.50	98.5	23.88
Frameshift indels	2.2	165.89	3	75.4
Nonstop	0.2	3.89	0	19.44
Missense	75.4	1972.11	52.5	26.16
In-frame deletion	0.8	2.11	0.5	2.64
In-frame insertion	0.6	0.89	0	1.48
In-frame indels	1.4	3.00	0.5	2.14

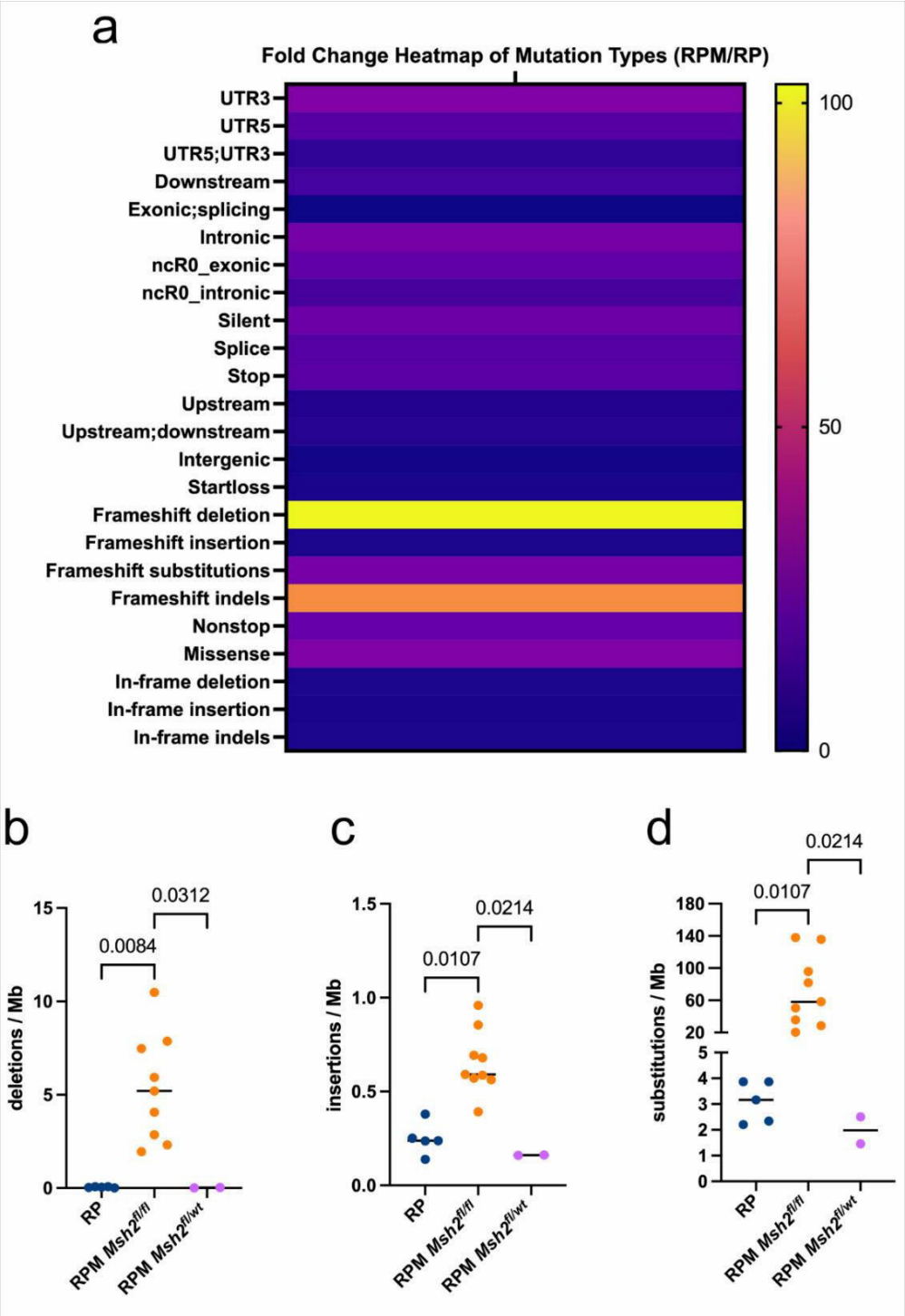

Figure 3.7 Mutation landscape in RPM tumors.
a) Fold change heatmap of mutation counts in RPM homozygous vs RP tumors of key mutations detected in WES data. Identification of frameshift mutations, including **b)** deletions, **c)** insertions, and **d**) substitutions in the RP, RPM *Msh2*$^{fl/fl}$, and RPM *Msh2*$^{fl/wt}$ background. Kruskal-Wallis statistical test **(b-d)**. *Figure originally created by the author and published in Ibruli et al. 2024.*

3.6 Mutational signature analysis

Msh2 deletion is known to induce MSI and mutational profiles associated with deficiencies in DNA mismatch repair. We analyzed the WES data of our RPM model for potential mutational signatures using COSMIC as a reference panel, focusing on the single-base substitutions SBS15 and SBS21 signatures that typically represent MMRd (Crisafulli 2024; Farmanbar et al. 2022).

RPM mice harboring homozygous loss of *Msh2* exhibited a strong enrichment of MMRd-associated signatures. These tumors exhibited significantly higher total mutation count, exceeding 6000 mutations in some samples, and showed an increase in various mutational processes, including signatures related to aging and unknown categories. However, SBS15 and SBS21 remained dominant in the RPM with $Msh2^{fl/fl}$ group, confirming the crucial role of *Msh2* in maintaining genome integrity. By contrast, RP and $Msh2^{fl/wt}$ tumors showed significantly fewer mutations and a predominance of aging- or non-MMR-related signatures **(Figure 3.8a)**.

To confirm this observation, the activity of MMRd signatures (SBS15 and SBS21), defined as the relative contribution of MMR mutations among all detected mutations in a tumor, was quantified **(Figure 3.8b)**. Indeed, the analysis showed that the homozygous RPM mice exhibited a 1.76-fold increase compared to RP mice (median of 0.6227 vs. 0.3545 in RP, p=0.0041) and a 1.57-fold increase compared to heterozygous RPM (median of 0.6227 vs. 0.3970 in RPM $Msh2^{fl/wt}$). However, traces of these signatures in RP subjects could still be detected, suggesting spontaneous or therapy-induced impairment of DNA repair pathways during tumor progression, which can contribute to subclonal diversity.

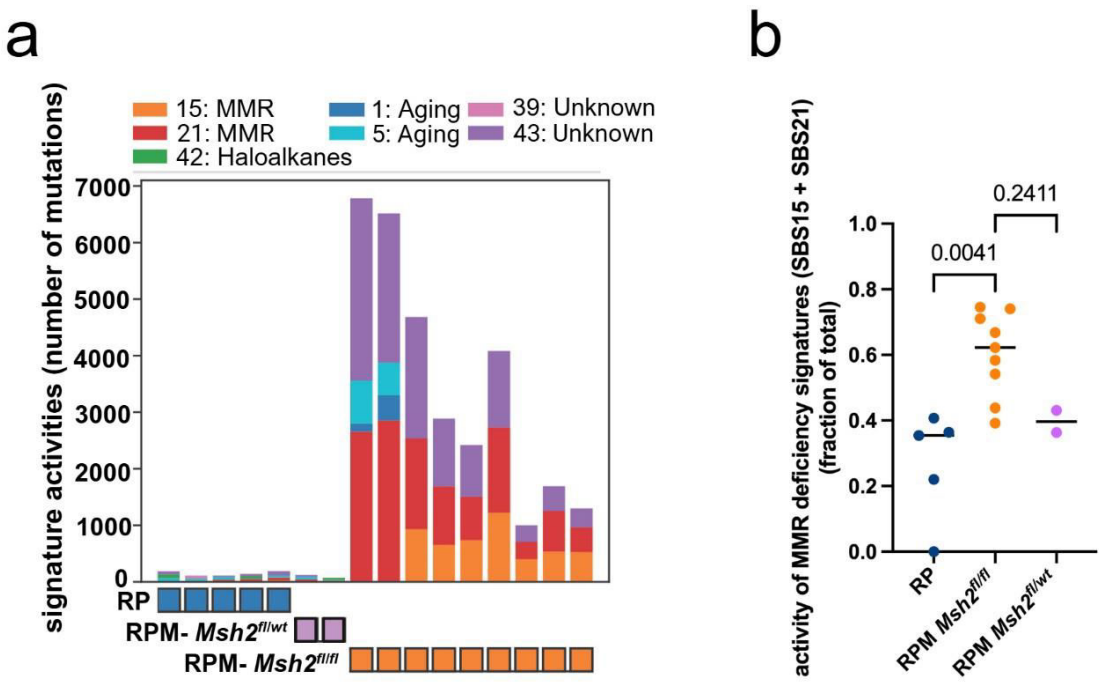

Figure 3.8 Mutational signature analysis.
a) Analysis of mutational signatures based on WES data in RP and RPM animals using COSMIC. **b)** The proportion of SBS15 and SBS21 signatures was analyzed in RP, RPM *Msh2*$^{fl/fl}$, and RPM *Msh2*$^{fl/wt}$ tumors to evaluate MMRd activity. Kruskal-Wallis statistical test **(b)**. *Figure originally created by the author and published in Ibruli et al. 2024.*

3.7 Neoantigen prediction and immunogenicity in RPM mice

To assess any functional consequences of the mutations in the RPM tumors, the WES data was analyzed to predict the immunogenic potential of the mutations. Some mutations can produce neoantigens, which are new mutated peptides that the immune system recognizes as foreign and, thus, can elicit immune responses (Zhang et al., 2021). Neoantigens commonly display strong affinity to HLA-I molecules (Garcia-Garijo et al. 2019). To identify the presence of such mutations in our model, neoantigen prediction analysis was carried out utilizing the HLA-I binding tool from the immune epitope database (Reynisson et al. 2021). Interestingly, this analysis revealed that RPM tumors harboring *Msh2*$^{fl/fl}$ contained significantly more potential neoantigens than RP (p=0.0106) and RPM *Msh2*$^{fl/wt}$ (p=0.0213) **(Figure 3.9a,b)**.

In addition, to further characterize the predicted HLA-I binders, we focused on the murine *H2kb* allele, which is a component of the MHC-I in mice and is responsible for presenting neoantigens on cell surfaces (Vijver et al. 2023). Furthermore, we focused

our analysis on the mutated peptides that were nine amino acids long (9mers) since they are the most common class of neoantigens binding to MHC-I molecules, including H2kb (Molano et al. 1998). We observed that the RPM *Msh2*$^{fl/fl}$ tumors had significantly more neoantigenic 9mers than both RP and RPM *Msh2*$^{fl/wt}$ **(Figure 3.9c)**. Subsequently, we categorized the identified 9mers into strong and weak H2kb binders and compared their frequency across our mice lines. Consistently, the RPM *Msh2*$^{fl/fl}$ tumors exhibited a significantly higher number of strong and weak H2kb binders than the RP (p=0.0084) and *Msh2*$^{fl/wt}$ (p=0.0312) samples **(Figure 3.9d,e)**. These findings strongly suggest that a homozygous loss of *Msh2* in SCLC results in tumors with a high immunogenicity potential.

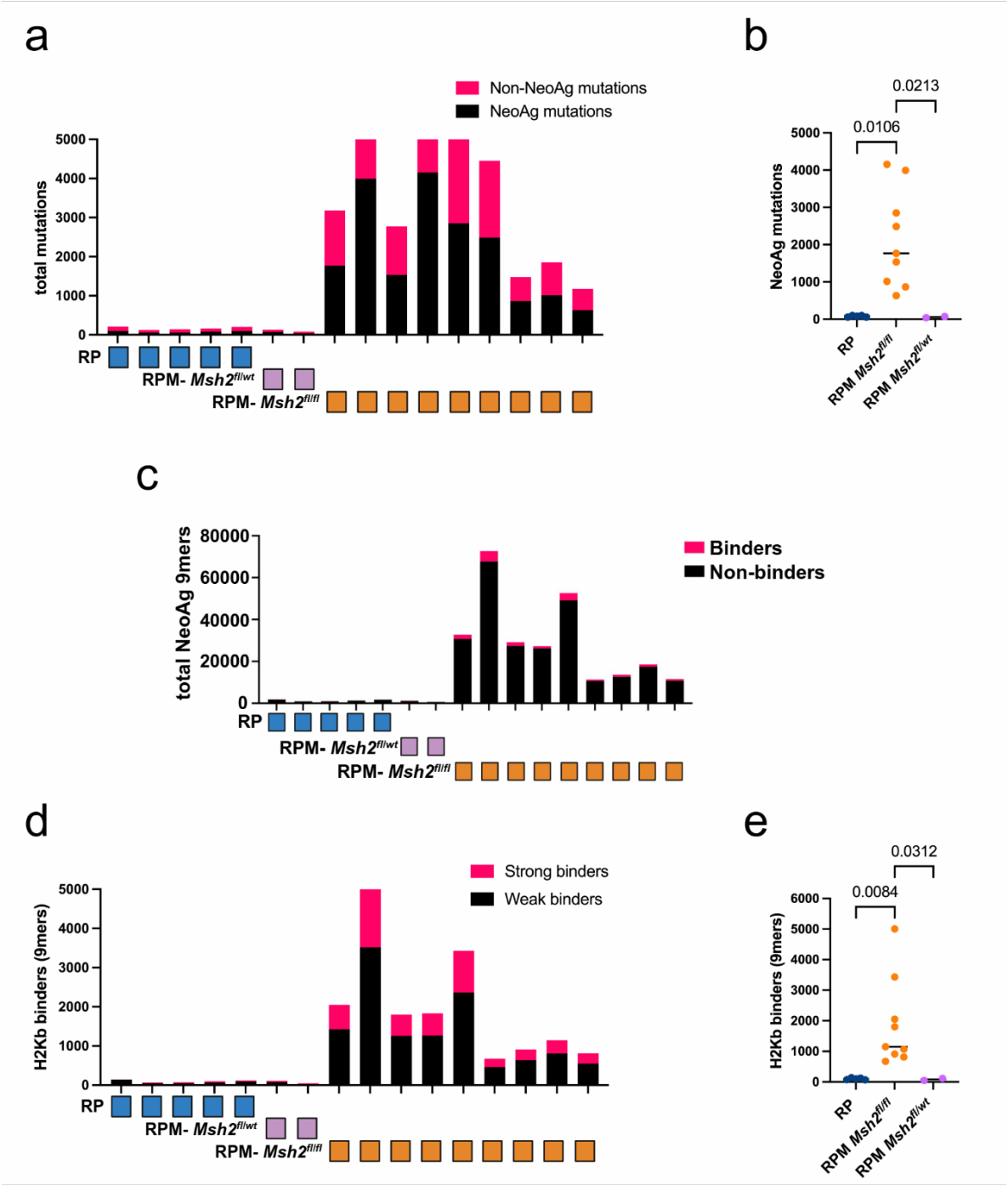

Figure 3.9 Prediction of neoantigens based on WES data.
a) Analysis of neoantigen and non-neoantigen mutations, and **b)** the corresponding statistical analysis. **c)** Estimation of H2Kb binders and non-binders, **d)** Assessment of H2Kb strong and weak binders, and **e)** the corresponding statistical analysis for H2Kb binders (9mers). All analyses are performed in *n*=5 RP, *n*=9 RPM with *Msh2*$^{fl/fl}$, and *n*=2 RPM *Msh2*$^{fl/wt}$. Kruskal-Wallis statistical test **(b,d)**. *Figure originally created by the author and published in Ibruli et al. 2024.*

3.8 Immune profiling of RPM tumors via flow cytometry

To characterize the impact of the MMR deficiency and *Msh2* loss on the TME, flow cytometry was performed on lung lesions of RPM *Msh2*$^{fl/fl}$ animals and compared them to RP subjects. We established an antibody panel to identify major immune cell types, such as leukocytes, T cells, B cells, macrophages, granulocytes, NK cells, and Treg cells. Moreover, we focused on CD4$^+$ T cells and analyzed their functional status, including activation, proliferation, and exhaustion states. In addition, we examined the expression of MHC-I, PD-L1, and PD-L2 on the surface of SCLC cells. **Figure 3.10** illustrates the gating strategy for profiling immune cells in tumors. After initial selection based on their size and granularity (FSC-A and SSC-A), alive immune cells were gated with CD45$^+$ expression, a standard hematopoietic marker. The remaining CD45- cells were considered tumor cells. The immune cell population was further subdivided using CD11b, a common myeloid marker, with CD45$^+$ and CD11b$^+$ cells assigned to the myeloid population and CD45$^+$ CD11b- cells to the lymphoid population. Lymphoid cells were subsequently gated for CD3 expression to identify the total T cell population and CD19 to identify B cells. T cells were further categorized into CD4$^+$ and CD8$^+$ subsets. CD4$^+$ T cells were further analyzed for Foxp3 expression to identify Tregs. On the other hand, CD45$^+$ immune cell population was used to determine macrophages (CD11b$^+$ CD11c$^+$), granulocytes (Ly-6C$^+$ Ly-6G$^+$), and NK cells (Nkp46$^+$).

Flow cytometry analysis of immune cell populations in the tumor microenvironment of RPM lesions revealed no significant difference in the overall number of the major immune cell types compared to RP tumors **(Figure 3.11a-b)**. This suggests that *Msh2* loss in murine SCLC tumors does not lead to substantial immune composition changes. In addition, the expression of the OX-40 activation marker and Ki-67 proliferation marker on the surface of CD4$^+$ T cells did not differ significantly **(Figure 3.11c-d)**. While there were no apparent differences in the expression of exhaustion markers, including Tim-3, Lag-3, and CTLA-4, there was a tendency toward higher expression of these markers in CD4$^+$ T cells of RPM tumors compared to RP lesions **(Figure 3.11e)**. Interestingly, we observed a significant increase in the expression of the PD-1 checkpoint on the surface of CD4$^+$ T cells in RPM tumors as opposed to RP, indicating potential immune modulation **(Figure 3.11f)**. The expression of MHC-I,

PD-L1, and PD-L2 functional markers on SCLC cells remained unchanged between the two mouse models **(Figure 3.11g)**. Overall, the flow cytometry results indicate that the *Msh2* loss in murine SCLC does not cause significant alteration of immune cell composition in the tumor microenvironment. However, the elevated expression of PD-1 on $CD4^+$ T cells suggests a potential impact on the immune modulation of these tumors.

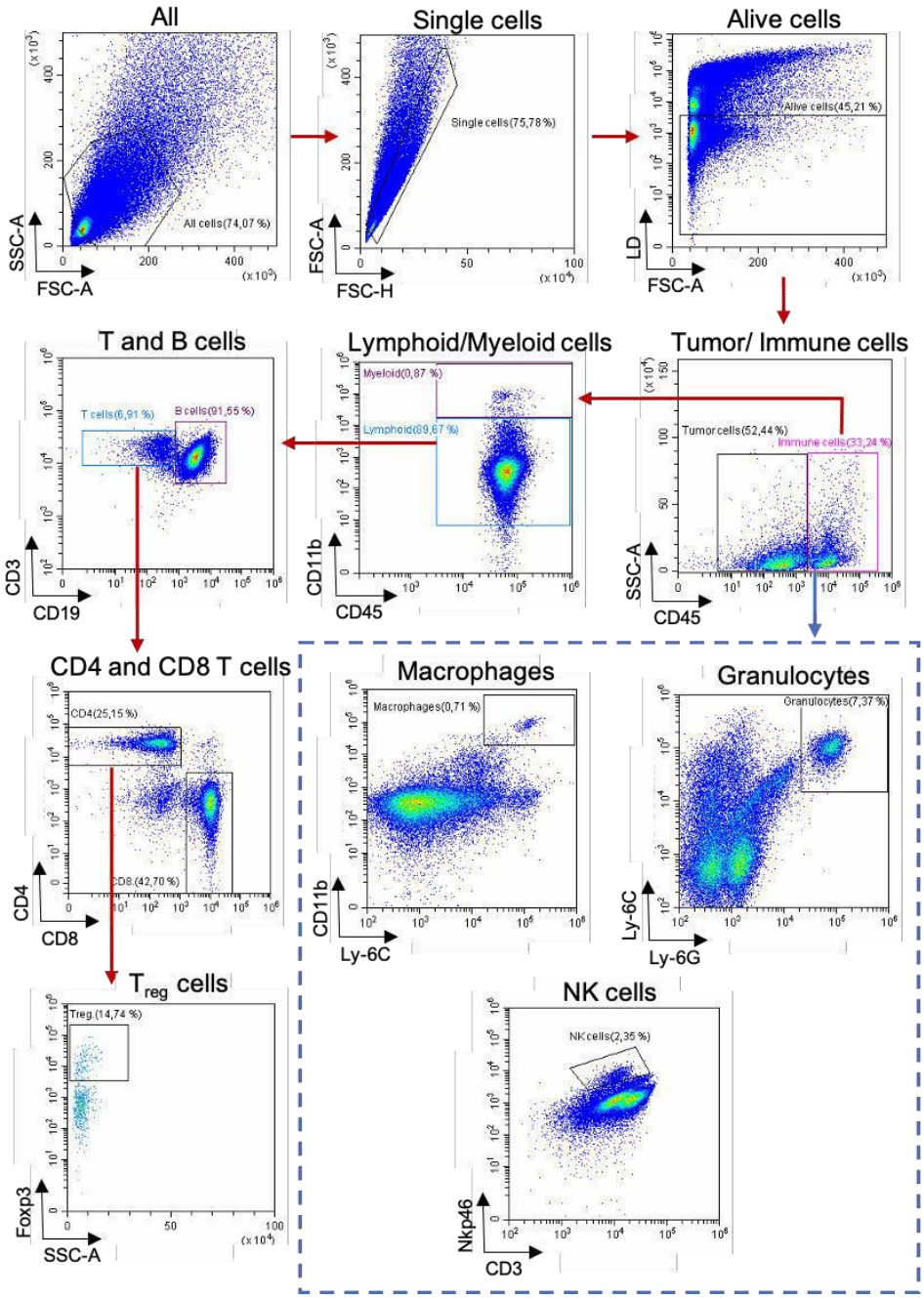

Figure 3.10 Gating strategy to profile the tumor resident immune cells in RPM mice. Representative flow cytometry plots showing the gating strategy (enclosed area) for immune cell profiling of RPM tumors. All: based on FSC-A and SSC-A characteristic and exclusion of cell debris; Single cells: exclusion of non-single cells; Alive cells: exclusion of dead cells with viability dye; Immune cells: total CD45$^+$ cells within alive cells; Tumor cells: total CD45- cells within alive cells; Myeloid cells: CD11b$^+$ and Lymphoid cells: CD11b- within alive CD45$^+$ cells; T cells: CD3$^+$ cells and B cells: CD19$^+$ within the lymphoid population; CD4$^+$ and CD8$^+$ T cells within CD3$^+$ cells; and Treg cells: Foxp3$^+$ within CD4$^+$ T cells. Within the CD45$^+$ cells are macrophages (CD11b$^+$ Ly-6C$^+$), granulocytes (Ly-6C$^+$ Ly-6G$^+$), and NK cells (NKp46$^+$). Arrows indicate the direction of sequential gating steps.

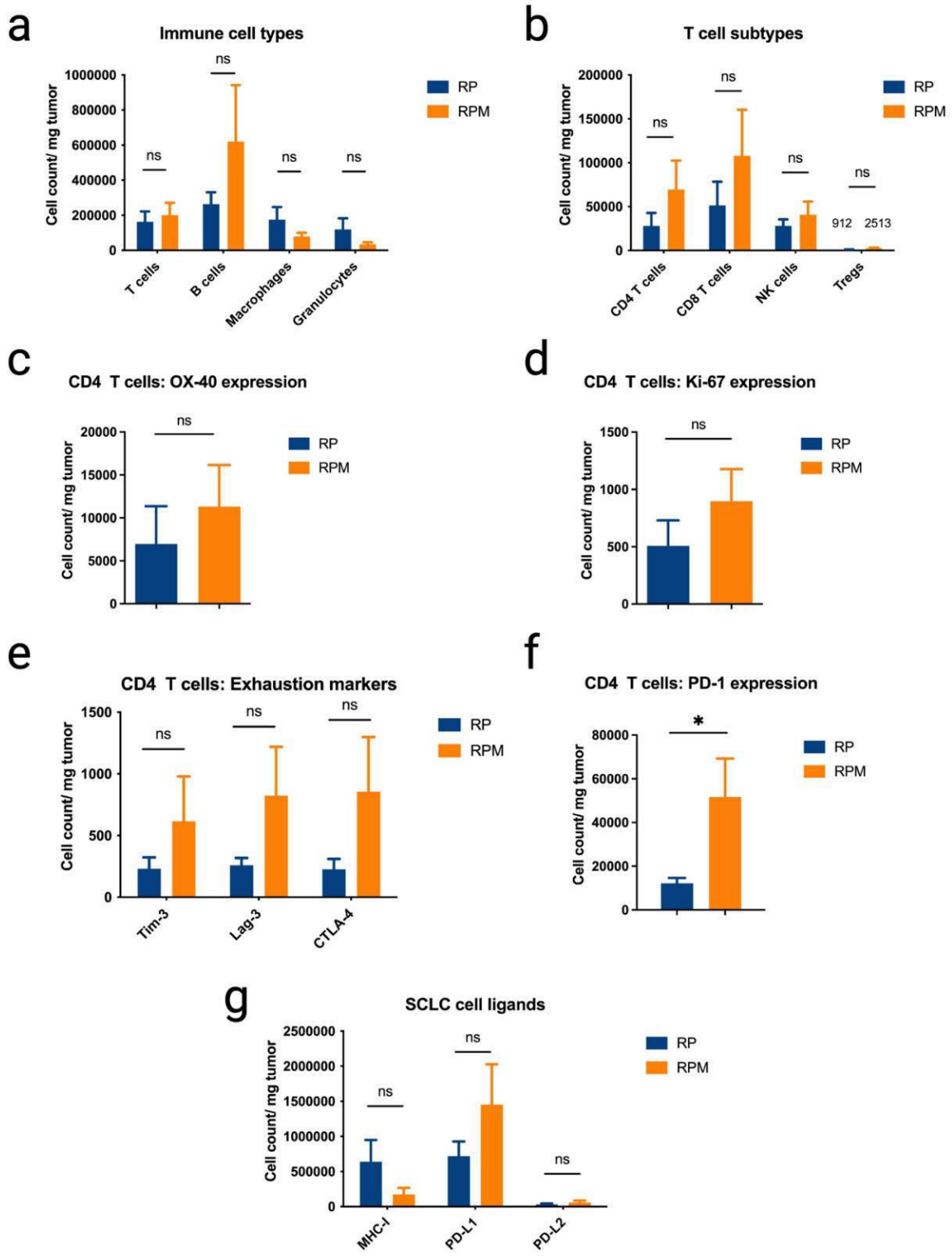

Figure 3.11 Immune profiling of RPM animals via flow cytometry.
Identification and quantification (as total cell count/mg tumor tissue) via flow cytometry of **a)** major immune cell populations, and **b)** T cell subsets. Analysis of $CD4^+$ T cells for expression of **c)** OX-40 activation marker, **d)** Ki-67 proliferation marker, **e)** exhaustion markers, and **f)** PD-1 checkpoint. **g)** Assessment of ligand expression on SCLC tumor cells. Statistical analysis was performed using the Mann-Whitney test, **p-value*=0.04 for PD-1 expression, *n*=10 mice.

3.9 Treatment responses in RPM model

3.9.1 Cisplatin-based chemotherapy and immune checkpoint inhibition

To investigate the *Msh2*/MMR-deficient tumors´ sensitivity towards variable therapies, we designed *in vivo* treatment cohorts and analyzed the effects on overall survival and tumor volume of the subjects. Following the detection of tumors of at least 5 mm^3 via MRI imaging, RPM with *Msh2*$^{fl/fl}$ and RP animals were assigned random treatments that reflect the current clinical practice, including cisplatin/etoposide, anti-PD-1 antibody, and a combination of both **(Figure 3.12)**. Cisplatin and etoposide are chemotherapy agents, standard in the management of human SCLC since this cancer entity is initially highly responsive to chemotherapy. However, SCLC patients almost always relapse shortly after, rendering chemotherapy treatment insufficient (Jiang et al. 2021). This issue can be overcome in some patients by adding an ICI, representing the current first-line treatment in clinics (Horn et al. 2018). However, the genetic and epigenetic factors that increase ICI sensitivity in SCLC are still not fully understood, leading to random assignment in patients and, thus, a low success rate.

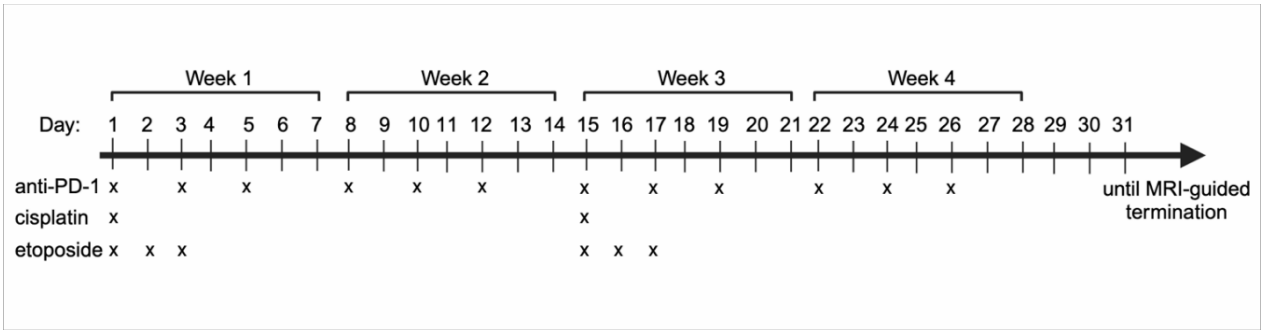

Figure 3.12 Scheme of chemotherapy and ICI treatment schedules.
Tumor-bearing animals were administered with anti-PD-1 antibody i.p. at a dose of 200 mg three times per week for three weeks or until predefined study endpoints were achieved. Cisplatin was injected i.p. at 4 mg/kg body weight once every 14 days, while etoposide was given i.p. at 8 mg/kg on days 1, 2, and 3 of a 14-day cycle. The figure was generated with licensed Biorender.com.

As expected, the mice that received cisplatin/etoposide as treatment, irrespective of the genomic background, showed significantly lengthened survival in relation to the control cohorts. While both tumor models responded remarkably to chemotherapy, RPM animals displayed increased sensitivity, surviving approximately 42 more days than PBS-treated controls (median: 83 days vs. 41 days; $p<0.0001$). In contrast, RP

mice showed a modest increase in survival of 20.5 days, with a median of 73.5 days vs. 53 days in the control group (p=0.0015) **(Figure 3.13a-b)**. Strikingly, RPM mice demonstrated a marked survival benefit following ICI treatment, with a median survival of 51.5 days compared to 41 days in the control group (p=0.0422), whereas RP animals did not exhibit any measurable response **(Figure 3.13c-d)**. When both therapy agents were combined, both mouse models showed significantly improved survival rates, with the RPM model harboring higher efficiency, similar to the mono-chemotherapy cohort **(Figure 3.13e-f)**. These findings indicate that *Msh2*-loss and MMR deficiency in an RP background make SCLC tumors more sensitive to ICI treatment.

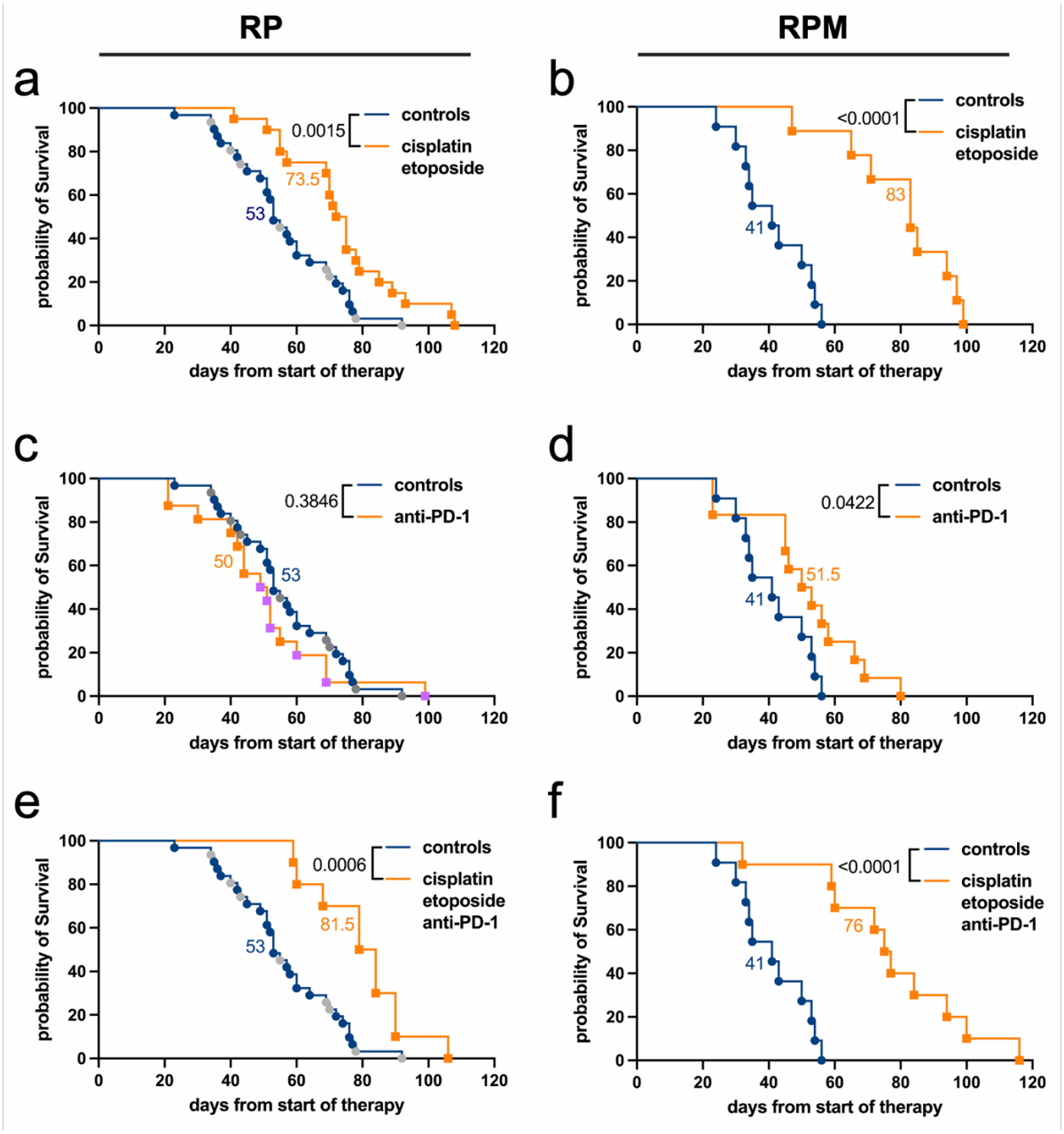

Figure 3.13 Efficacy of chemotherapy and ICI treatments in RPM and RP animals. Kaplan-Meier survival curves for cisplatin/etoposide treatment of **a)** RP mice (*n*=20) and **b)** RPM mice (*n*=9). Kaplan-Meier survival curves for anti-PD-1 treatment of **c)** RP mice (*n*=16) and **d)** RPM mice (*n*=12). Kaplan-Meier survival curves for combined cisplatin/etoposide and anti-PD-1 antibody treatment of **e)** RP mice (*n*=10) and **f)** RPM mice (*n*=10). For all graphs, vehicle controls (PBS-treated animals) of the respective mouse model were included: *n*=31 RP and *n*=11 RPM. Log-rank (Mantel-Cox) statistical test. *Figure originally created by the author and published in Ibruli et al. 2024*

3.9.2 Treg suppression therapy

In addition to investigating the efficacy of standard clinical treatments of SCLC in the RPM model, we aimed to determine whether incorporating Treg suppression would yield additional benefits. Treg suppression therapies, especially prior to exposing patients to immunotherapy, have demonstrated marked survival improvements in various cancer entities, including melanoma, NSCLC, and renal cell carcinoma (Gelibter et al. 2024; Liu et al. 2023; Verma et al. 2019). Tregs can inhibit effector T cell function, thereby suppressing anti-tumor immune responses (Dowling et al. 2018a). This way, the immune system can elicit effective anti-tumor responses, which also leads to enhanced immunotherapy benefits (Y. Li et al. 2024). Several Treg-targeting strategies, such as anti-CTLA-4 antibodies, have shown promise in preclinical and clinical settings. CTLA-4 is primarily expressed on activated T cells and plays a key role in Treg function by supporting the immunosuppressive activity of Tregs. Therefore, blocking CTLA-4 might lead to Treg dysfunction and could promote the activation of effector T cells (Dowling et al. 2018b). In addition to anti-CTLA-4 therapy, we also employed a CDK4/6 inhibitor (CDK4/6i), palbociclib. CDK4/6i is an emerging cancer treatment strategy that targets cell cycle, leading to reduced Treg proliferation and disruption of the immunosuppressive TME. Moreover, it has shown synergistic effects when used in combination with immunotherapy (Wander et al. 2022).

To determine which Treg suppressor works best in the RP background, we injected mice with either anti-CTLA-4 antibody or palbociclib and compared Treg counts in spleens using flow cytometry. We observed that while the anti-CTLA-4 antibody had no effect, palbociclib halved the Treg numbers **(Figure 3.14)**. Thus, we selected CDK4/6i as the Treg suppression therapy in our treatment regimens and administered it to randomly assigned RP and RPM mice, as depicted in **Figure 3.15**.

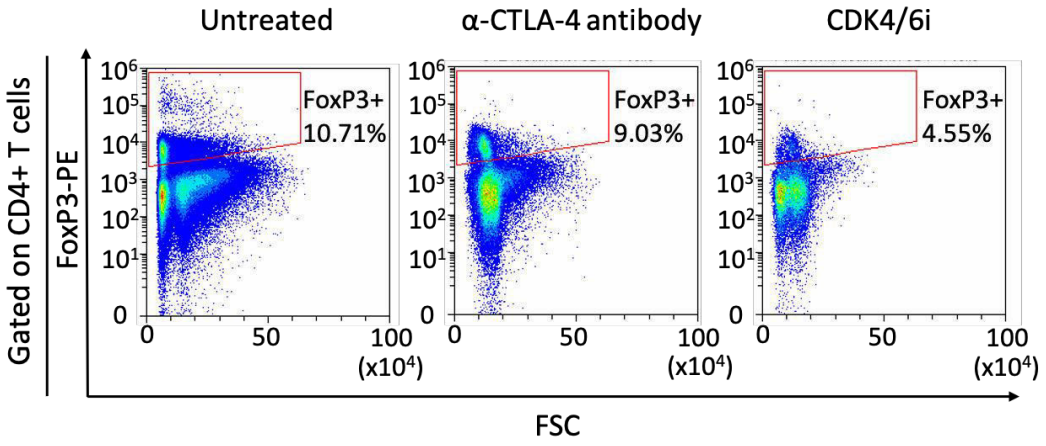

Figure 3.14 Validation of Treg suppression treatments in the spleen.
Representative flow cytometry plots of $CD4^+$ $FoxP3^+$ Treg cells isolated from the spleens of mice treated with either anti-CTLA-4 antibody (clone 9D9, BioXCell) administered i.p. at 10 mg/kg, three times per week for one week or CDK4/6i palbociclib (LC Laboratories) dosed at 100 mg/kg and injected daily via oral gavage for one week.

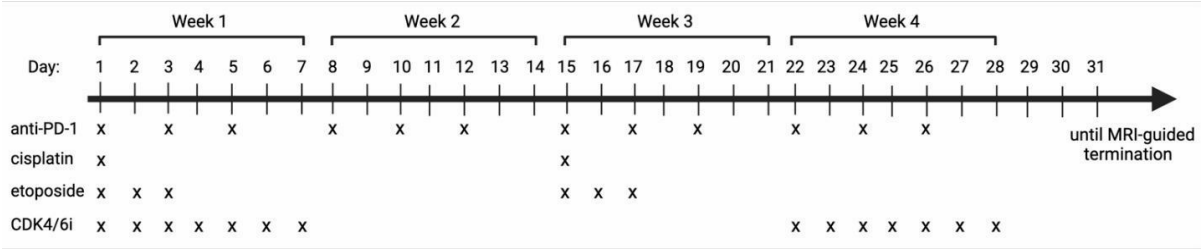

Figure 3.15 Scheme of Treg suppression treatment schedules.
Tumor-bearing animals were administered with anti-PD-1 antibody i.p. at a dose of 200mg three times per week for three weeks or until predefined termination criteria were met. Cisplatin was injected i.p. at 4 mg/kg body weight once every 14 days, while etoposide was given i.p. at 8 mg/kg on days 1, 2, and 3 of a 14-day cycle. The CDK4/6 inhibitor palbociclib was dosed at 100 mg/kg and administered via oral gavage for seven consecutive days every three weeks. The figure was generated with licensed Biorender.com.

Interestingly, we observed that the RP animals did not respond to CDK4/6i treatment alone **(Figure 3.16a)**. In contrast, RPM mice exhibited a significant survival improvement, with a median survival of 60 days compared to 41 days in the vehicle-treated controls (p=0.0022) **(Figure 3.16b)**. Consistently, combined treatment with CDK4/6i and first-line therapy resulted in a remarkable increase in survival of RPM mice by approximately 36 days (median survival of 77 days vs. 41 days in the controls, p<0.001) **(Figure 3.16d)**. Surprisingly, while the combination therapy

improved the survival of RP animals by 13 days, it had no statistically significant effect **(Figure 3.16c)**.

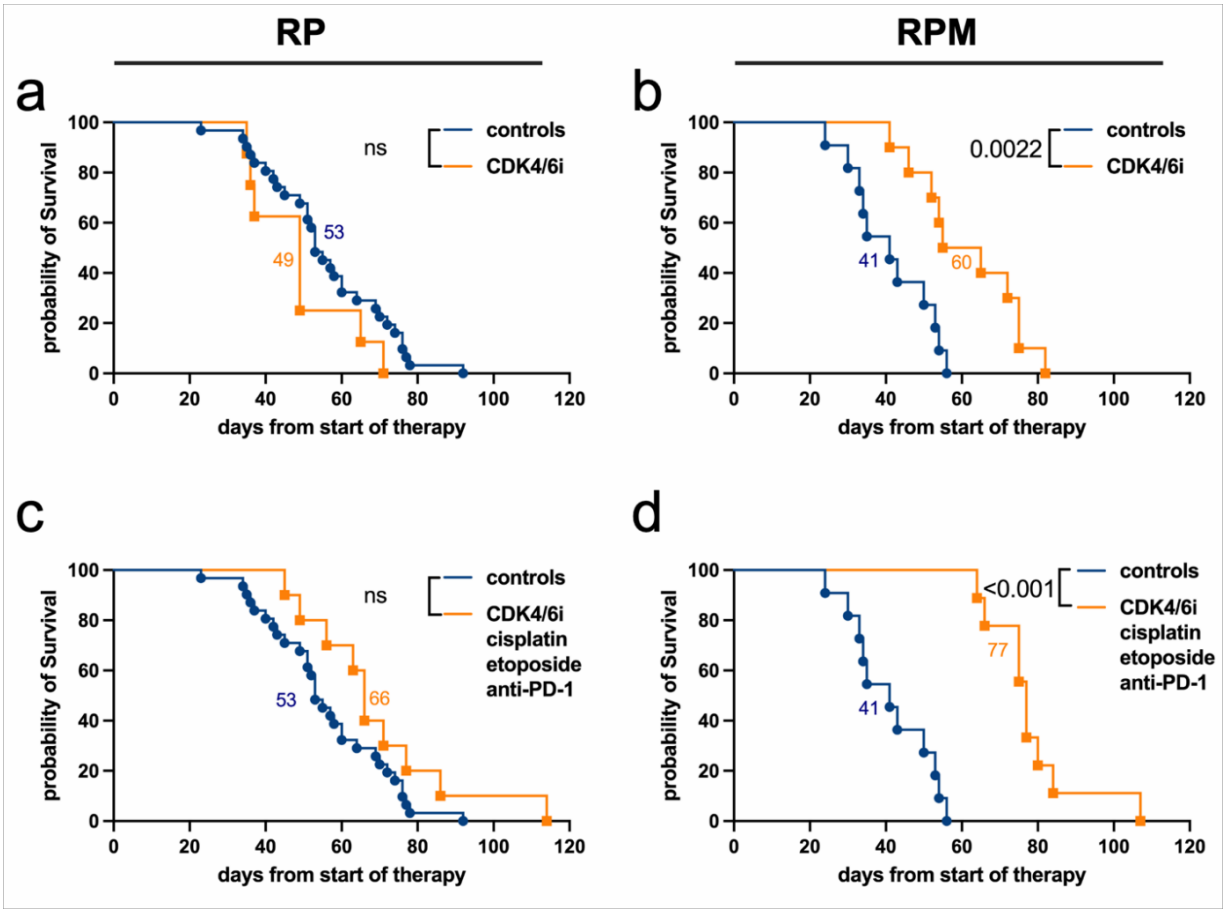

Figure 3.16 Efficacy of CDK4/6 inhibition in RPM and RP animals.
Kaplan-Meier survival curves for CDK4/6i palbociclib treatment of **a)** RP mice (*n*=8) and **b)** RPM mice (*n*=10). Kaplan-Meier survival curves for combined CDK4/6i, cisplatin/etoposide, and anti-PD-1 antibody treatment of **c)** RP mice (*n*=10) and **d)** RPM mice (*n*=9). For all graphs, vehicle controls (PBS-treated animals) of the respective mouse model were included: *n*=31 RP and *n*=11 RPM. Log-rank (Mantel-Cox) statistical test.

3.10 Immune profiling via IMC

3.10.1 Establishment of an antibody panel for immune microenvironment characterization

To characterize the spatial immune landscape in the RPM and RP models and determine the effects of various treatment strategies, we conducted IMC analysis via the Hyperion system. IMC is an advanced technology that enables the detection of up to 40 markers simultaneously on a single tissue slide. It employs metal-tagged antibodies separated by time-of-flight (TOF) mass spectrometry, enabling spatial biology analysis and studying complex cellular interactions within tumors (Giesen et al. 2014).

We designed a 35-marker antibody panel that covers a wide range of immune cell populations, tumor cells, and components of the stromal compartment. In addition, we included markers to assess the functional states of immune cells, particularly T cells, such as activation, exhaustion, antigen presentation, and apoptosis **(Figure 3.17a)**. The staining protocol was optimized to ensure optimal sensitivity and reproducibility of all antibodies in murine-frozen SCLC samples. Spleens were stained to verify antibody specificity as they can serve as control tissues containing all the immune cell subsets of interest **(Figure 3.17b)**. In addition to spleen staining, **Figure 3.17c** depicts a representative staining image of a frozen RP tumor, pinpointing the spatial distribution of markers, such as NCAM, CD45, and α-SMA. These images demonstrate the successful application of the IMC panel in detecting immune cell populations in the SCLC models.

a

Lymphocytes	
CD45	Pan Leukocyte
CD4	Helper T cell
CD8α	Cytotoxic T cell
CD19	B cell
FoxP3	Regulatory T cell (T_{reg})
NK1.1	NK cell
TCRgd	gd T cell

Myeloid cells	
CD11b	Macrophage/Granulocyte
F4/80	Pan Macrophage
Ly6C	Recruited Macrophage
CD11c	DC/macrophage
Ly6G	Neutrophil
MMR	Activated macrophage

T cell status	
IFNγ	Activation
OX-40	Activation
CD44	Activation
TIM-3	Exhaustion
LAG-3	Exhaustion
CD73	T_{reg} immunosuppression
PD-1	Immune Checkpoint
CTLA-4	Immune Checkpoint
MHC-I	AG presentation/ activation
MHC-II	AG presentation/ activation

Tumor cells	
NCAM	SCLC cell
Ki-67	Proliferation
PD-L1	Immune Checkpoint
PD-L2	Immune Checkpoint

Stroma	
αSMA	Fibroblasts
CD31	Endothelium
Hif-1α	Hypoxia

Killing/ cell death	
Perforin	Necrosis
Granzyme B	Apoptosis
Cl. caspase-3	Apoptosis
CD178 (FasL)	Apoptosis

b

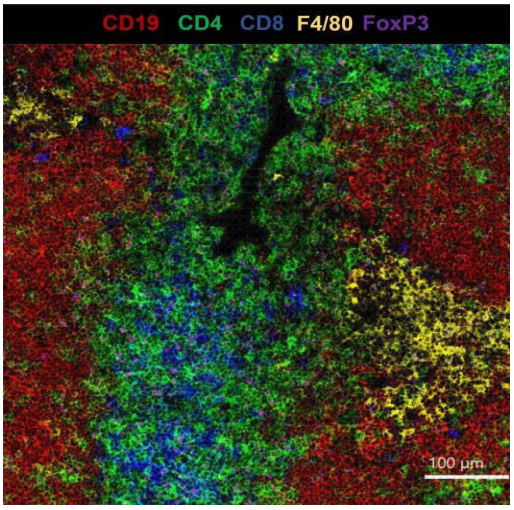

c

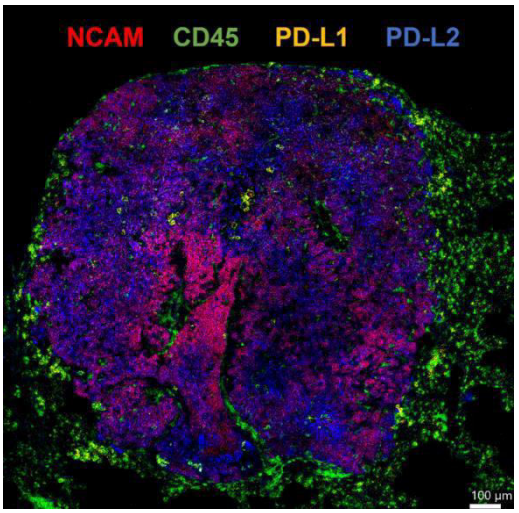

Figure 3.17. Validation of IMC antibodies in frozen spleen and RP tumors.
a) IMC panel of 35 antibodies to identify the lymphoid, myeloid, tumor, and stromal cells and detect the activation, proliferation, exhaustion, and cell death status. **b)** Validation of IMC antibodies in spleen frozen tissue. The representative image is false-colored for CD19 (red), CD4 (green), CD8α (blue), F4/80 (yellow), Foxp3 (magenta). **c)** Representative image of a frozen RP tumor stained for: NCAM (red), CD45 (green), PD-L1 (yellow), PD-L2 (blue). Scale bars = 100 µm.

3.10.2 Tumor morphology and immune infiltration in SCLC

To further characterize the morphology and immune infiltration in SCLC, we performed IMC staining in untreated RP and RPM lung lesions. In line with observations in human SCLC, murine SCLC tumors displayed a densely packed architecture with abundant expression of the NCAM/CD56, which serves as a tumor marker. The tumors also exhibited an immune “cold” phenotype, with minimal and uneven immune cell infiltration **(Figure 3.18a)**. $CD45^+$ immune cells (green) were predominantly localized in the tumor periphery (borders). Infiltrating immune cells inside the tumor tissue were sparse and mainly contained within the $CD31^+$ blood vessels (blue). These findings suggest limited penetration into the tumor parenchyma and impaired access to the tumor.

For comparison, we analyzed murine NSCLC tumors using EpCAM as an epithelial marker to identify tumor cells. Unlike SCLC, NSCLC tumors displayed a more glandular architecture with higher immune infiltration. $CD45^+$ lymphocytes were more abundant and uniformly distributed inside the tumor tissue. In addition, immune cells were not restricted to $CD31^+$ vascular structures **(Figure 3.18b)**. This stark difference in immune patterns reflects the well-established classification of SCLC as immune “cold” and NSCLC immune “hot” tumor entities.

In addition to the overall low immune cell infiltration in SCLC, we observed substantial intratumoral heterogeneity in the spatial distribution of immune cells within RP and RPM lesions. As illustrated in **Figure 3.18c**, some areas exhibited a high number of $CD45^+$ immune cells, while other areas nearby completely lacked immune cells. This uneven distribution makes the SCLC tumor microenvironment highly complex and poses a major challenge in defining the full immunological landscape by using analyses based on specific regions of the tissues.

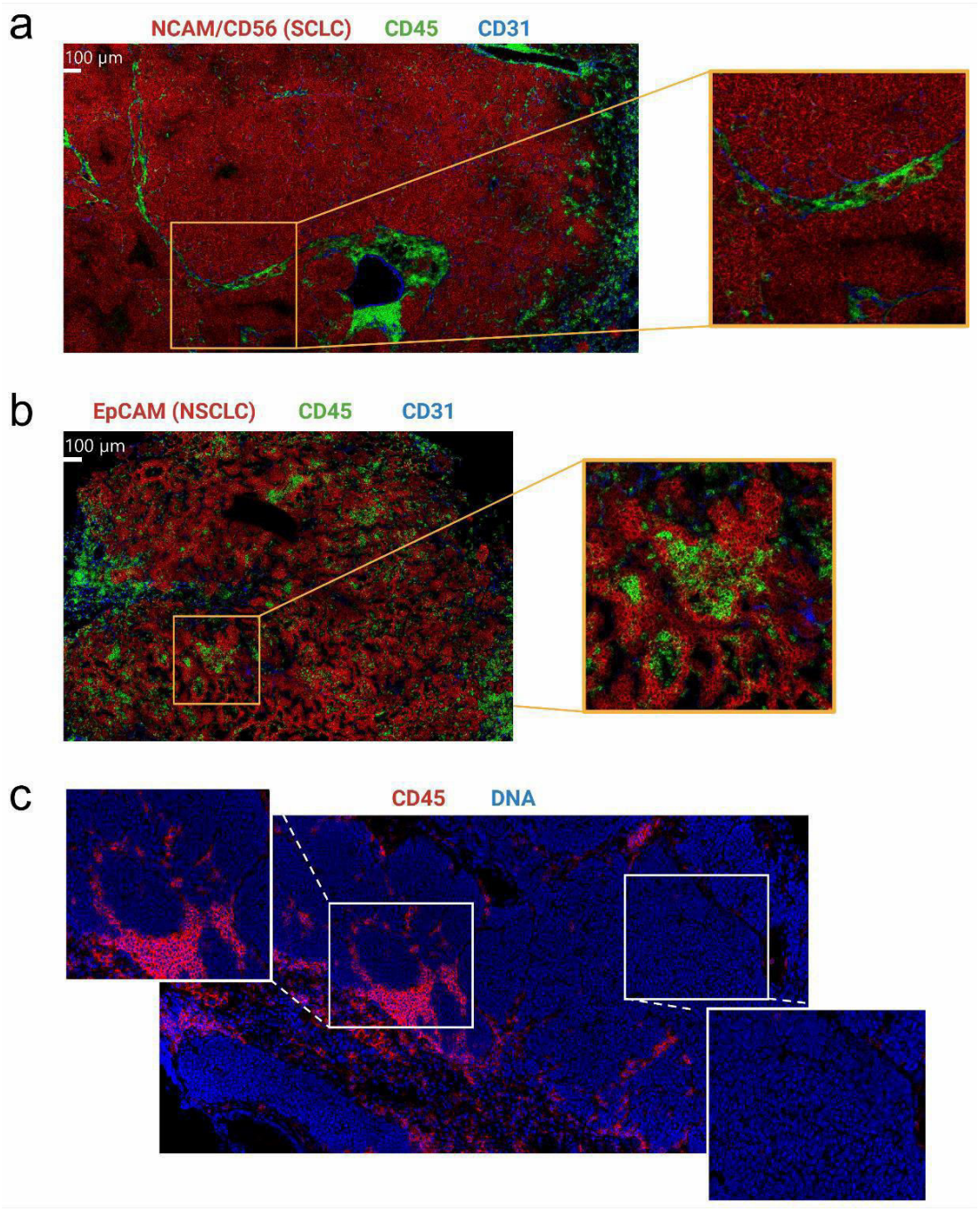

Figure 3.18 Immune infiltration and tumor morphology in murine SCLC and NSCLC tumors.

a) Representative IMC image of an untreated RP tumor showing NCAM/CD56$^+$ tumor cells (red), CD45$^+$ lymphocytes (green), and CD31$^+$ vessels (blue). **b)** Representative IMC image of a murine NSCLC tumor depicting EpCAM$^+$ tumor cells (red), CD45$^+$ lymphocytes (green), and CD31$^+$ vessels (blue). **c)** Representative image of an RP tumor illustrating intratumor heterogeneity in CD45$^+$ lymphocytes (red) infiltration. Nuclei are shown in blue (DNA). Scale bars = 100 µm.

3.10.3 Development of a comprehensive IMC analysis pipeline for murine SCLC

To investigate the immune microenvironment of RP and RPM tumors under different treatments, we constructed a TMA for high-throughput and standardized analysis of multiple samples. For each mouse, one lung lesion was dissected, from which two tissue cores were collected: one from inside the tumor core and one from the tumor-normal lung interface (tumor border). All cores were embedded into a TMA block and stained with a validated 35-marker IMC panel **(Figure 3.19a)**. Using this approach, simultaneous imaging and comparison of a high number of tumor ROIs in one acquisition session was facilitated. This minimizes batch effects and ensures uniform staining and laser ablation parameters.

The TMA included all treatment groups previously analyzed in the survival experiments, including untreated, chemotherapy alone, anti-PD-1 antibody alone, a combination of chemotherapy and anti-PD-1, CDK4/6i via palbociclib, and a combination of palbociclib with chemotherapy and anti-PD-1 antibody. To generate quantitative data from IMC images, we first tested single-cell segmentation, which involves identifying individual nuclei and expanding the segmentation to include the membrane components. However, it is very challenging to perform nuclei differentiation and segmentation in the densely packed SCLC tissue containing small and overlapping tumor cells, particularly when combined with the low resolution of the Hyperion imaging system. Specifically, the Hyperion system has a resolution of 1 µm, which is insufficient to distinguish tightly packed nuclei. To address this issue and achieve higher-resolution images of nuclei, IMC was combined with confocal imaging. First, high-resolution DAPI images were acquired using a confocal microscope prior to IMC ablation, resulting in a clearer visualization of nuclear boundaries. Next, the same sections were ablated on the Hyperion Imaging System for multiplex detection via IMC. DAPI and respective IMC images were then co-registered using a semi-automated pipeline, enabling spatial alignment.

Since single-cell segmentation is the standard method used to extract quantitative data from IMC data, we made considerable efforts to incorporate it into our analysis pipeline. Despite testing and optimizing high-resolution DAPI input and integrating

deep-learning-based segmentation tools such as the Mesmer model, we could not achieve reliable nuclear segmentation in large portions of the tumor cores. Many regions showed substantial nuclear overlap, and even manual corrections could not consistently identify reliable cell boundaries. As a result, this approach could not be validated, and we excluded it from our downstream analysis.

Instead, we developed a robust pixel-based analysis strategy. Each marker channel was binarized to detect positive signals and specific immune cell types were identified by co-localizing biologically relevant markers within the same pixels. To illustrate, $CD8^+$ T cells were defined by co-expression of CD3 and CD8 markers. Although this method cannot provide true single-cell resolution, it provides an alternative for reliable and reproducible quantification of immune cell types in tumors where segmentation is not feasible. Additionally, we applied manual tumor marks to distinguish between the tumor tissue and normal lung tissue to compare immune infiltration in each area **(Figure 3.19b)**.

To illustrate the results of our analysis pipeline, **Figure 3.20** depicts the steps applied to each IMC image. First, the tumor boundaries were manually defined, and the raw signal from key markers (CD45, α-SMA, and CD31) was visualized. Next, individual marker channels were binarized to detect positive signals and show the spatial distribution of immune and stromal cells. Finally, cell type mapping was performed based on the pixel-level co-localization of respective biologically relevant markers, enabling the classification of immune cell types inside or in the border of tumors. This pipeline allows us to analyze immune profiles across all TMA cores and treatment conditions, facilitating biological comparisons presented in the following section.

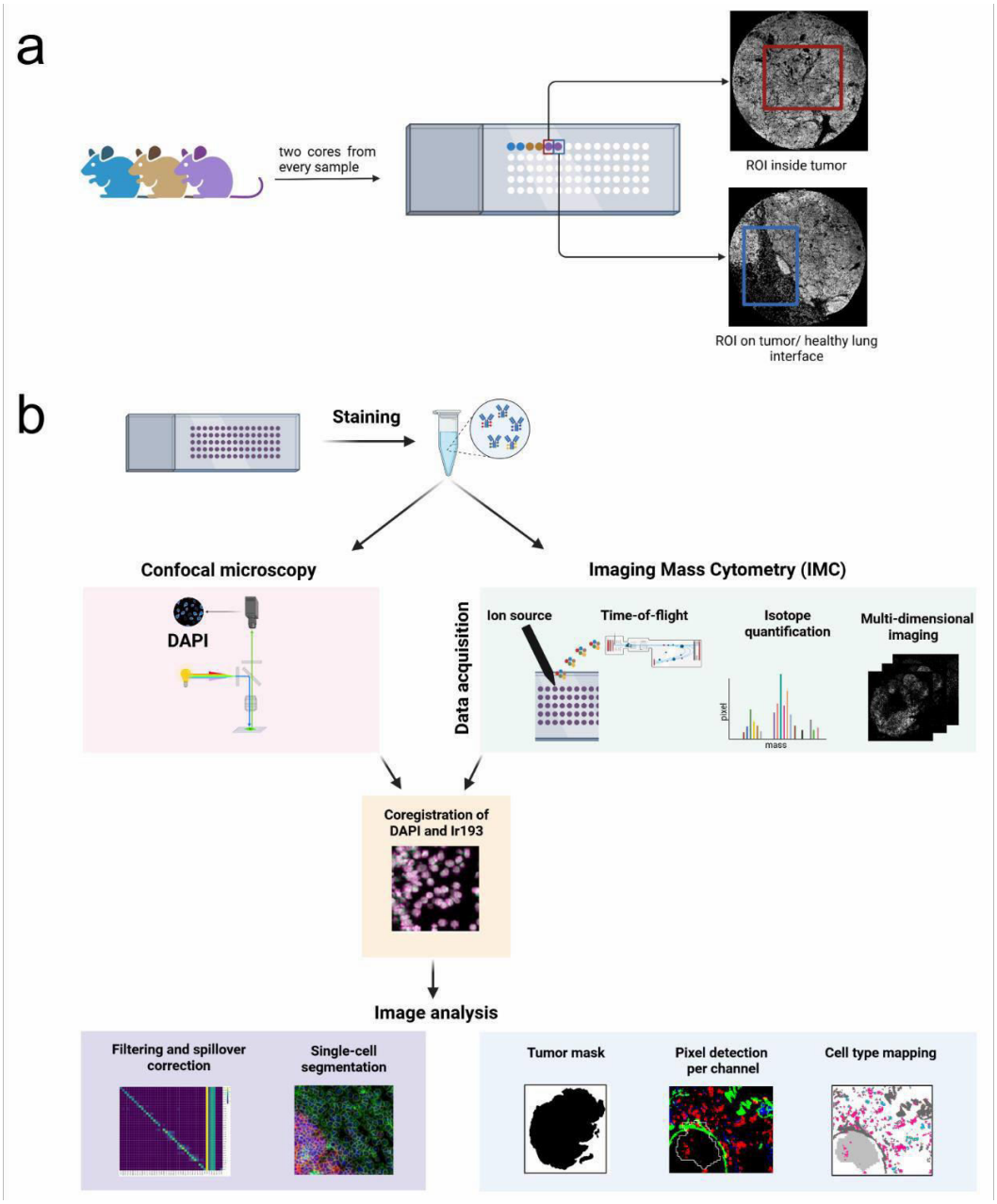

Figure 3.19 Workflow for high-throughput IMC analysis of RPM and RP tumor tissues. **a)** Schematic of TMA design and ROI selection. Two tissue cores, one from the tumor core and one from the tumor-normal lung interface, were extracted from each sample and embedded in a TMA block. ROIs were selected within each core. **b)** Overview of the IMC analysis pipeline. Four-micron frozen murine SCLC tissue slices were mounted on microscopy slides and stained with a combination of metal-tagged IMC antibodies. DAPI images were captured using a confocal microscope at 40x magnification. IMC images were generated with the Hyperion system, which utilizes the TOF principle to detect and quantify metal isotopes and produce multi-dimensional images. The data underwent initial processing, which involved co-registering the DAPI and IR193-DNA (IMC) channels for better detection of the nuclei. Images were initially pre-processed by image filtering and spillover correction. Single-cell segmentation was tested on RP and RPM tumor tissues via Mesmer, a deep-learning network. Subsequently, tumor masks were created to differentiate between intratumoral and extratumoral (border) regions. Each channel was analyzed by identifying positive pixels, which were then used for cell-type mapping. Created with Biorender.com.

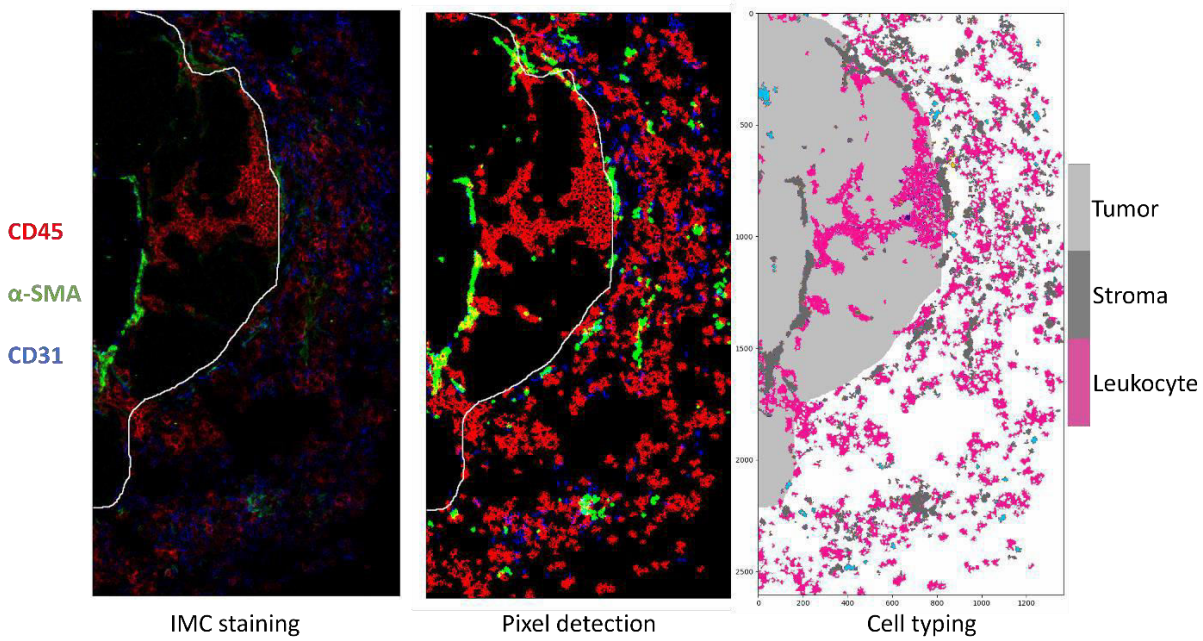

Figure 3.20 Stepwise output of the IMC analysis pipeline.
Representative example of pixel detection analysis applied to each IMC sample. **Left:** Raw signal of CD45 (red), α-SMA (green), and CD31 (blue) and the manually drawn tumor border overlaid in white. **Middle:** Binarized detection of markers to visualize the spatial distribution of immune and stromal cells. **Right:** Cell type mapping based on pixel-level co-localization of relevant markers.

3.10.4 IMC-based immune profiling of RPM and RP tumors under treatment

Due to the size and complexity of the dataset, as well as the very low frequency of immune cell subsets in SCLC tissue, we focused our analysis on the most abundant and relevant immune populations: total leukocytes ($CD45^+$), T cell subsets ($CD4^+$ and $CD8^+$), and B cells ($CD19^+$). These markers were quantified in all RP and RPM samples from baseline (vehicle group) and treated conditions.

We first performed a general comparison of untreated RP and RPM tumors to assess whether MMRd in the RPM model leads to differences in immune infiltration. This analysis complements the flow cytometry data by distinguishing between the tumor tissue versus the tumor-normal lung border/interface. We observed that in both models, immune cells were enriched at the border as compared to inside the tumor, consistent with the typical immune-excluded phenotype of SCLC (Rudin et al. 2021). However, RPM tumors showed markedly lower $CD45^+$ expression inside tumors than

RP, suggesting an even stronger immune exclusion effect in the MMR-deficient setting **(Figure 3.21a)**.

To explore these differences in more detail, we quantified major CD45$^+$ immune cell types, including CD4$^+$ T cells, CD8$^+$ T cells, and CD19$^+$ B cells. In the tumor interface (periphery), both RP and RPM samples showed similar expressions of all markers. The CD4$^+$ and CD8$^+$ T cell levels remained low and similar in both models. However, within the tumor core, we observed a significantly higher presence of CD19$^+$ B cells in RP tumors **(Figure 3.21b)**. These results show minor but potentially important differences between the two animal models, with B cells being particularly excluded in the RPM setting.

Next, we assessed the effect of different treatment regimens on the immune landscape inside tumor cores in RP and RPM models **(Figure 3.22)**. Treatments included monotherapies (cisplatin/etoposide, anti-PD-1, CDK4/6i) and combinations (cisplatin/etoposide + anti-PD-1; CDK4/6i + cisplatin/etoposide + anti-PD-1). Across all treatments, RPM tumors showed a consistently lower CD45$^+$ infiltration compared to RP. Notably, treatment with CDK4/6i + chemotherapy + anti-PD-1 led to a significantly higher CD45$^+$ lymphocyte infiltration in RP vs RPM tumors. CD4$^+$ T cells followed a similar trend, with significantly greater levels in RP compared to RPM under the triple combination. For CD8$^+$ T cells, expression levels remained low in both groups across all treatments, with the tendency of being lower in RPM tumors but with no significant changes. Interestingly, CD19$^+$ B cells were significantly reduced in untreated RPM samples compared to RP and remained almost undetectable in most treatment groups besides the chemotherapy-alone group. These findings may indicate that B cell exclusion is a feature of RPM tumors and is not reversed by therapy. In addition, the analysis of stroma content by measuring the expression of α-SMA$^+$ or CD31$^+$ pixels revealed comparable numbers across regimens. However, when exposed to the triple combination, RP mice showed a significant increase in stromal cells, suggesting more microenvironment remodeling in this setting.

Taken together, these findings indicate that, similar to RP mice, RPM tumors remain largely minimally infiltrated by immune cells. Various treatment strategies do not have a meaningful impact on RPM, unlike RP, which shows a less responsive microenvironment under certain treatments. The combination of CDK4/6i + cisplatin/etoposide + anti-PD-1 antibody was able to significantly increase CD45$^+$ cells, CD4$^+$ T cells, and stroma compartment in RP but had limited effect in RPM. These results suggest that MMRd contributes to a more resistant immune microenvironment, even under a combination of immunotherapy.

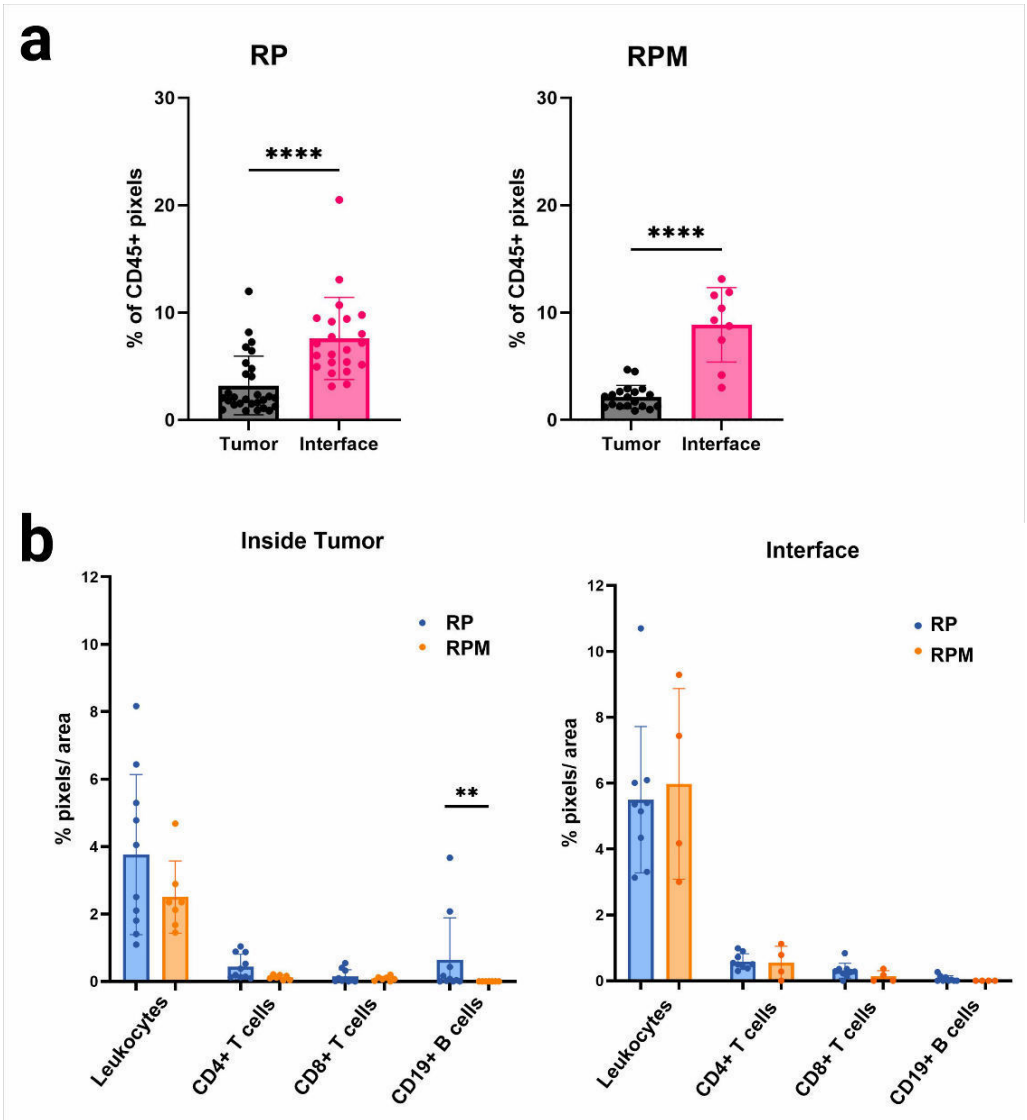

Figure 3.21 Immune cell distribution in untreated RP and RPM tumors.
a) Quantification of CD45$^+$ pixels in the tumor core vs. tumor-normal lung interface in untreated RP (left) and RPM (right) tumors. **b)** Quantification of CD45$^+$ leukocytes, CD4$^+$ T cells, CD8$^+$ T cells, and CD19$^+$ B cells in RP and RPM tumors inside the tumor and in the interface. Data are presented as mean ± SD; statistical comparisons were made using unpaired *t*-tests. $p < 0.01$ (**) and $p < 0.0001$ (****).

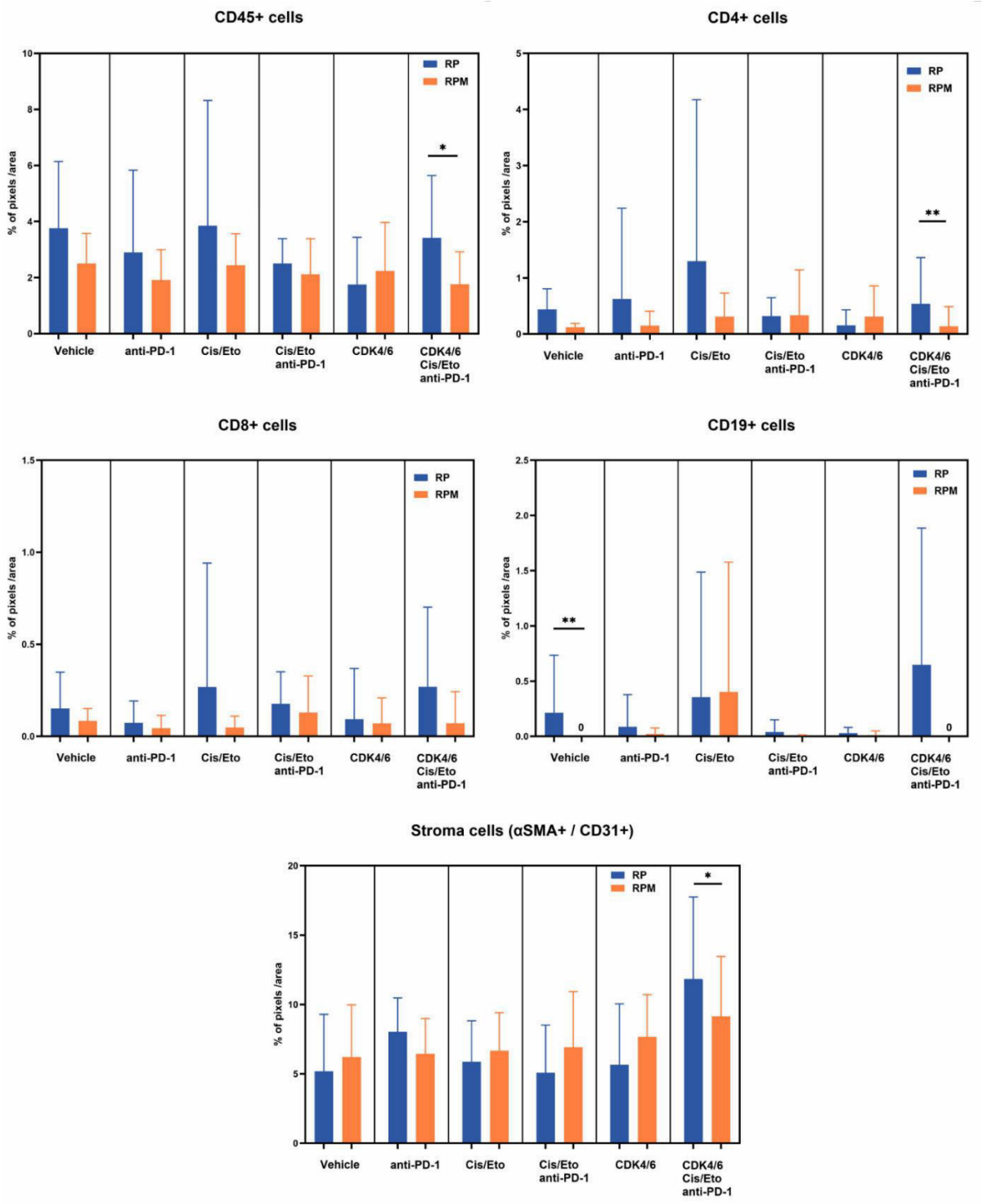

Figure 3.22 Immune and stromal composition inside the tumor core of RP and RPM models across treatment conditions.

Quantification of immune and stromal cell populations inside tumor tissues in RP (blue) and RPM (orange) tumors under the following treatments: vehicle, anti-PD-1, cisplatin/etoposide (Cis/Eto), Cis/Eto + anti-PD-1, CDK4/6i, and triple combination (CDK4/6i + Cis/Eto + anti-PD-1). Data are shown as mean ± SD. Statistical comparisons between RP and RPM within each treatment group were performed using the Mann–Whitney test. $p < 0.05$ (*), $p < 0.01$ (**).

4. Discussion

4.1 The novelty and rationale behind the RPM model

SCLC remains one of the most aggressive malignancies, characterized by rapid progression, early dissemination of metastases, and extremely poor survival outcomes (Kalemkerian et al. 2013; Krpina et al. 2023). Despite extensive research efforts, the molecular landscape of SCLC remains largely uncharacterized, contributing to restrictive efficacy and heterogeneity of current treatment strategies in clinical practice. This is largely attributed to the fact that, unlike many other tumors, SCLC is almost always diagnosed at advanced stages. At this point, surgical resection is no longer an option, and thus, tumor biopsies are especially limited. In addition, SCLC cells have a fast-growing and diffuse nature and longitudinal sampling is challenging (Byers et al. 2015). Consequently, GEMMs play a crucial role in SCLC research, providing a physiologically relevant platform to study tumor biology, immune interactions, and therapy responses.

The most important GEMM of SCLC is the *Rb1*$^{fl/fl}$*;Trp53*$^{fl/fl}$ (RP) model, which successfully reflects the main histopathological and neuroendocrine characteristics of the human disease (Meuwissen et al. 2003). This model harbors the conditional deletion of *Rb1* and *Trp53* tumor suppressor genes, which are almost universally inactivated in human SCLC samples (George et al. 2015, 2024). However, the RP model lacks extensive genomic instability and high TMB that are hallmarks of SCLC. In patients, most of this genomic instability is driven by chronic tobacco exposure, which results in extremely high mutation acquisition rates (Johnston-Early et al. 1980; Rudin et al. 2021). In addition to the smoking-driven mutational signature, recent large-scale proteogenomic studies have identified a distinct subset of clinical cases (~15%) that carry deficient MMR machinery genes, involving genes such as *MSH2*, *MSH6*, and *PMS3*. MMRd in these tumors results in disrupted DNA replication, accumulation of indel mutations, and MSI. Importantly, these patients exhibit worse OS compared to smoking-driven SCLC patients, underscoring the need for a specific model to represent this tumor subset (Q. Liu et al. 2024). However, no existing GEMM recapitulates MMRd in SCLC, limiting the investigation of tumor evolution, immune interactions, and treatment sensitivity in this subset of SCLC.

To address this gap, we have generated the first high-TMB GEMM of SCLC. By incorporating a conditional *Msh2* deletion in the RP background, we have created an MMR-deficient SCLC model (*Rb1*$^{fl/fl}$*;Trp53*$^{fl/fl}$*;Msh2*$^{fl/f}$ (RPM)), that better mimics the genetic landscape of MMR-deficient SCLC patients (Ibruli et al. 2024). This model enables the examination of how MMRd-related genomic instability influences tumor development, genomic instability, and immune responses. This is particularly relevant considering recent evidence that MMRd-SCLC exhibits different genetic features and a worse prognosis than smoking-driven SCLC (Q. Liu et al. 2024).

Given that MMRd has been strongly associated with improved responses to ICIs in colorectal and endometrial cancers (Eerkens et al. 2024; Sahin et al. 2019), the RPM model can extend the exploration of MMRd as a predictive biomarker of ICI response in SCLC. However, recent findings suggest that MMRd alone is not sufficient to elicit enhanced immune responses and sensitivity to ICIs. Despite the high TMB typically associated with a deficient MMR system, studies have shown that these tumors do not consistently present with increased T cell infiltration and efficient immune activation, contradicting the assumptions that MMRd always enhances anti-tumor immunity (Westcott et al. 2023). The RPM model allows the study of the tumor immune microenvironment and can determine whether MMRd-SCLC exhibits similar immune patterns observed in other MMRd tumor entities or whether it remains immune-cold. Additionally, exposing RPM mice to novel combination treatment strategies, such as Treg suppression and ICIs, may offer new insights in further enhancing ICI efficacy.

By addressing this important gap in SCLC research, the RPM model represents a significant advancement, which can potentially provide valuable insights into tumor progression, immune interactions, and therapeutic vulnerabilities. Ultimately, this model could improve patient stratification strategies, optimize combination therapies, and help develop personalized treatment approaches for SCLC patients.

4.2 Tumor growth, progression, and survival differences between RP and RPM models

An important observation in our study is a key difference in tumor kinetics between the RPM and RP models. Despite the increased genomic instability expected in RPM tumors due to *Msh2* loss, we observed a significantly delayed tumor onset compared to RP animals. This finding does not follow the general notion that tumors with higher mutation rates are characterized by accelerated oncogenesis. However, our results support the concept that although a rich mutational burden helps tumors to evolve, it may initially also slow tumor development by activating immune surveillance or reducing the ability of tumor cells to grow because of excessive genomic damage. Similar observations have been reported in other hypermutated tumor types, such as in preclinical models of gliomas, where a high TMB has been correlated with delayed tumor growth due to activated immune responses and lethal mutational load (Johanns et al. 2016).

Despite the delayed tumor onset, RPM tumors exhibited significantly more aggressive growth and ultimately led to earlier fatality compared to RP tumors. This was supported by both MRI-based tumor volume analysis and survival curves following tumor formation, where RPM mice showed poorer survival outcomes. These findings may indicate that MMR deficiency promotes rapid proliferation and evolution once the tumors can overcome the initial immune surveillance or replicative stress. This phenomenon has been also observed in other MMR-deficient tumors, such as endometrial cancers (Pakish et al. 2017), which demonstrated similar patterns of switching from delayed onset to aggressive progression. It is speculated that this behavior is attributed to rapid tumor evolution leading to a shift from anti-tumor immune responses to immune evasion . Overall, we hypothesize that *Msh2* loss accelerates tumorigenesis, consistent with the established role of deficient MMR in inducing genomic instability (Dietlein et al. 2014). This insight aligns with existing literature on the impact of MMRd on aggressive tumor features in other cancers like colorectal cancers (Oliveira, Bretes, and Furtado 2019), and highlights the potential clinical relevance of this study.

This study also reports that RPM and RP backgrounds hardly develop metastases regardless of different aggressiveness levels. Rarely occurring metastases were

confined mainly to the liver, aligned with the knowledge from other SCLC GEMMs (Kalemkerian et al. 2013). However, this observation contrasts the nature of human SCLC, which is almost always associated with distant metastases in the liver, brain, bones, and adrenal glands (Kalemkerian et al. 2013). This discrepancy may be related to species-specific differences in lung architecture, vascularization, or immune system efficacy (Vanharanta and Massagué 2013). Additionally, the lung tumor development via Adeno-Cre in the mouse models generates many primary lesions, which does not reflect the human scenario. It is possible that multiple lung tumors lead to early death and there might be no sufficient time for the development of metastases. The limited number of distant metastases in the RPM and RP mouse models indicates that, while they are important in investigating primary tumor biology, they cannot accurately model the metastatic behavior of human SCLC.

In summary, our data reveal a clear correlation between a deficient MMR system and the aggressiveness of tumors. Although the deletion of *Msh2* in our preclinical model led to delayed tumor formation, RPM tumors were significantly more aggressive than RP once the tumors developed. These findings underscore the complex interplay between genomic composition and tumor behavior, which is not represented in other SCLC models to date.

4.3 Genomic and molecular alterations in RPM tumors

The incorporation of *Msh2* loss in the RPM model was expected to result in significant alteration of the genomic landscape, considering the well-established impact of MMRd in promoting genomic instability across various solid tumors (Dietlein and Reinhardt 2014). WES analysis confirmed that RPM tumors exhibit a substantially higher TMB compared to RP tumors, aligning with findings in other MMRd cancers. The increased TMB is primarily attributed to the accumulation of insertions and deletions, particularly frameshift events, one of the main features of MMRd tumors. Our results are consistent with the established role of *Msh2* in correcting replication-associated DNA errors (Dietlein et al. 2014b; De Wind et al. 1995).

Recent large-scale proteogenomic studies have identified a distinct subgroup of SCLC, which is characterized by predominant defective MMR mechanisms. Liu et al. (2024) reported that 15% of their human SCLC subjects exhibited MMRd-related

mutational signatures characterized by mutations in the *MSH2*, *MSH6*, and *PMS3* mutations. Our findings align with this study by demonstrating that MMR is a significant contributor to genomic instability in some SCLC cases. Furthermore, we provide mechanistic insights by showing that *Msh2* loss alone is sufficient to induce a high-TMB phenotype in a preclinical SCLC setting without the need for additional external factors such as tobacco exposure. Interestingly, our study contrasts findings from Westcott et al. (2023), who also used *Msh2* loss to induce MMRd in GEMMs of lung and colon cancer. This study revealed that MMRd in their preclinical models exhibited no significant impact on the mutational load of SCLC, contradicting the conventional notion that MMRd is responsible for extensive genomic instability. The discrepancy between our study and theirs could be due to the different genetic backgrounds of the models used. Our RPM model introduces *Msh2* loss in the RP background, where the absence of *Rb1* and *Trp53* are the main drivers of tumorigenesis, mimicking human SCLC. Meanwhile, Westcott et al. studied *Msh2* inactivation in preclinical settings lacking these deletions, suggesting that the sole inactivation of *Msh2* has limited potential to influence TMB. The difference in our findings underscores the need for further investigation of how different genetic and external factors influence the extent of TMB in MMRd-SCLC.

To further examine the mutational landscape of RPM tumors, we performed a mutational signature analysis based on the COSMIC database and focused on the SBS15 and SBS21 signatures, which are predominantly involved in MMRd-induced tumorigenesis. While these signatures have been widely identified in colorectal, endometrial, and gastric cancers (Crisafulli et al. 2024; Farmanbar et al. 2022; Dominkuš et al. 2023), their role in SCLC remains poorly understood. We found that the RPM tumors showed a significantly elevated presence of these mutational signatures compared to RP controls, which mainly harbor background mutational processes. These results verify that in our preclinical model, *Msh2* alone is sufficient to induce mutational profiles observed in human MMRd cancers, supporting the relevance of the RPM model as a suitable platform to represent this SCLC subtype.

One of the most striking findings of our analysis is the identification of increased events of frameshift mutations, another established hallmark of MMRd tumors (Germano et al. 2018), in RPM tumors compared to RP subjects. It has been shown that frameshift

alterations produce dysfunctional proteins, which disrupt various signaling pathways and ultimately affect tumor biology (Germano et al. 2018). Additionally, frameshift mutations can create highly immunogenic neoantigens, as abnormal proteins can be recognized by the immune system more easily. Indeed, the neoantigens derived from frameshift alterations in colorectal and endometrial cancers have been demonstrated to elicit robust anti-tumor immune reactions (Gebert et al. 2021; Song and Zhang 2022). However, whether this phenomenon is similar in SCLC is yet to be explored. To address this question, we determined the neoantigen burden of RPM tumors and compared it to the RP background with support from a bioinformatician. We observed a significant enrichment of predicted H2Kb-binding neoantigens in RPM subjects, suggesting that *Msh2* loss can introduce tumor immunogenicity at the molecular level. However, this does not necessarily imply that the higher load of neoantigens translates to more effective immune responses in SCLC. Emerging evidence in other malignancies has shown that a stronger marker of immune activation is neoantigen clonality rather than the absolute neoantigen count. Highly clonal neoantigens, which are present in all tumor cells, can elicit strong T-cell reactions. On the contrary, subclonal neoantigens, present in only a fraction of tumor cells, have been shown to evade immune recognition (McGranahan et al. 2016; Rosenthal et al. 2019). RPM tumors generate most likely subclonal neoantigens, given their hypermutator nature. This could provide an explanation of why MMRd-SCLC cases have a worse OS compared to smoking-induced tumors (Q. Liu et al. 2024).

Overall, our findings indicate that MMRd is a critical driver of genomic instability, high TMB, and increased neoantigen load in a subset of SCLC cases. Furthermore, the RPM model provides a relevant preclinical model to further explore the MMRd in SCLC.

4.4 The impact of *Msh2* loss on the immune microenvironment assessed by flow cytometry

SCLC is widely recognized as an immune-cold tumor entity characterized by low levels of immune cell infiltration. It exhibits reduced antigen presentation, weak anti-tumor immune responses, and thus low sensitivity to immunotherapy, particularly ICIs (Chen et al. 2023; George et al. 2015). This is paradoxical, considering that SCLC is one of the cancers with the highest TMB, which typically results in enhanced immunogenicity.

A major question of this thesis was whether the MMRd via *Msh2* deletion could change the tumor immune microenvironment in SCLC. Despite the high TMB and elevated neoantigen load in RPM tumors, flow cytometry analysis revealed no major differences in the composition of immune cells when compared to RP tumors. Frequencies of the major immune cell types, including T cells, B cells, macrophages, granulocytes, and NK cells, were similar in both genotypes. These results indicate that MMRd and increased mutational burden in our model do not significantly impact immune cell recruitment. This finding contrasts the typical scenario in other MMRd models, such as MSI-high colorectal cancer, where high TMB often correlates with increased T cell infiltration (Jin et al. 2022). However, a recent study from Westcott et al. (2023) provides insights that align with ours. Their mouse models of MMR-deficient lung and colon cancer failed to exhibit increased T cell activation or improved response to ICI despite a high TMB and extensive neoantigen burden. This was attributed to elevated intratumoral heterogeneity that gave rise to subclonal neoantigens, resulting in ineffective immune responses.

Interestingly, while we detected no new patterns in the overall immune infiltration, the PD-1 expression on the surface of $CD4^+$ T cells was significantly higher in RPM tumors. PD-1 is a well-established marker of T cell exhaustion and chronic activation and has emerged as an important marker of T cell dysfunction (Thommen and Schumacher 2018). This finding may suggest that, although MMRd tumors contain more mutations and neoantigens, they can only elicit non-functional or only partial T-cell mediated anti-tumor responses. This phenomenon has been observed in other tumors and has been linked to additional factors, such as the presence of inhibitory molecules in the tumor microenvironment. The elevated PD-1 expression in the

absence of increased immune infiltration may also indicate early stages of T-cell involvement followed by functional suppression, as shown in other tumor types (Thommen and Schumacher 2018).

The lack of immune activation in RPM tumors may be explained by several immune suppression mechanisms that are involved in cancer. For instance, Treg cells, TAMs, and MDSCs can suppress effector T cell activity. We did not detect any considerable changes in either of these populations; however, our analysis was not focused on assessing their functional states deeply. Previous studies have reported similar scenarios. MMRd TME has been shown to shift towards an immunosuppressive state as a result of cytokine secretion or metabolic reprogramming. Indeed, MMR-deficient colorectal cancer models could upregulate *indoleamine 2,3-dioxygenase 1* (*IDO1)* and *TGF-β*, which are able to impair effective anti-tumor reactions even in the presence of immunogenic mutations (Azimnasab-sorkhabi et al. 2023; Chen et al. 2022; Llosa et al. 2015).

Furthermore, we detected no major differences in the expression of surface ligands, such as MHC-I, PD-L1, or PD-L2, which assist immune cells in recognizing tumor cells and acquiring checkpoint signaling. This is particularly unexpected, considering that RPM lesions have a high neoantigen load, which has been shown to upregulate MHC-I and promote antigen presentation. This may be a mechanism that MMRd-SCLC uses to evade immune activation. In fact, recent studies have reported that SCLC is generally characterized by low MHC-I expression, which may be attributed to epigenetic silencing. Thus, despite their high TMB, these tumors are less visible to cytotoxic T cells (Chen et al. 2023b; George et al. 2015).

Taken together, our data demonstrate that MMRd in our RPM model drives genomic instability, resulting in high TMB and elevated neoantigen load, but it does not significantly impact the tumor immune microenvironment. Thus, high TMB alone may not be sufficient to shape immune responses in SCLC, reinforcing the immune-cold phenotype of SCLC. This highlights the need to consider other factors, such as antigen presentation mechanisms, suppressive immune cells, and spatial distribution, in designing effective immunotherapies for MMRd-SCLC cases.

4.5 Response to standard therapy: Chemotherapy and ICI

The first-line treatment in the management of SCLC, particularly ES-SCLC, involves platinum-based chemotherapy in combination with ICIs (atezolizumab or durvalumab) (FDA 2019, 2020). While most patients respond initially very well to this treatment, almost all of them relapse rapidly, and the added benefit of ICIs varies substantially (T. Zhang et al. 2023). In this study, we evaluated the sensitivity of the RPM model to both chemotherapy and ICI to determine whether the presence of deficient MMR impacts the therapeutic response.

Consistent with observations in clinical practice, both RP and RPM mice responded to cisplatin/etoposide treatment, as evidenced by the significantly increased OS compared to vehicle-treated animals. However, RPM mice exhibited notably greater sensitivity by showing nearly double the survival benefit of RP controls. This may be due to the extensive DNA damage and replicative stress in MMR-deficient tumors, as previously described in other malignancies (Bouffet et al. 2016). In addition, *Msh2* deletion may prevent the RPM tumors from effectively repairing cisplatin-induced crosslinks, resulting in amplified cytotoxic effects and increased sensitivity to DNA-damaging agents (S. A. Martin, Lord, and Ashworth 2008).

Strikingly, while RP mice did not benefit from ICI alone, RPM animals exhibited a significant survival increase when exposed to anti-PD-1 therapy. This survival improvement was further enhanced when ICI was combined with chemotherapy, suggesting a potentially improved synergistic effect. The enhanced sensitivity to ICI may be attributed to the high TMB and extensive neoantigen panel in the RPM tumors, as they are both established features in other cancers. Le et al. (2015) demonstrated that patients with MMR-deficient colorectal, endometrial, and gastrointestinal cancers showed better survival outcomes than MMR-proficient tumors when treated with an anti-PD-1 antibody. Similarly, Rizvi et al. (2015a) reported that high TMB and increased neoantigen burden correlated with greater response to anti-PD-1 therapy in NSCLC cases. Additionally, this result aligns with our flow cytometry finding that PD-1 expression on the surface of $CD4^+$ T cells was elevated, indicating a chronically stimulated but exhausted T cell activity, which can be reactivated by PD-1 blockade (Thommen and Schumacher 2018).

Although our findings match with similar observations in other cancer types, where MMRd is associated with increased ICI sensitivity, the potential use of MMRd as a predictive biomarker in SCLC remains poorly understood. This is partly attributed to the scarcity of patient biopsies and the limited number of MMRd-SCLC cases. However, Liu et al. (2024) recently detected that a decent number of SCLC patients (~15%) in their cohort presented with dominant MMRd mutational signatures. Interestingly, they found that this subgroup showed poor OS, emphasizing that high TMB alone may not be sufficient in predicting immunotherapy response. Our RPM model shows a similar complexity by having a higher sensitivity to anti-PD-1 treatment but still lacking robust immune activation.

Interestingly, our findings contradict those reported by Westcott et al. (2023), who performed a similar investigation using *Msh2*-deleted mouse models of lung and colon malignancies. Their preclinical models did not show any survival benefit when treated with anti-PD-1, and they concluded that MMRd is not a reliable marker to predict ICI responsiveness. However, our MMRd-SCLC model exhibited a clear survival benefit following PD-1 blockade. There are two aspects that may account for this contrast. First, our preclinical models have different genetic backgrounds. Unlike their model, our RPM setting includes concurrent *Rb1* and *Trp53* deletion, reflecting a physiologically more relevant genetic makeup of clinical SCLC. Combining *Msh2*-deletion with *Rb1* and *Trp53* deficiency may play an important role in ICI susceptibility. Next, while we specifically mimic SCLC, Westcott generated adenocarcinoma-prone lung models, which are genetically and biologically distinct from SCLC. These observations highlight the importance of specific preclinical platforms to examine immunotherapy responses in MMRd tumors.

Taken together, our findings highlight the role of the RPM model in investigating therapy responses in MMRd-SCLC. We show that MMRd in our model not only improves chemotherapy effectiveness but also offers a selective advantage to anti-PD-1 treatment, especially in combination regimens. These results support the relevance of MMRd as a potential biomarker to stratify SCLC patients who would benefit from ICI therapy but also point out that additional factors beyond genetic alterations must be considered.

4.6 The role of Tregs and CDK4/6 inhibition in SCLC

In general, Tregs are a critical component of immunological self-tolerance and, in cancer, actively involved in immune suppression. It has been shown that Tregs can infiltrate tumors and control the activity of T and B cells, NK cells, DCs, and macrophages through cell-cell contact or the release of signaling molecules, including CTLA-4, IL-2, IL-10, and TGF-β (Josefowicz et al. 2012; Wing et al. 2010). Their immunomodulatory role is particularly relevant in the context of ICI resistance, in which Tregs can help even immunogenic tumors to evade T cell-mediated anti-tumor reactions (Tanaka et al. 2017; Togashi et al. 2019). Recent studies have described similar patterns in SCLC as well. Even though SCLC is an immune-cold tumor, immunosuppressive cell types like Tregs and TAMs have been linked to poor response to immunotherapy (Wang et al. 2024). Hence, new treatment strategies in various cancer types include depletion or functional suppression of Tregs. Depletion or suppression of Tregs results in the development of autoimmune diseases in humans and strong anti-tumor immune responses in cancer patients (Josefowicz et al. 2012).

To investigate whether targeting Tregs in our preclinical model improves survival outcomes, we tested two well-established Treg suppression methods: anti-CTLA-4 antibody therapy and CDK4/6 inhibition via palbociclib. CTLA-4 is an immune checkpoint receptor expressed on Tregs that downregulates immune responses by competing with CD28 for binding to B7 ligands on antigen-presenting cells (Walker et al. 2011). CDK4/6 are enzymes that regulate the G1/S checkpoint of the cell cycle, and their inhibition leads to cell cycle arrest and disruption of cell proliferation (Goel et al. 2022). It has been shown that CDK4/6i disrupts the proliferation of not only tumor cells but also immune cells, particularly Tregs (Goel et al. 2017; Zhang et al. 2023). Surprisingly, treatment with anti-CTLA-4 antibody did not change Treg levels in the spleens of the RP mice. This could be because the dose and timing of anti-CTLA-4 administration may have been insufficient to achieve effective Treg depletion in our model or because Tregs in SCLC may be less dependent on CTLA-4 signaling to function, as observed in other tumor types such as glioblastoma (Fecci et al. 2007). In contrast, palbociclib significantly reduced Treg numbers. This supports previous studies in breast and colorectal cancer models where CDK4/6i significantly reduced the $Foxp3^+$ Treg population (Deng et al. 2018; Goel et al. 2017).

Strikingly, RPM mice responded very well to palbociclib alone and in combination with the standard-of-care treatment in the clinics (chemotherapy + ICI). On the other hand, the RP tumors did not benefit from palbociclib alone, and additionally, they showed no improvement when exposed to the combination with chemotherapy and ICI. These results suggest that MMRd-SCLC may rely more on Treg-mediated immune suppression, which can lead to reactivation of the immune system when disrupted. A potential mechanism that enables the improved OS could be the CDK4/6i´s parallel effect on increasing effector T cell activation driven by the high neoantigen load in RPM tumors (S. Zhang et al. 2023). This was particularly effective in combination with chemotherapy and ICI, suggesting that an initial depletion of Tregs may boost the outcomes of both cytotoxic and immune-based treatments.

The combination of CDK4/6i and immunotherapy has drawn significant interest across various tumor entities. Although CDK4/6 inhibitors have been primarily utilized to disrupt tumor proliferation, they have been shown to impact immune cells, including reducing Treg proliferation and enhancing antigen presentation (Bonelli et al. 2019; S. Zhang et al. 2023). Of note, CDK4/6 treatment has been shown to sensitize melanoma to ICIs by promoting T-cell infiltration and reducing immunosuppression (Jerby-Arnon et al. 2018). Similarly, several early-phase clinical trials of NSCLC are investigating this combination as a strategy to overcome resistance to immunotherapy (Pujol et al. 2021). Importantly, the role of CDK4/6 inhibitors is currently being investigated in SCLC clinical trials. In particular, the ongoing phase II clinical study NCT03041311 assesses the combination of Trilaciclib, another CDK4/6i, with ICI and platinum-based chemotherapy in patients with ES-SCLC (Daniel et al. 2021; Goldschmidt et al. 2023). Preliminary results from this trial indicated that Trilaciclib significantly reduced severe neutropenia and enhanced peripheral T-cell clonal expansion, suggesting a favorable immunomodulatory effect without compromising anti-tumor efficacy. This ongoing trial highlights the clinical relevance of our findings, which can provide important insights and support the rationale for incorporating CDK4/6i in treatment regimens.

Nevertheless, a major drawback of using CDK4/6i to deplete Tregs is their non-specific activity. Besides interrupting Treg´s cell proliferation, they also arrest the cell cycle of tumor cells (Bonelli et al. 2019). This makes it difficult to interpret CDK4/6i effects, and

the improved survival observed in RPM mice might not be fully attributed to Treg suppression but also to cell-cycle arrest of highly proliferating tumor cells with deficient MMR. Furthermore, some studies have discussed CDK4/6i effects on effector immune cells (Schaer et al. 2018; Teh et al. 2020). Since the immune profile is not comprehensively investigated, the understanding of the immunological effects remains vague. In addition, several clinical trials reported serious toxicity of some CDK4/6 inhibitors, including palbociclib (Pujol et al. 2021; Yuan et al. 2021). The toxicity was mainly related to neutropenia, and it increased in combination with immunotherapy (S. Zhang et al. 2023). However, different inhibitors have distinct pharmacological activity and determining the most suitable agent and dosing schedule for every tumor type is essential. Some studies have suggested that reducing the duration of CDK4/6i treatment or including a short-term inhibition can achieve similar anti-tumor activity as a longer treatment (Jerby-Arnon et al. 2018; S. Zhang et al. 2023).

In summary, our study suggests that including an initial step of reducing the Treg number via CDK4/6 inhibition, could be a promising strategy to increase the survival outcomes in MMRd-SCLC co-treated with ICIs or chemotherapy. CDK4/6i can be particularly successful in combination with ICI in SCLC to convert this immunologically “cold” tumor into a “hot” one (S. Zhang et al. 2023). However, further research is required to understand its individual impact on cell cycle arrest, Treg suppression, and other immunological effects in order to fully define its role in the management of SCLC. Additionally, new studies should explore the safety and efficacy of CDK4/6i to exploit their full immunotherapeutic potential (Lelliott et al. 2022).

4.7 Immune profiling in murine SCLC models at baseline and following treatment via IMC

In this project, we used IMC to further characterize the immune infiltration patterns in our murine SCLC models (RPM and RP) at baseline (vehicle group) and under various treatment conditions. We established a high-dimensional imaging pipeline to analyze immune cells within tumor tissues and at the interface with normal lung tissue. Although our IMC panel initially included 35 markers, our quantitative analysis focused on a selected subset of the most important and relevant cell types, including

CD45$^+$ leukocytes, CD4$^+$ and CD8$^+$ T cells, CD19$^+$ B cells, and stromal cells identified by α-SMA and CD31 expression. This decision was made based on several factors. First, our staining results confirmed limited immune infiltration that is typical in murine and human SCLC tumors, consistent with previous reports describing SCLC as immunologically “cold” (Rudin et al. 2021). Additionally, we had to ensure the statistical robustness of this large and heterogeneous dataset. Lastly, we had practical constraints about the time and funding toward the end of the project. Therefore, the prioritization of the most abundant and biologically relevant cell populations allowed us to generate reproducible results even from this technically challenging dataset.

The IMC analysis confirmed and extended the previous findings from flow cytometry as well as complemented with some spatial information on the presence of immune cells in our murine SCLC models. At baseline, both RP and RPM tumors exhibited the classic immune-excluded phenotype, with the majority of CD45$^+$ cells accumulating at the tumor-normal lung border rather than penetrating the tumor core. The limited T cell infiltration is a hallmark of human SCLC and has been linked to poor immunotherapy response (Yang et al. 2018). Unlike NSCLC samples, RP and RPM tumors displayed a low and uneven distribution of infiltrating immune cells that seemed restricted in the vascular structures. The quantitative analysis further supported these observations by revealing low CD45$^+$ signals inside RP and RPM tumor tissues. This was more pronounced in the RPM samples, with even lower CD45$^+$ expression within tumor compartments than in RP. These findings suggest that both murine SCLC models display the typical immune “cold” phenotype, which is further enhanced in an MMR-deficient setting, possibly by reinforcing physical or molecular barriers. This mode of action has been proposed in other immune-excluded tumors as well (Joyce et al. 2015).

Further analysis of immune subsets revealed that CD4$^+$ and CD8$^+$ T cells were scarce across all samples and regions. This is consistent with the low activity of effector T-cell responses typically reported in SCLC (Baine et al. 2020; Rudin et al. 2021). Notably, we observed a significant difference in the presence of CD19$^+$ B cells. RPM tumors showed significantly lower B cell count than RP samples at baseline. This observation is in line with emerging evidence that links a higher B cell infiltration with increased anti-tumor immunity and improved survival outcomes (Helmink et al. 2020; Petitprez

et al. 2020). Significantly, this finding correlates with the survival experiments **(Figure 3.4c)**, in which RP mice exhibited a significantly prolonged survival at baseline compared to RPM. Thus, the higher presence of B cells in RP tumors may contribute to higher immune surveillance and lower tumor progression, a notion described in other solid tumors as well (Sharonov et al. 2020).

Next, we assessed the impact of different treatment regimens and observed limited effects on immune cell infiltration in central parts of the tumor, particularly in RPM. Surprisingly, the combination treatment with CDK4/6i, chemotherapy, and anti-PD-1 blockade led to significantly higher $CD45^+$ and $CD4^+$ T cells in RP tumors compared to RPM. This treatment also increased the stromal cell content in this model, which may reflect broader microenvironmental remodeling and contribute to improved immune cell trafficking. This phenomenon has been reported in other settings and has been shown to improve immunotherapy responses (Salmon et al. 2012).

However, there is a discrepancy between the IMC results and survival outcomes. While at baseline, higher B cell levels correlated with improved survival in RP mice compared to RPM, this correlation was not maintained after triple therapy. Although we observed higher $CD45^+$ and $CD4^+$ T cells within RP tumor cores compared to RPM, RPM mice survived significantly longer following treatment **(Figure 3.16d)**. This discrepancy suggests that survival outcomes after therapy cannot be explained by only the quantity of immune cells determined by IMC. Several explanations can be proposed. First, our IMC experiments captured the infiltration and spatial distribution of immune cells at only the endpoint of the experiment. Thus, this method may miss the dynamic processes involved at earlier time points, as previously pointed out in longitudinal studies of immunotherapy responses (Spitzer et al. 2017). Second, the total CD45+ and CD4+ pixel counts may not correlate with possible changes induced by the therapy, including enhanced antigen presentation or increased type I interferon signaling, which have been detected in immune priming triggered by CDK4/6i (Deng et al. 2018; Goel et al. 2017). Third, the improved survival outcomes in RPM could be attributed to tumor-intrinsic factors, such as increased sensitivity to DNA damage due to chemotherapy or enhanced tumor cell senescence by CDK4/6i. Both these mechanisms have been shown to enable anti-tumor activity (Barros et al. 2022; Goel et al. 2017). Moreover, changes in the stroma, including vessel structure and function,

might have improved drug delivery and oxygenation in RPM tumors without affecting immune infiltration patterns. Although the scope of this study does not include exploring any of these mechanisms, they are potential biological explanations to understand the lack of correlation between the immune system and survival outcomes in our setting.

Taken together, our findings suggest that overcoming the immune resistance in MMR-deficient SCLC tumors may require more complex therapy strategies that do not rely only on increasing T-cell infiltration. One option could be disrupting physical barriers to enable infiltration, which are very prominent in our murine SCLC samples, as previously suggested in fibrotic and desmoplastic tumors (Joyce et al. 2015). Additional insights into a broader range of immune cell subsets, spatial cell-cell interactions, and functional states of infiltrating cells in SCLC will be crucial to understanding the treatment impacts.

4.8 Implications for personalized medicine in SCLC

Personalized medicine has transformed cancer treatment by tailoring therapies based on molecular and immunological features of individual tumors (Goetz et al. 2018). However, this strategy is still not entirely applicable in SCLC, mainly due to limited tissue biopsies, the aggressive and rapid disease progression, and the lack of established molecular subtypes in clinical practice (George et al. 2015). Nonetheless, emerging data, like the ones reported in this study, highlight the potential importance of incorporating biomarkers such as TMB or MMRd status into clinical practice.

The newly generated RPM model demonstrates that MMRd in SCLC drives genomic instability and predicts sensitivity to immunotherapy and Treg suppression therapy. These findings align with literature reports in other cancer types, where MMRd and high TMB have been suggested as predictive biomarkers of response to ICIs. For instance, MMRd is an FDA-approved biomarker for anti-PD-1 administration in colorectal and endometrial cancers since anti-PD-1 treatment yields superior OS (Le et al. 2017). Similarly, high TMB is considered a potential predictor of immunotherapy benefits in NSCLC, with several ongoing clinical trials to confirm its utility (Hellmann et al. 2018; Rizvi et al. 2015).

In SCLC, the use of biomarkers to guide therapy approaches is still in the early stages. Nevertheless, our results suggest that the subset of patients presenting with MMR-deficient SCLC may benefit from PD-1 blockade or CDK4/6 inhibition. This opens the door for a new classification of SCLC based on genomic features. Therefore, we believe that integrating MMRd and TMB testing into routine diagnostic procedures could assist in building stratified treatment regimens. Additionally, these insights could help design clinical trials with more specific patient selection criteria, leading to potential increased clinical benefit and reduced exposure of some patients to unnecessary and ineffective drugs (Q. Liu et al. 2024; Westcott et al. 2023).

In summary, our study contributes to the growing body of evidence that supports the establishment of personalized treatments in SCLC. Incorporating genomic, molecular, and immunological biomarkers in standard molecular profiling in the clinics may transform SCLC clinical care from a one-size-fits-all strategy to individualized treatment approaches.

4.9 Study limitations and future directions

While our study provides a comprehensive characterization of a novel SCLC mouse model harboring MMRd and its therapeutic vulnerabilities, several limitations must be considered when interpreting these findings.

One important limitation is the fact that our GEMM does not incorporate tobacco-associated mutational signatures, which constitute the majority of human SCLC cases. Although the RPM model successfully generates a high TMB phenotype, it does not reflect the mutational composition driven by chronic smoking exposure. Instead, our RPM mouse line represents only a minority of human SCLC, approximately 15%, as reported in a recent cohort (Q. Liu et al. 2024). This narrows the translational potential of our findings by not covering the broader population of smoking-associated SCLC cases (George et al. 2015).

A second limitation of our model is the genetic simplicity. The RPM mouse incorporates only one MMR gene, *Msh2*, while human MMRd tumors often carry

alterations in multiple MMR genes, including *MSH6* or *PMS2* (Anon 2017; Hause et al. 2016). This important difference may account for variations in immune composition or therapy responses. Thus, while our model is valuable in understanding the loss of *Msh2* in SCLC, it does not capture the full heterogeneity of MMRd in patients.

Additionally, another drawback of our GEMM is the low metastatic potential. Both RPM and RP models rarely developed metastases, and if they did, they were mostly contained in the liver. This dramatically contrasts with human disease, which is highly invasive and characterized by early and rapid dissemination of metastases into the brain, bones, adrenal glands, and liver (Kalemkerian et al. 2013). This limitation does not allow for the investigation of the impact of MMRd in metastatic processes, immune responses in metastatic niches, or therapy resistance in such distal sites. This discrepancy could be explained by the differences in lung architecture and immune regulation of human and murine systems, and it underlines the need for a better representation of metastatic processes in preclinical SCLC models (Vanharanta et al. 2013).

Another important limitation of our study is linked to the extent of the immune profiling analysis. Our analyses were focused on assessing the immune cell composition and functional marker expression in effector T cells at the endpoint of tumors. However, a longitudinal analysis would be crucial to track how immune cell populations differ over time, which enables us to understand the kinetics of immune activation. Furthermore, while we provided more thorough insights into the immune composition inside and on the border of tumors when different therapy regimens were applied, we did not conduct high-resolution spatial profiling that could identify critical patterns in the immune microenvironment (Binnewies et al. 2018).

In addition to these constraints, we did not also explore other immunosuppressive pathways that could explain the lack of effective immune activation in RPM tumors. For instance, upregulation of TGF-β, IDO1, or MDSCs has been shown to dampen the immune activation induced by a high neoantigen load (Llosa et al. 2015; Spranger et al. 2015; Waldner et al. 2023). These mechanisms are well described in MMRd-colorectal and endometrial tumors. They should be evaluated in the future to improve the understanding of immune evasion in MMR-deficient SCLC cases.

Several limitations also apply to the therapeutic investigations used in this thesis. While we show that CDK4/6i via palbociclib can improve survival rates in RPM mice, its function is not exclusively due to Treg suppression. The primary activity of CDK4/6i is to induce the cell cycle arrest of cells, particularly proliferating tumor cells. In addition, CDK4/6i have been described as modulators of cytotoxic T cells or dendritic cells (Goel et al. 2022; S. Zhang et al. 2023). For this reason, the interpretation of the mode of action of palbociclib in our model is complicated. Moreover, we did not address any potential resistance mechanisms to ICIs or explore other combination therapies besides standard chemotherapy and CDK4/6i.

Another limitation of this study is the depth of IMC analysis. Although a 35-marker panel was established and staining protocols were optimized, the quantitative analysis focused on only a few immune cell types ($CD45^+$, $CD4^+$, $CD8^+$, and $CD19^+$ cells). This decision was necessary given the low immune infiltration observed in the stained samples, the complicated single-cell segmentation due to the densely packed tumor tissue, and practical constraints regarding the time and funding of this project. As a result, rare cell populations, functional markers, cell-cell interactions, and broader spatial analyses could not be conducted. Furthermore, IMC analysis was performed at the end of the treatment regimens and at a single time point, making it impossible to study the dynamics of therapy-induced changes in the immune microenvironment. Continuing the analysis of our existing dataset could reveal a broader understanding of therapeutic effects on our MMR-deficient SCLC mouse model compared to the standard RP mouse. Additionally, future studies should combine longitudinal IMC profiling with functional assays to provide a deeper understanding of how immune activation evolves over time under different therapies.

In summary, while the RPM model provides a physiologically relevant preclinical platform to gain valuable insights into MMR-deficient SCLC and its sensitivity to therapies, it does not fully recapitulate the genetic complexity, immune responses, and metastatic patterns of human SCLC. Addressing these limitations by generating more diverse models, performing longitudinal and spatial immune profiling, and expanding therapeutic options will be critical to fully disentangle the potential of personalized medicine in SCLC therapeutic approaches.

4.10 Outlook

The findings presented in this thesis provide new insights into how MMRd, specifically *Msh2* deletion, affects tumorigenesis, mutation load, and immune responses in SCLC. We successfully established a novel GEMM (RPM) by introducing *Msh2* loss in the well-characterized RP mouse model. We also show that the RPM model mimics important molecular properties of MMRd-SCLC, including high TMB, MMR-related mutational signatures, and an increased number of neoantigens.

However, further research is required to deepen the understanding of the impact of these mutations and neoantigens in the RPM model. For instance, CRISPR/Cas9 screening or an MHC-I binding assay could explore which neoantigens are actually immunogenic in RPM tumors. Additionally, longitudinal studies focusing on how RPM tumors change over time or under various treatment strategies could shed light on the mechanisms of immune escape and resistance to therapy.

In addition to genomic profiling, further studies should also investigate the tumor immune microenvironment in more detail. While this thesis indicates that MMR deficiency reshapes the immune microenvironment and promotes sensitivity to ICI, the immunosuppressive components of SCLC, including Tregs, MDSCs, and TAMs, remain not understood. Our IMC data should be further analyzed to retrieve spatial information, which, paired with spatial transcriptomics and single-cell RNA sequencing, could help characterize these cell types in detail.

Finally, the RPM model may serve as a preclinical platform to investigate new therapeutic strategies that exploit DNA repair deficiencies. For instance, synthetic lethality-based approaches (PARP or ATR inhibitors) or additional Treg-targeting therapies could have potential synergistic effects in combination with ICIs. Furthermore, personalized immunotherapies based on neoantigen profiling or immune cell properties might exhibit effectiveness in MMR-deficient SCLC.

In conclusion, our RPM model opens new avenues for conducting mechanistic explorations and translational research. The data generated from this thesis may contribute to the development of more precise and effective treatments for a subset of patients who are currently under-investigated.

References

Alexandrov, Ludmil B., Jaegil Kim, Nicholas J. Haradhvala, Mi Ni Huang, Alvin Wei Tian Ng, Yang Wu, Arnoud Boot, Kyle R. Covington, Dmitry A. Gordenin, Erik N. Bergstrom, S. M. Ashiqul Islam, Nuria Lopez-Bigas, Leszek J. Klimczak, John R. McPherson, Sandro Morganella, Radhakrishnan Sabarinathan, David A. Wheeler, Ville Mustonen, Gad Getz, Steven G. Rozen, Michael R. Stratton, Paul Boutros, Kin Chan, Akihiro Fujimoto, Marat Kazanov, Michael Lawrence, Iñigo Martincorena, Hidewaki Nakagawa, Paz Polak, Stephenie Prokopec, Steven A. Roberts, Natalie Saini, Tatsuhiro Shibata, Yuichi Shiraishi, Bin Tean Teh, Ignacio Vázquez-García, Fouad Yousif, and Willie Yu. 2020. "The Repertoire of Mutational Signatures in Human Cancer." *Nature* 578(7793):94–101. doi:10.1038/s41586-020-1943-3.

American Cancer Society. 2023. "What Is Lung Cancer?" https://www.cancer.org/cancer/types/lung-cancer/about/what-is.html.

Aseervatham, Jaya. 2023. "Dynamic Role of Exosome MicroRNAs in Cancer Cell Signaling and Their Emerging Role as Noninvasive Biomarkers." *Biology* 12(5).

Augustyn, Alexander, Mark Borromeo, Tao Wang, Junya Fujimoto, Chunli Shao, Patrick D. Dospoy, Victoria Lee, Christopher Tan, James P. Sullivan, Jill E. Larsen, Luc Girard, Carmen Behrens, Ignacio I. Wistuba, Yang Xie, Melanie H. Cobb, Adi F. Gazdar, Jane E. Johnson, John D. Minna, and Peter K. Vogt. 2014. "ASCL1 Is a Lineage Oncogene Providing Therapeutic Targets for High-Grade Neuroendocrine Lung Cancers." *Proceedings of the National Academy of Sciences of the United States of America* 111(41):14788–93. doi:10.1073/pnas.1410419111.

Azimnasab-sorkhabi, Parviz, Maryam Soltani-asl, Túlio Teruo Yoshinaga, Maria Lucia Zaidan Dagli, Cristina de Oliveira Massoco, and Jose Roberto Kfoury Junior. 2023. "Indoleamine-2,3 Dioxygenase: A Fate-Changer of the Tumor Microenvironment." *Molecular Biology Reports* 50(7):6133–45.

Baine, Marina K., Min Shu Hsieh, W. Victoria Lai, Jacklynn V. Egger, Achim A. Jungbluth, Yahya Daneshbod, Amanda Beras, Rowanne Spencer, Jessica Lopardo, Francis Bodd, Joseph Montecalvo, Jennifer L. Sauter, Jason C. Chang, Darren J. Buonocore, William D. Travis, Triparna Sen, John T. Poirier, Charles M. Rudin, and Natasha Rekhtman. 2020. "SCLC Subtypes Defined by ASCL1, NEUROD1, POU2F3, and YAP1: A Comprehensive Immunohistochemical and Histopathologic Characterization." *Journal of Thoracic Oncology* 15(12):1823–35. doi:10.1016/j.jtho.2020.09.009.

Barayan, Ranya, Xiaozhuo Ran, and Benjamin H. Lok. 2020. "PARP Inhibitors for Small Cell Lung Cancer and Their Potential for Integration into Current Treatment Approaches." *Journal of Thoracic Disease* 12(10):6240–52.

Barros, Eliana M., Stuart A. McIntosh, and Kienan I. Savage. 2022. "The DNA Damage Induced Immune Response: Implications for Cancer Therapy." *DNA Repair* 120. doi:10.1016/j.dnarep.2022.103409.

Batur, Sebnem, Dogu Vuralli Bakkaloglu, Nuray Kepil, and Sibel Erdamar. 2016. "Microsatellite Instability and B-Type Raf Proto-Oncogene Mutation in Colorectal Cancer: Clinicopathological Characteristics and Effects on Survival." *Bosnian Journal of Basic Medical Sciences* 16(4):254–60. doi:10.17305/bjbms.2016.1238.

Binnewies, Mikhail, Edward W. Roberts, Kelly Kersten, Vincent Chan, Douglas F. Fearon, Miriam Merad, Lisa M. Coussens, Dmitry I. Gabrilovich, Suzanne Ostrand-Rosenberg,

Catherine C. Hedrick, Robert H. Vonderheide, Mikael J. Pittet, Rakesh K. Jain, Weiping Zou, T. Kevin Howcroft, Elisa C. Woodhouse, Robert A. Weinberg, and Matthew F. Krummel. 2018. “Understanding the Tumor Immune Microenvironment (TIME) for Effective Therapy.” *Nature Medicine* 24(5):541–50. doi:10.1038/s41591-018-0014-x.

Bonelli, Mara, Silvia La Monica, Claudia Fumarola, and Roberta Alfieri. 2019. “Multiple Effects of CDK4/6 Inhibition in Cancer: From Cell Cycle Arrest to Immunomodulation.” *Biochemical Pharmacology* 170.

Borlongan, Mia C., Dipongkor Saha, and Hongbin Wang. 2024. “Tumor Microenvironment: A Niche for Cancer Stem Cell Immunotherapy.” *Stem Cell Reviews and Reports* 20(1):3–24.

Bouffet, Eric, Valérie Larouche, Brittany B. Campbell, Daniele Merico, Richard De Borja, Melyssa Aronson, Carol Durn, Joerg Krueger, Vanja Cabric, Vijay Ramaswamy, Nataliya Zhukova, Gary Mason, Roula Farah, Samina Afzal, Michal Yalon, Gideon Rechavi, Vanan Magimairajan, Michael F. Walsh, Shlomi Constantini, Rina Dvir, Ronit Elhasid, Alyssa Reddy, Michael Osborn, Michael Sullivan, Jordan Hansford, Andrew Dodgshun, Nancy Klauber-Demore, Lindsay Peterson, Sunil Patel, Scott Lindhorst, Jeffrey Atkinson, Zane Cohen, Rachel Laframboise, Peter Dirks, Michael Taylor, David Malkin, Steffen Albrecht, Roy W. R. Dudley, Nada Jabado, Cynthia E. Hawkins, Adam Shlien, and Uri Tabori. 2016. “Immune Checkpoint Inhibition for Hypermutant Glioblastoma Multiforme Resulting from Germline Biallelic Mismatch Repair Deficiency.” *Journal of Clinical Oncology* 34(19):2206–11. doi:10.1200/JCO.2016.66.6552.

Byers, Lauren Averett, and Charles M. Rudin. 2015. “Small Cell Lung Cancer: Where Do We Go from Here?” *Cancer* 121(5):664–72.

Chen, Baode, Chenglin Mu, Zhiwei Zhang, Xuelin He, and Xia Liu. 2022. “The Love-Hate Relationship Between TGF-β Signaling and the Immune System During Development and Tumorigenesis.” *Frontiers in Immunology* 13.

Chen, Yunfei, Hui Li, and Yun Fan. 2023a. “Shaping the Tumor Immune Microenvironment of SCLC: Mechanisms, and Opportunities for Immunotherapy.” *Cancer Treatment Reviews* 120.

Chen, Yunfei, Hui Li, and Yun Fan. 2023b. “Shaping the Tumor Immune Microenvironment of SCLC: Mechanisms, and Opportunities for Immunotherapy.” *Cancer Treatment Reviews* 120.

Cheng, Weishi, Kai Kang, Ailin Zhao, and Yijun Wu. 2024. “Dual Blockade Immunotherapy Targeting PD-1/PD-L1 and CTLA-4 in Lung Cancer.” *Journal of Hematology and Oncology* 17(1).

Crisafulli, Giovanni. 2024. “Mutational Signatures in Colorectal Cancer: Translational Insights, Clinical Applications, and Limitations.” *Cancers* 16(17).

Dai, Jie, Yangzhou Su, Suye Zhong, Li Cong, Bang Liu, Junjun Yang, Yongguang Tao, Zuping He, Chao Chen, and Yiqun Jiang. 2020. “Exosomes: Key Players in Cancer and Potential Therapeutic Strategy.” *Signal Transduction and Targeted Therapy* 5(1).

Dakal, Tikam Chand, Bhanupriya Dhabhai, Anuja Pant, Kareena Moar, Kanika Chaudhary, Vikas Yadav, Vipin Ranga, Narendra Kumar Sharma, Abhishek Kumar, Pawan Kumar Maurya, Jarek Maciaczyk, Ingo G. H. Schmidt-Wolf, and Amit Sharma. 2024. “Oncogenes and Tumor Suppressor Genes: Functions and Roles in Cancers.” *MedComm* 5(6).

Daniel, Davey, Vladimer Kuchava, Igor Bondarenko, Oleksandr Ivashchuk, Sreekanth Reddy, Jana Jaal, Iveta Kudaba, Lowell Hart, Amiran Matitashvili, Yili Pritchett, Shannon R.

Morris, Jessica A. Sorrentino, Joyce M. Antal, and Jerome Goldschmidt. 2021. "Trilaciclib Prior to Chemotherapy and Atezolizumab in Patients with Newly Diagnosed Extensive-Stage Small Cell Lung Cancer: A Multicentre, Randomised, Double-Blind, Placebo-Controlled Phase II Trial." *International Journal of Cancer* 148(10):2557–70. doi:10.1002/ijc.33453.

Deng, Jiehui, Eric S. Wang, Russell W. Jenkins, Shuai Li, Ruben Dries, Kathleen Yates, Sandeep Chhabra, Wei Huang, Hongye Liu, Amir R. Aref, Elena Ivanova, Cloud P. Paweletz, Michaela Bowden, Chensheng W. Zhou, Grit S. Herter-Sprie, Jessica A. Sorrentino, John E. Bisi, Patrick H. Lizotte, Ashley A. Merlino, Max M. Quinn, Lauren E. Bufe, Annan Yang, Yanxi Zhang, Hua Zhang, Peng Gao, Ting Chen, Megan E. Cavanaugh, Amanda J. Rode, Eric Haines, Patrick J. Roberts, Jay C. Strum, William G. Richards, Jochen H. Lorch, Sareh Parangi, Viswanath Gunda, Genevieve M. Boland, Raphael Bueno, Sangeetha Palakurthi, Gordon J. Freeman, Jerome Ritz, W. Nicholas Haining, Norman E. Sharpless, Haribabu Arthanari, Geoffrey I. Shapiro, David A. Barbie, Nathanael S. Gray, and Kwok Kin Wong. 2018. "CDK4/6 Inhibition Augments Antitumor Immunity by Enhancing T-Cell Activation." *Cancer Discovery* 8(2):216–33. doi:10.1158/2159-8290.CD-17-0915.

Denninghoff, Valeria, Alessandro Russo, Diego de Miguel-Pérez, Umberto Malapelle, Amin Benyounes, Allison Gittens, Andres Felipe Cardona, and Christian Rolfo. 2021. "Small Cell Lung Cancer: State of the Art of the Molecular and Genetic Landscape and Novel Perspective." *Cancers* 13(7).

Depristo, Mark A., Eric Banks, Ryan Poplin, Kiran V. Garimella, Jared R. Maguire, Christopher Hartl, Anthony A. Philippakis, Guillermo Del Angel, Manuel A. Rivas, Matt Hanna, Aaron McKenna, Tim J. Fennell, Andrew M. Kernytsky, Andrey Y. Sivachenko, Kristian Cibulskis, Stacey B. Gabriel, David Altshuler, and Mark J. Daly. 2011. "A Framework for Variation Discovery and Genotyping Using Next-Generation DNA Sequencing Data." *Nature Genetics* 43(5):491–501. doi:10.1038/ng.806.

Dietlein, Felix, and H. Christian Reinhardt. 2014. "Molecular Pathways: Exploiting Tumor-Specific Molecular Defects in DNA Repair Pathways for Precision Cancer Therapy." *Clinical Cancer Research* 20(23):5882–87. doi:10.1158/1078-0432.CCR-14-1165.

Dietlein, Felix, Lisa Thelen, and H. Christian Reinhardt. 2014a. "Cancer-Specific Defects in DNA Repair Pathways as Targets for Personalized Therapeutic Approaches." *Trends in Genetics* 30(8):326–39.

Dietlein, Felix, Lisa Thelen, and H. Christian Reinhardt. 2014b. "Cancer-Specific Defects in DNA Repair Pathways as Targets for Personalized Therapeutic Approaches." *Trends in Genetics* 30(8):326–39.

Dilruba, Shahana, and Ganna V. Kalayda. 2016. "Platinum-Based Drugs: Past, Present and Future." *Cancer Chemotherapy and Pharmacology* 77(6):1103–24.

Ding, Jianhua, and Chaihong Yeong. 2024. "Advances in DLL3-Targeted Therapies for Small Cell Lung Cancer: Challenges, Opportunities, and Future Directions." *Frontiers in Oncology* 14.

Dingemans, A. M. C., M. Früh, A. Ardizzoni, B. Besse, C. Faivre-Finn, L. E. Hendriks, S. Lantuejoul, S. Peters, N. Reguart, C. M. Rudin, D. De Ruysscher, P. E. Van Schil, J. Vansteenkiste, and M. Reck. 2021. "Small-Cell Lung Cancer: ESMO Clinical Practice Guidelines for Diagnosis, Treatment and Follow-Up☆." *Annals of Oncology* 32(7):839–53. doi:10.1016/j.annonc.2021.03.207.

Dong, Liu, Haoqin Jiang, Zhihua Kang, and Ming Guan. 2023. “Biomarkers for Chemotherapy and Drug Resistance in the Mismatch Repair Pathway.” *Clinica Chimica Acta* 544.

Dora, David, Christopher Rivard, Hui Yu, Shivaun Lueke Pickard, Viktoria Laszlo, Tunde Harko, Zsolt Megyesfalvi, Elek Dinya, Csongor Gerdan, Gabor Szegvari, Fred R. Hirsch, Balazs Dome, and Zoltan Lohinai. 2021. “Characterization of Tumor-associated Macrophages and the Immune Microenvironment in Limited-stage Neuroendocrine-high and -low Small Cell Lung Cancer.” *Biology* 10(6). doi:10.3390/biology10060502.

Dowling, Mark R., Andrey Kan, Susanne Heinzel, Julia M. Marchingo, Philip D. Hodgkin, and Edwin D. Hawkins. 2018a. “Regulatory T Cells Suppress Effector T Cell Proliferation by Limiting Division Destiny.” *Frontiers in Immunology* 9. doi:10.3389/fimmu.2018.02461.

Dowling, Mark R., Andrey Kan, Susanne Heinzel, Julia M. Marchingo, Philip D. Hodgkin, and Edwin D. Hawkins. 2018b. “Regulatory T Cells Suppress Effector T Cell Proliferation by Limiting Division Destiny.” *Frontiers in Immunology* 9. doi:10.3389/fimmu.2018.02461.

Dumoulin, Daphne W., Paolo Bironzo, and Francesco Passiglia. 2023. “Rare Thoracic Cancers: A Comprehensive Overview of Diagnosis and Management of Small Cell Lung Cancer, Malignant Pleural Mesothelioma and Thymic Epithelial Tumours.” *European Respiratory Review* 32(167). doi:10.1183/16000617.0174-2022.

Dyson, Nicholas J. 2016. “RB1: A Prototype Tumor Suppressor and an Enigma.” doi:10.1101/gad.282145.

Edelbrock, Michael A., Saravanan Kaliyaperumal, and Kandace J. Williams. 2013. “Structural, Molecular and Cellular Functions of MSH2 and MSH6 during DNA Mismatch Repair, Damage Signaling and Other Noncanonical Activities.” *Mutation Research - Fundamental and Molecular Mechanisms of Mutagenesis* 743–744:53–66.

Eerkens, Anneke L., Koen Brummel, Annegé Vledder, Sterre T. Paijens, Marta Requesens, Dominik Loiero, Nienke van Rooij, Annechien Plat, Floris Jan Haan, Patty Klok, Refika Yigit, Thijs Roelofsen, Natascha M. de Lange, Rie Klomp, David Church, Arja ter Elst, René Wardenaar, Diana Spierings, Floris Foijer, Viktor Hendrik Koelzer, Tjalling Bosse, Joost Bart, Mathilde Jalving, Anna K. L. Reyners, Marco de Bruyn, and Hans W. Nijman. 2024. “Neoadjuvant Immune Checkpoint Blockade in Women with Mismatch Repair Deficient Endometrial Cancer: A Phase I Study.” *Nature Communications* 15(1). doi:10.1038/s41467-024-52098-8.

Farid, Saira, and Stephen V. Liu. 2020. “Chemo-Immunotherapy as First-Line Treatment for Small-Cell Lung Cancer.” *Therapeutic Advances in Medical Oncology* 12.

Farmanbar, Amir, Sanaz Firouzi, Robert Kneller, and Hossein Khiabanian. 2022. “Mutational Signatures Reveal Ternary Relationships between Homologous Recombination Repair, APOBEC, and Mismatch Repair in Gynecological Cancers.” *Journal of Translational Medicine* 20(1). doi:10.1186/s12967-022-03259-0.

FDA. 2017. *HIGHLIGHTS OF PRESCRIBING INFORMATION*. www.fda.gov/medwatch.

FDA. 2019. *HIGHLIGHTS OF PRESCRIBING INFORMATION*. www.fda.gov/medwatch.

FDA. 2020. *HIGHLIGHTS OF PRESCRIBING INFORMATION*. www.fda.gov/medwatch.

Fecci, Peter E., Hidenobu Ochiai, Duane A. Mitchell, Peter M. Grossi, Alison E. Sweeney, Gary E. Archer, Thomas Cummings, James P. Allison, Darell D. Bigner, and John H. Sampson. 2007. “Systemic CTLA-4 Blockade Ameliorates Glioma-Induced Changes to the CD4 + T Cell Compartment without Affecting Regulatory T-Cell Function.” *Clinical Cancer Research* 13(7):2158–67. doi:10.1158/1078-0432.CCR-06-2070.

Florea, Ana Maria, and Dietrich Büsselberg. 2011. “Cisplatin as an Anti-Tumor Drug: Cellular Mechanisms of Activity, Drug Resistance and Induced Side Effects.” *Cancers* 3(1):1351–71.

Frankish, Adam, Mark Diekhans, Irwin Jungreis, Julien Lagarde, Jane E. Loveland, Jonathan M. Mudge, Cristina Sisu, James C. Wright, Joel Armstrong, If Barnes, Andrew Berry, Alexandra Bignell, Carles Boix, Silvia Carbonell Sala, Fiona Cunningham, Tomás Di Domenico, Sarah Donaldson, Ian T. Fiddes, Carlos García Girón, Jose Manuel Gonzalez, Tiago Grego, Matthew Hardy, Thibaut Hourlier, Kevin L. Howe, Toby Hunt, Osagie G. Izuogu, Rory Johnson, Fergal J. Martin, Laura Martínez, Shamika Mohanan, Paul Muir, Fabio C. P. Navarro, Anne Parker, Baikang Pei, Fernando Pozo, Ferriol Calvet Riera, Magali Ruffier, Bianca M. Schmitt, Eloise Stapleton, Marie Marthe Suner, Irina Sycheva, Barbara Uszczynska-Ratajczak, Maxim Y. Wolf, Jinuri Xu, Yucheng T. Yang, Andrew Yates, Daniel Zerbino, Yan Zhang, Jyoti S. Choudhary, Mark Gerstein, Roderic Guigó, Tim J. P. Hubbard, Manolis Kellis, Benedict Paten, Michael L. Tress, and Paul Flicek. 2021. “GENCODE 2021.” *Nucleic Acids Research* 49(D1):D916–23. doi:10.1093/nar/gkaa1087.

Friker, Lea L., Thomas Perwein, Andreas Waha, Evelyn Dörner, Rebecca Klein, Mirjam Blattner-Johnson, Julian P. Layer, Dominik Sturm, Gunther Nussbaumer, Robert Kwiecien, Isabel Spier, Stefan Aretz, Kornelius Kerl, Ulrike Hennewig, Marius Rohde, Axel Karow, Ingmar Bluemcke, Ann Kristin Schmitz, Harald Reinhard, Pablo Hernáiz Driever, Susanne Wendt, Annette Weiser, Ana S. Guerreiro Stücklin, Nicolas U. Gerber, André O. von Bueren, Claudia Khurana, Norbert Jorch, Maria Wiese, Christian P. Kratz, Matthias Eyrich, Michael Karremann, Ulrich Herrlinger, Michael Hölzel, David T. W. Jones, Marion Hoffmann, Torsten Pietsch, Gerrit H. Gielen, and Christof M. Kramm. 2025. “MSH2, MSH6, MLH1, and PMS2 Immunohistochemistry as Highly Sensitive Screening Method for DNA Mismatch Repair Deficiency Syndromes in Pediatric High-Grade Glioma.” *Acta Neuropathologica* 149(1):11. doi:10.1007/s00401-025-02846-x.

Ganti, Apar Kishor P., Billy W. Loo, Michael Bassetti, Collin Blakely, Anne Chiang, Thomas A. D’Amico, Christopher D’Avella, Afshin Dowlati, Robert J. Downey, Martin Edelman, Charles Florsheim, Kathryn A. Gold, Jonathan W. Goldman, John C. Grecula, Christine Hann, Wade Iams, Puneeth Iyengar, Karen Kelly, Maya Khalil, Marianna Koczywas, Robert E. Merritt, Nisha Mohindra, Julian Molina, Cesar Moran, Saraswati Pokharel, Sonam Puri, Angel Qin, Chad Rusthoven, Jacob Sands, Rafael Santana-Davila, Michael Shafique, Saiama N. Waqar, Kristina M. Gregory, and Miranda Hughes. 2021. “Small Cell Lung Cancer, Version 2.2022.” *JNCCN Journal of the National Comprehensive Cancer Network* 19(12):1441–64. doi:10.6004/JNCCN.2021.0058.

Garcia-Garijo, Andrea, Carlos Alberto Fajardo, and Alena Gros. 2019. “Determinants for Neoantigen Identification.” *Frontiers in Immunology* 10(JUN).

Gatalica, Zoran, Semir Vranic, Joanne Xiu, Jeffrey Swensen, and Sandeep Reddy. 2016. “High Microsatellite Instability (MSI-H) Colorectal Carcinoma: A Brief Review of Predictive Biomarkers in the Era of Personalized Medicine.” *Familial Cancer* 15(3):405–12.

Gay, Carl M., C. Allison Stewart, Elizabeth M. Park, Lixia Diao, Sarah M. Groves, Simon Heeke, Barzin Y. Nabet, Junya Fujimoto, Luisa M. Solis, Wei Lu, Yuanxin Xi, Robert J. Cardnell, Qi Wang, Giulia Fabbri, Kasey R. Cargill, Natalie I. Vokes, Kavya Ramkumar, Bingnan Zhang, Carminia M. Della Corte, Paul Robson, Stephen G. Swisher, Jack A. Roth, Bonnie S. Glisson, David S. Shames, Ignacio I. Wistuba, Jing Wang, Vito Quaranta, John Minna, John V. Heymach, and Lauren Averett Byers. 2021. “Patterns of

Transcription Factor Programs and Immune Pathway Activation Define Four Major Subtypes of SCLC with Distinct Therapeutic Vulnerabilities." *Cancer Cell* 39(3):346-360.e7. doi:10.1016/j.ccell.2020.12.014.

Gazdar, Adi F., Paul A. Bunn, and John D. Minna. 2017. "Small-Cell Lung Cancer: What We Know, What We Need to Know and the Path Forward." *Nature Reviews Cancer* 17(12):725–37.

Gebert, Johannes, Ozkan Gelincik, Mine Oezcan-Wahlbrink, Jason D. Marshall, Alejandro Hernandez-Sanchez, Katharina Urban, Mark Long, Eduardo Cortes, Elena Tosti, Eva Maria Katzenmaier, Yurong Song, Ali Elsaadi, Nan Deng, Eduardo Vilar, Vera Fuchs, Nina Nelius, Yan P. Yuan, Aysel Ahadova, Shizuko Sei, Robert H. Shoemaker, Asad Umar, Lei Wei, Song Liu, Peer Bork, Winfried Edelmann, Magnus von Knebel Doeberitz, Steven M. Lipkin, and Matthias Kloor. 2021. "Recurrent Frameshift Neoantigen Vaccine Elicits Protective Immunity With Reduced Tumor Burden and Improved Overall Survival in a Lynch Syndrome Mouse Model." *Gastroenterology* 161(4):1288-1302.e13. doi:10.1053/j.gastro.2021.06.073.

Gelibter, Alain, Angela Asquino, Lidia Strigari, Ilaria Grazia Zizzari, Lucrezia Tuosto, Fabio Scirocchi, Angelica Pace, Marco Siringo, Elisa Tramontano, Serena Bianchini, Filippo Bellati, Andrea Botticelli, Donatella Paoli, Daniele Santini, Marianna Nuti, Aurelia Rughetti, and Chiara Napoletano. 2024. "CD137+ and Regulatory T Cells as Independent Prognostic Factors of Survival in Advanced Non-Oncogene Addicted NSCLC Patients Treated with Immunotherapy as First-Line." *Journal of Translational Medicine* 22(1). doi:10.1186/s12967-024-05142-6.

George, Julie, Jing Shan Lim, Se Jin Jang, Yupeng Cun, Luka Ozretia, Gu Kong, Frauke Leenders, Xin Lu, Lynnette Fernández-Cuesta, Graziella Bosco, Christian Müller, Ilona Dahmen, Nadine S. Jahchan, Kwon Sik Park, Dian Yang, Anthony N. Karnezis, Dedeepya Vaka, Angela Torres, Maia Segura Wang, Jan O. Korbel, Roopika Menon, Sung Min Chun, Deokhoon Kim, Matt Wilkerson, Neil Hayes, David Engelmann, Brigitte Pützer, Marc Bos, Sebastian Michels, Ignacija Vlasic, Danila Seidel, Berit Pinther, Philipp Schaub, Christian Becker, Janine Altmüller, Jun Yokota, Takashi Kohno, Reika Iwakawa, Koji Tsuta, Masayuki Noguchi, Thomas Muley, Hans Hoffmann, Philipp A. Schnabel, Iver Petersen, Yuan Chen, Alex Soltermann, Verena Tischler, Chang Min Choi, Yong Hee Kim, Pierre P. Massion, Yong Zou, Dragana Jovanovic, Milica Kontic, Gavin M. Wright, Prudence A. Russell, Benjamin Solomon, Ina Koch, Michael Lindner, Lucia A. Muscarella, Annamaria La Torre, John K. Field, Marko Jakopovic, Jelena Knezevic, Esmeralda Castaños-Vélez, Luca Roz, Ugo Pastorino, Odd Terje Brustugun, Marius Lund-Iversen, Erik Thunnissen, Jens Köhler, Martin Schuler, Johan Botling, Martin Sandelin, Montserrat Sanchez-Cespedes, Helga B. Salvesen, Viktor Achter, Ulrich Lang, Magdalena Bogus, Peter M. Schneider, Thomas Zander, Sascha Ansén, Michael Hallek, Jürgen Wolf, Martin Vingron, Yasushi Yatabe, William D. Travis, Peter Nürnberg, Christian Reinhardt, Sven Perner, Lukas Heukamp, Reinhard Büttner, Stefan A. Haas, Elisabeth Brambilla, Martin Peifer, Julien Sage, and Roman K. Thomas. 2015. "Comprehensive Genomic Profiles of Small Cell Lung Cancer." *Nature* 524(7563):47–53. doi:10.1038/nature14664.

George, Julie, Lukas Maas, Nima Abedpour, Maria Cartolano, Laura Kaiser, Rieke N. Fischer, Andreas H. Scheel, Jan Philipp Weber, Martin Hellmich, Graziella Bosco, Caroline Volz, Christian Mueller, Ilona Dahmen, Felix John, Cleidson Padua Alves, Lisa Werr, Jens Peter Panse, Martin Kirschner, Walburga Engel-Riedel, Jessica Jürgens, Erich Stoelben,

Michael Brockmann, Stefan Grau, Martin Sebastian, Jan A. Stratmann, Jens Kern, Horst Dieter Hummel, Balazs Hegedüs, Martin Schuler, Till Plönes, Clemens Aigner, Thomas Elter, Karin Toepelt, Yon Dschun Ko, Sylke Kurz, Christian Grohé, Monika Serke, Katja Höpker, Lars Hagmeyer, Fabian Doerr, Khosro Hekmath, Judith Strapatsas, Karl Otto Kambartel, Geothy Chakupurakal, Annette Busch, Franz Georg Bauernfeind, Frank Griesinger, Anne Luers, Wiebke Dirks, Rainer Wiewrodt, Andrea Luecke, Ernst Rodermann, Andreas Diel, Volker Hagen, Kai Severin, Roland T. Ullrich, Hans Christian Reinhardt, Alexander Quaas, Magdalena Bogus, Cornelius Courts, Peter Nürnberg, Kerstin Becker, Viktor Achter, Reinhard Büttner, Jürgen Wolf, Martin Peifer, and Roman K. Thomas. 2024. "Evolutionary Trajectories of Small Cell Lung Cancer under Therapy." *Nature* 627(8005):880–89. doi:10.1038/s41586-024-07177-7.

Germano, Giovanni, Nabil Amirouchene-Angelozzi, Giuseppe Rospo, and Alberto Bardelli. 2018. "The Clinical Impact of the Genomic Landscape of Mismatch Repair–Deficient Cancers." *Cancer Discovery* 8(12):1518–28.

Giesen, Charlotte, Hao A. O. Wang, Denis Schapiro, Nevena Zivanovic, Andrea Jacobs, Bodo Hattendorf, Peter J. Schüffler, Daniel Grolimund, Joachim M. Buhmann, Simone Brandt, Zsuzsanna Varga, Peter J. Wild, Detlef Günther, and Bernd Bodenmiller. 2014. "Highly Multiplexed Imaging of Tumor Tissues with Subcellular Resolution by Mass Cytometry." *Nature Methods* 11(4):417–22. doi:10.1038/nmeth.2869.

Glatzer, Markus, Sabine Schmid, Marco Radovic, Martin Früh, and Paul Martin Putora. 2017. "The Role of Radiation Therapy in the Management of Small Cell Lung Cancer." *Breathe* 13(4):e87–94.

Goel, Shom, Johann S. Bergholz, and Jean J. Zhao. 2022. "Targeting CDK4 and CDK6 in Cancer." *Nature Reviews Cancer* 22(6):356–72.

Goel, Shom, Molly J. Decristo, April C. Watt, Haley Brinjones, Jaclyn Sceneay, Ben B. Li, Naveed Khan, Jessalyn M. Ubellacker, Shaozhen Xie, Otto Metzger-Filho, Jeremy Hoog, Matthew J. Ellis, Cynthia X. Ma, Susanne Ramm, Ian E. Krop, Eric P. Winer, Thomas M. Roberts, Hye Jung Kim, Sandra S. McAllister, and Jean J. Zhao. 2017. "CDK4/6 Inhibition Triggers Anti-Tumour Immunity." *Nature* 548(7668):471–75. doi:10.1038/nature23465.

Goetz, Laura H., and Nicholas J. Schork. 2018. "Personalized Medicine: Motivation, Challenges, and Progress." *Fertility and Sterility* 109(6):952–63.

Goldschmidt, Jerome, Lowell Hart, Jeffrey Scott, Kristen Boykin, Ray Bailey, Trevor Heritage, Lorena Lopez-Gonzalez, Zheng Yi Zhou, Marie Louise Edwards, Alisha Monnette, Augustina Ogbonnaya, Kathryn Deyoung, Divea Venkatasetty, Ping Shi, Lindsay Aton, Huan Huang, Paul R. Conkling, and Lucio Gordan. 2023. "Real-World Outcomes of Trilaciclib Among Patients with Extensive-Stage Small Cell Lung Cancer Receiving Chemotherapy." *Advances in Therapy* 40(10):4189–4215.

Gurjao, Carino, Dina Tsukrov, Maxim Imakaev, Lovelace J. Luquette, and Leonid A. Mirny. 2020. "Is Tumor Mutational Burden Predictive of Response to Immunotherapy?"

Hamilton, Gerhard, and Barbara Rath. 2019. "Immunotherapy for Small Cell Lung Cancer: Mechanisms of Resistance." *Expert Opinion on Biological Therapy* 19(5):423–32.

Hanahan, Douglas, and Robert A. Weinberg. 2011. "Hallmarks of Cancer: The next Generation." *Cell* 144(5):646–74.

Hause, Ronald J., Colin C. Pritchard, Jay Shendure, and Stephen J. Salipante. 2016. "Classification and Characterization of Microsatellite Instability across 18 Cancer Types." *Nature Medicine* 22(11):1342–50. doi:10.1038/nm.4191.

He, Yuchen, Luyuan Zhang, Ruoyu Zhou, Yumin Wang, and Hao Chen. 2022. "The Role of DNA Mismatch Repair in Immunotherapy of Human Cancer." *International Journal of Biological Sciences* 18(7):2821–32.

Hellmann, Matthew D., Margaret K. Callahan, Mark M. Awad, Emiliano Calvo, Paolo A. Ascierto, Akin Atmaca, Naiyer A. Rizvi, Fred R. Hirsch, Giovanni Selvaggi, Joseph D. Szustakowski, Ariella Sasson, Ryan Golhar, Patrik Vitazka, Han Chang, William J. Geese, and Scott J. Antonia. 2018. "Tumor Mutational Burden and Efficacy of Nivolumab Monotherapy and in Combination with Ipilimumab in Small-Cell Lung Cancer." *Cancer Cell* 33(5):853-861.e4. doi:10.1016/j.ccell.2018.04.001.

Helmink, and S. Z. K. Woodman. 2020. "B Cells and Tertiary Lymphoid Structures Promote Immunotherapy." *Nature* 577(7791):549–55. doi:10.1038/s41586-0191922-8.

Hiddinga, Birgitta I., Jo Raskin, Annelies Janssens, Patrick Pauwels, and Jan P. Van Meerbeeck. 2021a. "Recent Developments in the Treatment of Small Cell Lung Cancer." *European Respiratory Review* 30(161).

Hiddinga, Birgitta I., Jo Raskin, Annelies Janssens, Patrick Pauwels, and Jan P. Van Meerbeeck. 2021b. "Recent Developments in the Treatment of Small Cell Lung Cancer." *European Respiratory Review* 30(161).

Hoang, Phuc H., and Maria Teresa Landi. 2022. "DNA Methylation in Lung Cancer: Mechanisms and Associations with Histological Subtypes, Molecular Alterations, and Major Epidemiological Factors." *Cancers* 14(4).

Horita, Nobuyuki, Masaki Yamamoto, Takashi Sato, Toshinori Tsukahara, Hideyuki Nagakura, Ken Tashiro, Yuji Shibata, Hiroki Watanabe, Kenjiro Nagai, Miyo Inoue, Kentaro Nakashima, Ryota Ushio, Masaharu Shinkai, Makoto Kudo, and Takeshi Kaneko. 2015. "Topotecan for Relapsed Small-Cell Lung Cancer: Systematic Review and Meta-Analysis of 1347 Patients." *Scientific Reports* 5. doi:10.1038/srep15437.

Horn, Leora, Aaron S. Mansfield, Aleksandra Szczęsna, Libor Havel, Maciej Krzakowski, Maximilian J. Hochmair, Florian Huemer, György Losonczy, Melissa L. Johnson, Makoto Nishio, Martin Reck, Tony Mok, Sivuonthanh Lam, David S. Shames, Juan Liu, Beiying Ding, Ariel Lopez-Chavez, Fairooz Kabbinavar, Wei Lin, Alan Sandler, and Stephen V. Liu. 2018. "First-Line Atezolizumab plus Chemotherapy in Extensive-Stage Small-Cell Lung Cancer." *New England Journal of Medicine* 379(23):2220–29. doi:10.1056/nejmoa1809064.

Huang, Yu Han, Olaf Klingbeil, Xue Yan He, Xiaoli S. Wu, Gayatri Arun, Bin Lu, Tim D. D. Somerville, Joseph P. Milazzo, John E. Wilkinson, Osama E. Demerdash, David L. Spector, Mikala Egeblad, Junwei Shi, and Christopher R. Vakoc. 2018. "POU2F3 Is a Master Regulator of a Tuft Cell-like Variant of Small Cell Lung Cancer." *Genes and Development* 32(13–14):915–28. doi:10.1101/gad.314815.118.

Hung, Ming Chun, Wan Ping Wang, and Ya Hui Chi. 2022. "AKT Phosphorylation as a Predictive Biomarker for PI3K/MTOR Dual Inhibition-Induced Proteolytic Cleavage of MTOR Companion Proteins in Small Cell Lung Cancer." *Cell and Bioscience* 12(1). doi:10.1186/s13578-022-00862-y.

Ibruli, Olta, France Rose, Filippo Beleggia, Anna Schmitt, Maria Cartolano, Lucia Torres Fernandez, Julia Saggau, Debora Bonasera, Martha Kiljan, Gokcen Gozum, Luca Lichius, Jiali Cai, Li Na Niu, Manoela Iannicelli Caiaffa, Jan M. Herter, Henning Walczak, Gianmaria Liccardi, Holger Grüll, Reinhard Büttner, Graziella Bosco, Julie George, Roman K. Thomas, Kasia Bozek, Hans Christian Reinhardt, and Grit S. Herter-Sprie. 2024. "A Novel Mouse Model Recapitulating the MMR-Defective SCLC Subtype

Uncovers an Actionable Sensitivity to Immune Checkpoint Blockade." *Journal of Cancer Research and Clinical Oncology* 150(11). doi:10.1007/s00432-024-05942-9.

Iclozan, Cristina, Scott Antonia, Alberto Chiappori, Dung Tsa Chen, and Dmitry Gabrilovich. 2013. "Therapeutic Regulation of Myeloid-Derived Suppressor Cells and Immune Response to Cancer Vaccine in Patients with Extensive Stage Small Cell Lung Cancer." *Cancer Immunology, Immunotherapy* 62(5):909–18. doi:10.1007/s00262-013-1396-8.

Inamura, Kentaro. 2017. "Lung Cancer: Understanding Its Molecular Pathology and the 2015 WHO Classification." *Frontiers in Oncology* 7(AUG). doi:10.3389/fonc.2017.00193.

Ireland, Abbie S., Alexi M. Micinski, David W. Kastner, Bingqian Guo, Sarah J. Wait, Kyle B. Spainhower, Christopher C. Conley, Opal S. Chen, Matthew R. Guthrie, Danny Soltero, Yi Qiao, Xiaomeng Huang, Szabolcs Tarapcsák, Siddhartha Devarakonda, Milind D. Chalishazar, Jason Gertz, Justin C. Moser, Gabor Marth, Sonam Puri, Benjamin L. Witt, Benjamin T. Spike, and Trudy G. Oliver. 2020. "MYC Drives Temporal Evolution of Small Cell Lung Cancer Subtypes by Reprogramming Neuroendocrine Fate." *Cancer Cell* 38(1):60-78.e12. doi:10.1016/j.ccell.2020.05.001.

Jeong, Minho, and Kee Beom Kim. 2025. "Recent Research on Role of P53 Family in Small-Cell Lung Cancer." *Cancers* 17(7).

Jerby-Arnon, Livnat, Parin Shah, Michael S. Cuoco, Christopher Rodman, Mei Ju Su, Johannes C. Melms, Rachel Leeson, Abhay Kanodia, Shaolin Mei, Jia Ren Lin, Shu Wang, Bokang Rabasha, David Liu, Gao Zhang, Claire Margolais, Orr Ashenberg, Patrick A. Ott, Elizabeth I. Buchbinder, Rizwan Haq, F. Stephen Hodi, Genevieve M. Boland, Ryan J. Sullivan, Dennie T. Frederick, Benchun Miao, Tabea Moll, Keith T. Flaherty, Meenhard Herlyn, Russell W. Jenkins, Rohit Thummalapalli, Monika S. Kowalczyk, Israel Cañadas, Bastian Schilling, Adam N. R. Cartwright, Adrienne M. Luoma, Shruti Malu, Patrick Hwu, Chantale Bernatchez, Marie Andrée Forget, David A. Barbie, Alex K. Shalek, Itay Tirosh, Peter K. Sorger, Kai Wucherpfennig, Eliezer M. Van Allen, Dirk Schadendorf, Bruce E. Johnson, Asaf Rotem, Orit Rozenblatt-Rosen, Levi A. Garraway, Charles H. Yoon, Benjamin Izar, and Aviv Regev. 2018. "A Cancer Cell Program Promotes T Cell Exclusion and Resistance to Checkpoint Blockade." *Cell* 175(4):984-997.e24. doi:10.1016/j.cell.2018.09.006.

Jia, Deshui, Arnaud Augert, Dong Wook Kim, Emily Eastwood, Nan Wu, Ali H. Ibrahim, Kee Beom Kim, Colin T. Dunn, Smitha P. S. Pillai, Adi F. Gazdar, Hamid Bolouri, Kwon Sik Park, and David Macpherson. 2018. "Crebbp Loss Drives Small Cell Lung Cancer and Increases Sensitivity to HDAC Inhibition." *Cancer Discovery* 8(11):1422–37. doi:10.1158/2159-8290.CD-18-0385.

Jiang, Shiyu, Liling Huang, Hongnan Zhen, Peijie Jin, Jing Wang, and Zhihuang Hu. 2021. "Carboplatin versus Cisplatin in Combination with Etoposide in the First-Line Treatment of Small Cell Lung Cancer: A Pooled Analysis." *BMC Cancer* 21(1). doi:10.1186/s12885-021-09034-6.

Jin, Zhaohui, and Frank A. Sinicrope. 2022. *SPECIAL SERIES: PRECISION MEDICINE AND IMMUNOTHERAPY IN GI MALIGNANCIES Review Articles Mismatch Repair-Deficient Colorectal Cancer: Building on Checkpoint Blockade*. Vol. 40. https://doi.org/10.

Johanns, Tanner M., Jeffrey P. Ward, Christopher A. Miller, Courtney Wilson, Dale K. Kobayashi, Diane Bender, Yujie Fu, Anton Alexandrov, Elaine R. Mardis, Maxim N. Artyomov, Robert D. Schreiber, and Gavin P. Dunn. 2016. "Endogenous Neoantigen-Specific CD8 T Cells Identified in Two Glioblastoma Models Using a Cancer

Immunogenomics Approach." *Cancer Immunology Research* 4(12):1007–15. doi:10.1158/2326-6066.CIR-16-0156.

Johnston-Early, Anita, Martin H. Cohen, John D. Minna, Lillian M. Paxton, Byron E. Fossieck, Daniel C. Ihde, Paul A. Bunn, Mary J. Matthews, and Robert Makuch. 1980. *Smoking Abstinence and Small Cell Lung Cancer Survival An Association*. http://jama.jamanetwork.com/.

Josefowicz, Steven Z., Li Fan Lu, and Alexander Y. Rudensky. 2012. "Regulatory T Cells: Mechanisms of Differentiation and Function." *Annual Review of Immunology* 30:531–64.

Joyce. 2015. "T Cell Exclusion, Immune Privilege, and the Tumor Microenvironment." *Science* 348(6230):69–74.

Kalemkerian, Gregory P., Wallace Akerley, Paul Bogner, Hossein Borghaei, Laura Qm Chow, Robert J. Downey, Leena Gandhi, Apar Kishor, P. Ganti, Ramaswamy Govindan, John C. Grecula, James Hayman, Rebecca Suk Heist, Leora Horn, Thierry Jahan, Marianna Koczywas, Billy W. Loo, Robert E. Merritt, Cesar A. Moran, Harvey B. Niell, Janis O'malley, Jyoti D. Patel, Neal Ready, Charles M. Rudin, Charles C. Williams, Kristina Gregory, and Miranda Hughes. 2013. *Small Cell Lung Cancer: Clinical Practice Guidelines in Oncology*. www.smokefree.gov.

Kim, Hye Jung, and Harvey Cantor. 2014. "CD4 T-Cell Subsets and Tumor Immunity: The Helpful and the Not-so-Helpful." *Cancer Immunology Research* 2(2):91–98.

Kong, Xueqing, Jinyi Zhang, Shuwei Chen, Xianyang Wang, Qing Xi, Han Shen, and Rongxin Zhang. 2024. "Immune Checkpoint Inhibitors: Breakthroughs in Cancer Treatment." *Cancer Biology & Medicine* 21(6).

Kontomanolis, Emmanuel N., Antonios Koutras, Athanasios Syllaios, Dimitrios Schizas, Aikaterini Mastoraki, Nikolaos Garmpis, Michail Diakosavvas, Kyveli Angelou, Georgios Tsatsaris, Athanasios Pagkalos, Thomas Ntounis, and Zacharias Fasoulakis. 2020. "Role of Oncogenes and Tumor-Suppressor Genes in Carcinogenesis: A Review." *Anticancer Research* 40(11):6009–15.

Krpina, Kristina, Semir Vranić, Krešimir Tomić, Miroslav Samaržija, and Lara Batičić. 2023. "Small Cell Lung Carcinoma: Current Diagnosis, Biomarkers, and Treatment Options with Future Perspectives." *Biomedicines* 11(7).

Kucherlapati, Melanie H., Kyeryoung Lee, Andrew A. Nguyen, Alan B. Clark, Harry Hou, Andrew Rosulek, Hua Li, Kan Yang, Kunhua Fan, Martin Lipkin, Roderick T. Bronson, Linda Jelicks, Thomas A. Kunkel, Raju Kucherlapati, and Winfried Edelmann. 2010. "An Msh2 Conditional Knockout Mouse for Studying Intestinal Cancer and Testing Anticancer Agents." *Gastroenterology* 138(3). doi:10.1053/j.gastro.2009.11.009.

Landscape of Microsatellite Instability Across 39 Cancer Types. 2017. http://ocg.cancer.gov/.

Le, Dung T., Jennifer N. Durham, Kellie N. Smith, Hao Wang, Bjarne R. Bartlett, Laveet K. Aulakh, Steve Lu, Holly Kemberling, Cara Wilt, Brandon S. Luber, Fay Wong, Nilofer S. Azad, Agnieszka A. Rucki, Dan Laheru, Ross Donehower, Atif Zaheer, George A. Fisher, Todd S. Crocenzi, James J. Lee, Tim F. Greten, Austin G. Duffy, Kristen K. Ciombor, Aleksandra D. Eyring, Bao H. Lam, Andrew Joe, S. Peter Kang, Matthias Holdhoff, Ludmila Danilova, Leslie Cope, Christian Meyer, Shibin Zhou, Richard M. Goldberg, Deborah K. Armstrong, Katherine M. Bever, Amanda N. Fader, Janis Taube, Franck Housseau, David Spetzler, Nianqing Xiao, Drew M. Pardoll, Nickolas Papadopoulos, Kenneth W. Kinzler, James R. Eshleman, Bert Vogelstein, Robert A. Anders, and Luis A.

Diaz. 2017. “Mismatch Repair Deficiency Predicts Response of Solid Tumors to PD-1 Blockade.” *Science* 357(6349):409–13. doi:10.1126/science.aan6733.

Le, Dung T., Jennifer N. Uram, Hao Wang, Bjarne R. Bartlett, Holly Kemberling, Aleksandra D. Eyring, Andrew D. Skora, Brandon S. Luber, Nilofer S. Azad, Dan Laheru, Barbara Biedrzycki, Ross C. Donehower, Atif Zaheer, George A. Fisher, Todd S. Crocenzi, James J. Lee, Steven M. Duffy, Richard M. Goldberg, Albert de la Chapelle, Minori Koshiji, Feriyl Bhaijee, Thomas Huebner, Ralph H. Hruban, Laura D. Wood, Nathan Cuka, Drew M. Pardoll, Nickolas Papadopoulos, Kenneth W. Kinzler, Shibin Zhou, Toby C. Cornish, Janis M. Taube, Robert A. Anders, James R. Eshleman, Bert Vogelstein, and Luis A. Diaz. 2015. “PD-1 Blockade in Tumors with Mismatch-Repair Deficiency.” *New England Journal of Medicine* 372(26):2509–20. doi:10.1056/nejmoa1500596.

Lelliott, Emily J., Karen E. Sheppard, and Grant A. McArthur. 2022. “Harnessing the Immunotherapeutic Potential of CDK4/6 Inhibitors in Melanoma: Is Timing Everything?” *Npj Precision Oncology* 6(1). doi:10.1038/s41698-022-00273-9.

Li, Guo Min. 2008. “Mechanisms and Functions of DNA Mismatch Repair.” *Cell Research* 18(1):85–98.

Li, Heng, and Richard Durbin. 2009. “Fast and Accurate Short Read Alignment with Burrows-Wheeler Transform.” *Bioinformatics* 25(14):1754–60. doi:10.1093/bioinformatics/btp324.

Li, Xiangzhao, Shifen Zhang, Jiamin Zeng, Sha sha Song, Xiaoqing Liu, Wei Kang, Minyi Liang, Rui Yang, Hong Li, and Li Liang. 2023. “Heterogeneous Expression of Mismatch Repair Proteins and Interpretation of Immunohistochemical Results in Colorectal Cancer and Endometrial Cancer.” *Pathology Research and Practice* 248. doi:10.1016/j.prp.2023.154647.

Li, Yu, Cangang Zhang, Aimin Jiang, Anqi Lin, Zaoqu Liu, Xiangshu Cheng, Wanting Wang, Quan Cheng, Jian Zhang, Ting Wei, and Peng Luo. 2024. “Potential Anti-Tumor Effects of Regulatory T Cells in the Tumor Microenvironment: A Review.” *Journal of Translational Medicine* 22(1).

Li, Zhengrui, Jing Li, Xiaolei Bai, Xufeng Huang, and Qi Wang. 2024. “Tumor Microenvironment as a Complex Milieu Driving Cancer Progression: A Mini Review.” *Clinical and Translational Oncology*.

Lin, Xin, Kuan Kang, Pan Chen, Zhaoyang Zeng, Guiyuan Li, Wei Xiong, Mei Yi, and Bo Xiang. 2024a. “Regulatory Mechanisms of PD-1/PD-L1 in Cancers.” *Molecular Cancer* 23(1).

Lin, Xin, Kuan Kang, Pan Chen, Zhaoyang Zeng, Guiyuan Li, Wei Xiong, Mei Yi, and Bo Xiang. 2024b. “Regulatory Mechanisms of PD-1/PD-L1 in Cancers.” *Molecular Cancer* 23(1).

Lin, Zhengjun, Songzhu Zou, and Kunming Wen. 2023. “The Crosstalk of CD8+ T Cells and Ferroptosis in Cancer.” *Frontiers in Immunology* 14.

Liu, Min qi, and Xiaoping Yang. 2025. “Patient-Derived Xenograft Models: Current Status, Challenges, and Innovations in Cancer Research.” *Genes & Diseases* 101520. doi:10.1016/j.gendis.2025.101520.

Liu, Qian, Jing Zhang, Chenchen Guo, Mengcheng Wang, Chenfei Wang, Yilv Yan, Liangdong Sun, Di Wang, Lele Zhang, Huansha Yu, Likun Hou, Chunyan Wu, Yuming Zhu, Gening Jiang, Hongwen Zhu, Yanting Zhou, Shanhua Fang, Tengfei Zhang, Liang Hu, Junqiang Li, Yansheng Liu, Hui Zhang, Bing Zhang, Li Ding, Ana I. Robles, Henry Rodriguez, Daming Gao, Hongbin Ji, Hu Zhou, and Peng Zhang. 2024. “Proteogenomic Characterization of Small Cell Lung Cancer Identifies Biological Insights and Subtype-Specific Therapeutic Strategies.” *Cell* 187(1):184-203.e28. doi:10.1016/j.cell.2023.12.004.

Liu, Wuyi, Huyue Zhou, Wenjing Lai, Changpeng Hu, Rufu Xu, Peng Gu, Menglin Luo, Rong Zhang, and Guobing Li. 2024. “The Immunosuppressive Landscape in Tumor Microenvironment.” *Immunologic Research* 72(4):566–82.

Liu, Yanbin, Zhenjiang Liu, Yixiao Yang, Jun Cui, Jingwei Sun, and Yarong Liu. 2023. “The Prognostic and Biology of Tumour-Infiltrating Lymphocytes in the Immunotherapy of Cancer.” *British Journal of Cancer* 129(7):1041–49.

Llosa, Nicolas J., Michael Cruise, Ada Tam, Elizabeth C. Wicks, Elizabeth M. Hechenbleikner, Janis M. Taube, Richard L. Blosser, Hongni Fan, Hao Wang, Brandon S. Luber, Ming Zhang, Nickolas Papadopoulos, Kenneth W. Kinzler, Bert Vogelstein, Cynthia L. Sears, Robert A. Anders, Drew M. Pardoll, and Franck Housseau. 2015. “The Vigorous Immune Microenvironment of Microsatellite Instable Colon Cancer Is Balanced by Multiple Counter-Inhibitory Checkpoints.” *Cancer Discovery* 5(1):43–51. doi:10.1158/2159-8290.CD-14-0863.

Marcus, Leigh, Steven J. Lemery, Patricia Keegan, and Richard Pazdur. 2019. “FDA Approval Summary: Pembrolizumab for the Treatment of Microsatellite Instability-High Solid Tumors.” *Clinical Cancer Research* 25(13):3753–58. doi:10.1158/1078-0432.CCR-18-4070.

Marshall, Jean S., Richard Warrington, Wade Watson, and Harold L. Kim. 2018. “An Introduction to Immunology and Immunopathology.” *Allergy, Asthma and Clinical Immunology* 14.

Martin, Lainie P., Thomas C. Hamilton, and Russell J. Schilder. 2008. “Platinum Resistance: The Role of DNA Repair Pathways.” *Clinical Cancer Research* 14(5):1291–95.

Martin, Sarah A., Christopher J. Lord, and Alan Ashworth. 2008. “DNA Repair Deficiency as a Therapeutic Target in Cancer.” *Current Opinion in Genetics and Development* 18(1):80–86.

Mascaux, C., M. Paesmans, T. Berghmans, F. Branle, J. J. Lafitte, F. Lemaıˆtre Lemaıˆtre, A. P. Meert, P. Vermylen, and J. P. Sculier. 2000. *A Systematic Review of the Role of Etoposide and Cisplatin in the Chemotherapy of Small Cell Lung Cancer with Methodology Assessment and Meta-Analysis European Lung Cancer Working Party (ELCWP)*. Vol. 30. www.elsevier.nl/locate/lungcan.

McFadden, David G., Thales Papagiannakopoulos, Amaro Taylor-Weiner, Chip Stewart, Scott L. Carter, Kristian Cibulskis, Arjun Bhutkar, Aaron McKenna, Alison Dooley, Amanda Vernon, Carrie Sougnez, Scott Malstrom, Megan Heimann, Jennifer Park, Frances Chen, Anna F. Farago, Talya Dayton, Erica Shefler, Stacey Gabriel, Gad Getz, and Tyler Jacks. 2014. “Genetic and Clonal Dissection of Murine Small Cell Lung Carcinoma Progression by Genome Sequencing.” *Cell* 156(6):1298–1311. doi:10.1016/j.cell.2014.02.031.

McGranahan, Nicholas, Andrew J. S. Furness, Rachel Rosenthal, Sofie Ramskov, Rikke Lyngaa, Sunil Kumar Saini, Mariam Jamal-Hanjani, Gareth A. Wilson, Nicolai J. Birkbak, Crispin T. Hiley, Thomas B. K. Watkins, Seema Shafi, Nirupa Murugaesu, Richard Mitter, Ayse U. Akarca, Joseph Linares, Teresa Marafioti, Jake Y. Henry, Eliezer M. Van Allen, Diana Miao, Bastian Schilling, Dirk Schadendorf, Levi A. Garraway, Vladimir Makarov, Naiyer A. Rizvi, Alexandra Snyder, Matthew D. Hellmann, Taha Merghoub, Jedd D. Wolchok, Sachet A. Shukla, Catherine J. Wu, Karl S. Peggs, Timothy A. Chan, Sine R. Hadrup, Sergio A. Quezada, and Charles Swanton. 2016. “Clonal Neoantigens Elicit T Cell Immunoreactivity and Sensitivity to Immune Checkpoint Blockade.” *Science* 351(6280):1463–69. doi:10.1126/science.aaf1490.

McKenna, Aaron, Matthew Hanna, Eric Banks, Andrey Sivachenko, Kristian Cibulskis, Andrew Kernytsky, Kiran Garimella, David Altshuler, Stacey Gabriel, Mark Daly, and Mark A. DePristo. 2010. "The Genome Analysis Toolkit: A MapReduce Framework for Analyzing next-Generation DNA Sequencing Data." *Genome Research* 20(9):1297–1303. doi:10.1101/gr.107524.110.

McLaren, William, Laurent Gil, Sarah E. Hunt, Harpreet Singh Riat, Graham R. S. Ritchie, Anja Thormann, Paul Flicek, and Fiona Cunningham. 2016. "The Ensembl Variant Effect Predictor." *Genome Biology* 17(1). doi:10.1186/s13059-016-0974-4.

McLaughlin, Jessica, Jonathan Berkman, and Patrick Nana-Sinkam. 2023. "Targeted Therapies in Non-Small Cell Lung Cancer: Present and Future." *Faculty Reviews* 12. doi:10.12703/r/12-22.

McMeekin, D. Scott, David L. Tritchler, David E. Cohn, David G. Mutch, Heather A. Lankes, Melissa A. Geller, Matthew A. Powell, Floor J. Backes, Lisa M. Landrum, Richard Zaino, Russell D. Broaddus, Nilsa Ramirez, Feng Gao, Shamshad Ali, Kathleen M. Darcy, Michael L. Pearl, Paul A. DiSilvestro, Shashikant B. Lele, and Paul J. Goodfellow. 2016. "Clinicopathologic Significance of Mismatch Repair Defects in Endometrial Cancer: An NRG Oncology/Gynecologic Oncology Group Study." Pp. 3062–68 in *Journal of Clinical Oncology*. Vol. 34. American Society of Clinical Oncology.

Meuwissen, Ralph, Sabine C. Linn, R. Ilona Linnoila, John Zevenhoven, Wolter J. Mooi, and Anton Berns. n.d. *Induction of Small Cell Lung Cancer by Somatic Inactivation of Both Trp53 and Rb1 in a Conditional Mouse Model*.

Molano, Alberto, Hediye Erdjument-Bromage, Daved H. Fremont, Ilhem Messaoudi, Paul Tempst, and Janko Nikolić-Žugić. 1998. "Peptide Selection by an MHC H-2Kb Class I Molecule Devoid of the Central Anchor ('C') Pocket." *The Journal of Immunology* 160(6):2815–23. doi:10.4049/jimmunol.160.6.2815.

Mollaoglu, Gurkan, Matthew R. Guthrie, Stefanie Böhm, Johannes Brägelmann, Ismail Can, Paul M. Ballieu, Annika Marx, Julie George, Christine Heinen, Milind D. Chalishazar, Haixia Cheng, Abbie S. Ireland, Kendall E. Denning, Anandaroop Mukhopadhyay, Jeffery M. Vahrenkamp, Kristofer C. Berrett, Timothy L. Mosbruger, Jun Wang, Jessica L. Kohan, Mohamed E. Salama, Benjamin L. Witt, Martin Peifer, Roman K. Thomas, Jason Gertz, Jane E. Johnson, Adi F. Gazdar, Robert J. Wechsler-Reya, Martin L. Sos, and Trudy G. Oliver. 2017. "MYC Drives Progression of Small Cell Lung Cancer to a Variant Neuroendocrine Subtype with Vulnerability to Aurora Kinase Inhibition." *Cancer Cell* 31(2):270–85. doi:10.1016/j.ccell.2016.12.005.

Montecucco, Alessandra, Francesca Zanetta, and Giuseppe Biamonti. 2015. "Molecular Mechanisms of Etoposide." *EXCLI Journal* 14:95–108.

Nguyen, Nam H. K., Roya Rafiee, Abderrahmane Tagmount, Amin Sobh, Alex Loguinov, Angelica K. de Jesus Sosa, Abdelrahman H. Elsayed, Mohammed Gbadamosi, Nathan Seligson, Christopher R. Cogle, Jeffery Rubnitz, Raul Ribeiro, James Downing, Xueyuan Cao, Stanley B. Pounds, Christopher D. Vulpe, and Jatinder K. Lamba. 2023. "Genome-Wide CRISPR/Cas9 Screen Identifies Etoposide Response Modulators Associated with Clinical Outcomes in Pediatric AML." *Blood Advances* 7(9):1769–83. doi:10.1182/bloodadvances.2022007934.

Nne, A., A. Upérin, R. Odrigo, A. Rriagada, J. Ean -P Ierre, P. Ignon, C. Écile, L. E. P. Échoux, A. Nna, G. Regor, Ichard J. S. Tephens, P. Aul, E. G. K. Ristjansen, Ruce E. J. Ohnson, and Enry W. Agner. 1999. *PROPHYLACTIC CRANIAL IRRADIATION FOR PATIENTS WITH*

SMALL-CELL LUNG CANCER IN COMPLETE REMISSION A BSTRACT Background Prophylactic Cranial Irradiation Re.

Oliveira, André F., Luís Bretes, and Irene Furtado. 2019. "Review of PD-1/PD-L1 Inhibitors in Metastatic DMMR/MSI-H Colorectal Cancer." *Frontiers in Oncology* 9(MAY).

Oser, Matthew G., David MacPherson, Trudy G. Oliver, Julien Sage, and Kwon Sik Park. 2024. "Genetically-Engineered Mouse Models of Small Cell Lung Cancer: The next Generation." *Oncogene* 43(7):457–69.

Pakish, Janelle B., Qian Zhang, Zhongyuan Chen, Han Liang, Gary B. Chisholm, Ying Yuan, Samuel C. Mok, Russell R. Broaddus, Karen H. Lu, and Melinda S. Yates. 2017. "Immune Microenvironment in Microsatellite-Instable Endometrial Cancers: Hereditary or Sporadic Origin Matters." *Clinical Cancer Research* 23(15):4473–81. doi:10.1158/1078-0432.CCR-16-2655.

Pan, Yueyun, Yinda Yu, Xiaojian Wang, and Ting Zhang. 2020. "Tumor-Associated Macrophages in Tumor Immunity." *Frontiers in Immunology* 11.

Patel, Ayushi S., Seungyeul Yoo, Ranran Kong, Takashi Sato, Abhilasha Sinha, Sarah Karam, Li Bao, Maya Fridrikh, Katsura Emoto, German Nudelman, Charles A. Powell, Mary Beth Beasley, Jun Zhu, and Hideo Watanabe. 2021. *Prototypical Oncogene Family Myc Defines Unappreciated Distinct Lineage States of Small Cell Lung Cancer*. https://www.science.org.

Paul, Sourav, and Girdhari Lal. 2017. "The Molecular Mechanism of Natural Killer Cells Function and Its Importance in Cancer Immunotherapy." *Frontiers in Immunology* 8(SEP).

Paz-Ares, Luis, Mikhail Dvorkin, Yuanbin Chen, Niels Reinmuth, Katsuyuki Hotta, Dmytro Trukhin, Galina Statsenko, Maximilian J. Hochmair, Mustafa Özgüroğlu, Jun Ho Ji, Oleksandr Voitko, Artem Poltoratskiy, Santiago Ponce, Francesco Verderame, Libor Havel, Igor Bondarenko, Andrzej Kazarnowicz, György Losonczy, Nikolay V. Conev, Jon Armstrong, Natalie Byrne, Norah Shire, Haiyi Jiang, Jonathan W. Goldman, Emilio Batagelj, Ignacio Casarini, Anea Viviana Pastor, Susana Noemi Sena, Juan Jose Zarba, Otto Burghuber, Sylvia Hartl, Bernd Lamprecht, Michael Studnicka, Luis Alberto Schlittler, Fabricio Augusto Martinelli de Oliveira, Aknar Calabrich, Gustavo Colagiovanni Girotto, Peo Dos Reis, Carlos Fausto Nino Gorini, Peo Rafael Martins De Marchi, Clarissa Serodio da Rocha Baldotto, Claudia Sette, Mauro Zukin, Assen Dudov, Rumyana Ilieva, Krassimir Koynov, Rositsa Krasteva, Ivan Tonev, Spartak Valev, Violetka Venkova, Minghong Bi, Chengshui Chen, Yuan Chen, Zhendong Chen, Jian Fang, Jifeng Feng, Zhigang Han, Jie Hu, Yi Hu, Wei Li, Zongan Liang, Zhong Lin, Rui Ma, Shenglin Ma, Kejun Nan, Yongqian Shu, Kai Wang, Mengzhao Wang, Gang Wu, Nong Yang, Zhixiong Yang, Helong Zhang, Wei Zhang, Jun Zhao, Yanqiu Zhao, Caicun Zhou, Jianying Zhou, Xiangdong Zhou, Vitezslav Kolek, Leona Koubkova, Jaromir Roubec, Jana Skrickova, Milada Zemanova, Christos Chouaid, Werner Hilgers, Hervé Lena, Denis Moro-Sibilot, Gilles Robinet, Pierre Jean Souquet, Jürgen Alt, Helge Bischoff, Christian Grohe, Eckart Laack, Susanne Lang, Jens Panse, Christian Schulz, Krisztina Bogos, Eszter Csánky, Anea Fülöp, Zsolt Horváth, Judit Kósa, Ibolya Laczó, Gábor Pajkos, Zsuzsanna Pápai, Zsolt Pápai Székely, Veronika Sárosi, Attila Somfay, Éva Somogyiné Ezer, Anás Telekes, Jair Bar, Maya Gottfried, Norman Isaac Heching, Alona Zer Kuch, Roberta Bartolucci, Anna Cecilia Bettini, Angelo Delmonte, Marina Chiara Garassino, Mauro Minelli, Fausto Roila, Shinji Atagi, Koichi Azuma, Hisatsugu Goto, Koichi Goto, Yu Hara, Hidetoshi Hayashi, Toyoaki Hida, Kenya Kanazawa, Shintaro Kanda, Young Hak Kim, Shoichi Kuyama,

Tadashi Maeda, Masahiro Morise, Yasuharu Nakahara, Makoto Nishio, Naoyuki Nogami, Isamu Okamoto, Haruhiro Saito, Masahiro Shinoda, Shigeki Umemura, Tatsuya Yoshida, Niels Claessens, Robin Cornelissen, Lizza Heniks, Jeroen Hiltermann, Egbert Smit, Agnes Staal van den Brekel, Dariusz Kowalski, Slawomir Mańdziuk, Robert Mróz, Marek Wojtukiewicz, Tudor Ciuleanu, Doina Ganea, Anei Ungureanu, Alexander Luft, Vladimir Moiseenko, Dina Sakaeva, Alexey Smolin, Alexander Vasilyev, Lyubov Vladimirova, Igor Anasina, Jozef Chovanec, Pavol Demo, Robert Godal, Peter Kasan, Marian Stresko, Michal Urda, Eun Kyung Cho, Joo Hang Kim, Sang We Kim, Gyeong Won Lee, Jong Seok Lee, Ki Hyeong Lee, Kyung Hee Lee, Yun Gyoo Lee, Maria Amelia Insa Molla, Manuel Domine Gomez, Juan Ignacio Delgado Mingorance, Dolores Isla Casado, Marta Lopez Brea, Margarita Majem Tarruella, Teresa Morán Bueno, Alejano Navarro Mendivil, Santiago Ponce Aix, Maria Rosario Garcia Campelo, Gee Chen Chang, Yen Hsun Chen, Chao Hua Chiu, Te Chun Hsia, Kang Yun Lee, Chien Te Li, Chin Chou Wang, Yu Feng Wei, Shang Yin Wu, Ahmet Alacacıoğlu, Irfan Çiçin, Ahmet Demirkazik, Mustafa Erman, Tuncay Göksel, Hryhoriy Adamchuk, Oleksii Kolesnik, Anna Kryzhanivska, Yuriv Ostapenko, Serhii Shevnia, Yaroslav Shparyk, Grygorii Ursol, Nataliia Voitko, Ihor Vynnychenko, Sunil Babu, Anne Chiang, Winston Chua, Shaker Dakhil, Afshin Dowlati, Basir Haque, Rodney Jamil, Jeanna Knoble, Shailena Lakhanpal, Kailhong Mi, Petros Nikolinakos, Steven Powell, Helen Ross, Eric Schaefer, Jeffrey Schneider, Joseph Spahr, David Spigel, Joseph Stilwill, Christopher Sumey, and Michael Williamson. 2019. “Durvalumab plus Platinum–Etoposide versus Platinum–Etoposide in First-Line Treatment of Extensive-Stage Small-Cell Lung Cancer (CASPIAN): A Randomised, Controlled, Open-Label, Phase 3 Trial.” *The Lancet* 394(10212):1929–39. doi:10.1016/S0140-6736(19)32222-6.

Peifer, Martin, Lynnette Fernández-Cuesta, Martin L. Sos, Julie George, Danila Seidel, Lawryn H. Kasper, Dennis Plenker, Frauke Leenders, Ruping Sun, Thomas Zander, Roopika Menon, Mirjam Koker, Ilona Dahmen, Christian Müller, Vincenzo Di Cerbo, Hans Ulrich Schildhaus, Janine Altmüller, Ingelore Baessmann, Christian Becker, Bram De Wilde, Jo Vandesompele, Diana Böhm, Sascha Ansén, Franziska Gabler, Ines Wilkening, Stefanie Heynck, Johannes M. Heuckmann, Xin Lu, Scott L. Carter, Kristian Cibulskis, Shantanu Banerji, Gad Getz, Kwon Sik Park, Daniel Rauh, Christian Grütter, Matthias Fischer, Laura Pasqualucci, Gavin Wright, Zoe Wainer, Prudence Russell, Iver Petersen, Yuan Chen, Erich Stoelben, Corinna Ludwig, Philipp Schnabel, Hans Hoffmann, Thomas Muley, Michael Brockmann, Walburga Engel-Riedel, Lucia A. Muscarella, Vito M. Fazio, Harry Groen, Wim Timens, Hannie Sietsma, Erik Thunnissen, Egber Smit, Daniëlle A. M. Heideman, Peter J. F. Snijders, Federico Cappuzzo, Claudia Ligorio, Stefania Damiani, John Field, Steinar Solberg, Odd Terje Brustugun, Marius Lund-Iversen, Jörg Sänger, Joachim H. Clement, Alex Soltermann, Holger Moch, Walter Weder, Benjamin Solomon, Jean Charles Soria, Pierre Validire, Benjamin Besse, Elisabeth Brambilla, Christian Brambilla, Sylvie Lantuejoul, Philippe Lorimier, Peter M. Schneider, Michael Hallek, William Pao, Matthew Meyerson, Julien Sage, Jay Shendure, Robert Schneider, Reinhard Büttner, Jürgen Wolf, Peter Nürnberg, Sven Perner, Lukas C. Heukamp, Paul K. Brindle, Stefan Haas, and Roman K. Thomas. 2012. “Integrative Genome Analyses Identify Key Somatic Driver Mutations of Small-Cell Lung Cancer.” *Nature Genetics* 44(10):1104–10. doi:10.1038/ng.2396.

Peltomäki, Päivi, Minna Nyström, Jukka Pekka Mecklin, and Toni T. Seppälä. 2023. “Lynch Syndrome Genetics and Clinical Implications.” *Gastroenterology* 164(5):783–99. doi:10.1053/j.gastro.2022.08.058.

Petitprez, Florent, Aurélien de Reyniès, Emily Z. Keung, Tom Wei Wu Chen, Cheng Ming Sun, Julien Calderaro, Yung Ming Jeng, Li Ping Hsiao, Laetitia Lacroix, Antoine Bougoüin, Marco Moreira, Guillaume Lacroix, Ivo Natario, Julien Adam, Carlo Lucchesi, Yec’han Laizet, Maud Toulmonde, Melissa A. Burgess, Vanessa Bolejack, Denise Reinke, Khalid M. Wani, Wei Lien Wang, Alexander J. Lazar, Christina L. Roland, Jennifer A. Wargo, Antoine Italiano, Catherine Sautès-Fridman, Hussein A. Tawbi, and Wolf H. Fridman. 2020. “B Cells Are Associated with Survival and Immunotherapy Response in Sarcoma.” *Nature* 577(7791):556–60. doi:10.1038/s41586-019-1906-8.

Popova, Nadezhda V., and Manfred Jücker. 2022. “The Functional Role of Extracellular Matrix Proteins in Cancer.” *Cancers* 14(1).

Del Prete, Annalisa, Valentina Salvi, Alessandra Soriani, Mattia Laffranchi, Francesca Sozio, Daniela Bosisio, and Silvano Sozzani. 2023. “Dendritic Cell Subsets in Cancer Immunity and Tumor Antigen Sensing.” *Cellular and Molecular Immunology* 20(5):432–47.

Pujol, Jean Louis, Johan Vansteenkiste, Luis Paz-Ares Rodríguez, Vanesa Gregorc, Julien Mazieres, Mark Awad, Pasi A. Jänne, Michael Chisamore, Anwar M. Hossain, Yanyun Chen, and J. Thaddeus Beck. 2021a. “Abemaciclib in Combination With Pembrolizumab for Stage IV KRAS-Mutant or Squamous NSCLC: A Phase 1b Study.” *JTO Clinical and Research Reports* 2(11). doi:10.1016/j.jtocrr.2021.100234.

Pujol, Jean Louis, Johan Vansteenkiste, Luis Paz-Ares Rodríguez, Vanesa Gregorc, Julien Mazieres, Mark Awad, Pasi A. Jänne, Michael Chisamore, Anwar M. Hossain, Yanyun Chen, and J. Thaddeus Beck. 2021b. “Abemaciclib in Combination With Pembrolizumab for Stage IV KRAS-Mutant or Squamous NSCLC: A Phase 1b Study.” *JTO Clinical and Research Reports* 2(11). doi:10.1016/j.jtocrr.2021.100234.

Pužar Dominkuš, Pia, and Petra Hudler. 2023. “Mutational Signatures in Gastric Cancer and Their Clinical Implications.” *Cancers* 15(15).

Raso, Maria Gabriela, Neus Bota-Rabassedas, and Ignacio I. Wistuba. 2021a. “Pathology and Classification of SCLC.” *Cancers* 13(4):1–11.

Raso, Maria Gabriela, Neus Bota-Rabassedas, and Ignacio I. Wistuba. 2021b. “Pathology and Classification of SCLC.” *Cancers* 13(4):1–11.

Raso, Maria Gabriela, Neus Bota-Rabassedas, and Ignacio I. Wistuba. 2021c. “Pathology and Classification of SCLC.” *Cancers* 13(4):1–11.

Raso, Maria Gabriela, Neus Bota-Rabassedas, and Ignacio I. Wistuba. 2021d. “Pathology and Classification of SCLC.” *Cancers* 13(4):1–11.

Reynisson, Birkir, Bruno Alvarez, Sinu Paul, Bjoern Peters, and Morten Nielsen. 2021. “NetMHCpan-4.1 and NetMHCIIpan-4.0: Improved Predictions of MHC Antigen Presentation by Concurrent Motif Deconvolution and Integration of MS MHC Eluted Ligand Data.” *Nucleic Acids Research* 48(W1):W449–54. doi:10.1093/NAR/GKAA379.

Rizvi, Naiyer A., Matthew D. Hellmann, Alexandra Snyder, Pia Kvistborg, Vladimir Makarov, Jonathan J. Havel, William Lee, Jianda Yuan, Phillip Wong, Teresa S. Ho, Martin L. Miller, Natasha Rekhtman, Andre L. Moreira, Fawzia Ibrahim, Cameron Bruggeman, Billel Gasmi, Roberta Zappasodi, Yuka Maeda, Chris Sander, Edward B. Garon, Taha Merghoub, Jedd D. Wolchok, Ton N. Schumacher, and Timothy A. Chan. 2015a. “Mutational Landscape Determines Sensitivity to PD-1 Blockade in Non-Small Cell Lung Cancer.” *Science* 348(6230):124–28. doi:10.1126/science.aaa1348.

Rizvi, Naiyer A., Matthew D. Hellmann, Alexandra Snyder, Pia Kvistborg, Vladimir Makarov, Jonathan J. Havel, William Lee, Jianda Yuan, Phillip Wong, Teresa S. Ho, Martin L. Miller, Natasha Rekhtman, Andre L. Moreira, Fawzia Ibrahim, Cameron Bruggeman, Billel Gasmi, Roberta Zappasodi, Yuka Maeda, Chris Sander, Edward B. Garon, Taha Merghoub, Jedd D. Wolchok, Ton N. Schumacher, and Timothy A. Chan. 2015b. "Mutational Landscape Determines Sensitivity to PD-1 Blockade in Non-Small Cell Lung Cancer." *Science* 348(6230):124–28. doi:10.1126/science.aaa1348.

Rosenthal, Rachel, Elizabeth Larose Cadieux, Roberto Salgado, Maise Al-Bakir, David A. Moore, Crispin T. Hiley, Tom Lund, Miljana Tanić, James L. Reading, Kroopa Joshi, Jake Y. Henry, Ehsan Ghorani, Gareth A. Wilson, Nicolai J. Birkbak, Mariam Jamal-Hanjani, Selvaraju Veeriah, Zoltan Szallasi, Sherene Loi, Matthew D. Hellmann, Andrew Feber, Benny Chain, Javier Herrero, Sergio A. Quezada, Jonas Demeulemeester, Peter Van Loo, Stephan Beck, Nicholas McGranahan, Charles Swanton, Mariam Jamal-Hanjani, Selvaraju Veeriah, Justyna Czyzewska-Khan, Diana Johnson, Joanne Laycock, Rachel Rosenthal, Pat Gorman, Robert E. Hynds, Gareth Wilson, Gareth Wilson, Thomas B. K. Watkins, Nicholas McGranahan, Mickael Escudero, Aengus Stewart, Andrew Rowan, Crispin Hiley, Christopher Abbosh, Jacki Goldman, Richard Kevin Stone, Tamara Denner, Sophia Ward, Emma Nye, Kroopa Joshi, Assma Ben Aissa, Yien Ning Sophia Wong, Andy Georgiou, Sergio Quezada, John A. Hartley, Helen L. Lowe, David Lawrence, Martin Hayward, Nikolaos Panagiotopoulos, Mary Falzon, Elaine Borg, Teresa Marafioti, Sam M. Janes, Martin Forster, Tanya Ahmad, Siow Ming Lee, Dionysis Papadatos-Pastos, Dawn Carnell, Ruheena Mendes, Jeremy George, Asia Ahmed, Magali Taylor, Junaid Choudhary, Yvonne Summers, Raffaele Califano, Paul Taylor, Rajesh Shah, Piotr Krysiak, Kendadai Rammohan, Eustace Fontaine, Richard Booton, Matthew Evison, Phil Crosbie, Stuart Moss, Leena Joseph, Paul Bishop, Anne Marie Quinn, Helen Doran, Angela Leek, Phil Harrison, Katrina Moore, Rachael Waddington, Juliette Novasio, Fiona Blackhall, Jane Rogan, Elaine Smith, Caroline Dive, Jonathan Tugwood, Ged Brady, Dominic G. Rothwell, Jackie Pierce, Sakshi Gulati, Babu Naidu, Gerald Langman, Simon Trotter, Hollie Bancroft, Amy Kerr, Salma Kadiri, Gary Middleton, Madava Djearaman, Dean Fennell, Jacqui A. Shaw, John Le Quesne, David A. Moore, Apostolos Nakas, Sridhar Rathinam, William Monteiro, Hilary Marshall, Louise Nelson, Joan Riley, Lindsay Primrose, Luke Martinson, Girija Anand, Sajid Khan, Marianne Nicolson, Keith Kerr, Shirley Palmer, Hardy Remmen, Joy Miller, Keith Buchan, Mahendran Chetty, Lesley Gomersall, Jason Lester, Fiona Morgan, Haydn Adams, Helen Davies, Malgorzata Kornaszewska, Richard Attanoos, Sara Lock, Mairead MacKenzie, Maggie Wilcox, Harriet Bell, Allan Hackshaw, Yenting Ngai, Sean Smith, Nicole Gower, Christian Ottensmeier, Serena Chee, Benjamin Johnson, Aiman Alzetani, Emily Shaw, Eric Lim, Paulo De Sousa, Monica Tavares Barbosa, Alex Bowman, Simon Jordan, Alexandra Rice, Hilgardt Raubenheimer, Harshil Bhayani, Morag Hamilton, Natalie Mensah, Lyn Ambrose, Anand Devaraj, Hema Chavan, Andrew G. Nicholson, Kelvin Lau, Michael Sheaff, Peter Schmid, John Conibear, Veni Ezhil, Vineet Prakash, Peter Russell, Teresa Light, Tracey Horey, Sarah Danson, Jonathan Bury, John Edwards, Jennifer Hill, Sue Matthews, Yota Kitsanta, Kim Suvarna, Patricia Fisher, Michael Shackcloth, John Gosney, Sarah Feeney, Julius Asante-Siaw, Kim Ryanna, Alan Dawson, Mohamad Tuffail, Amrita Bajaj, Jan Brozik, Harriet Walter, Nicolas Carey, Gillian Price, Kayleigh Gilbert, Joanne Webb, Akshay Patel, Anshuman Chaturvedi, Felice Granato, Katie Baker, Mathew Carter, Lynsey Priest, Matthew G. Krebs, Colin Lindsay, Fabio Gomes,

Francesca Chemie, Robert George, Davide Patrini, Reena Khiroya, Penny Shaw, Marcin Skrzypski, Mariana Werner Sunderland, James L. L. Reading, Carmella Beastall, Nagina Mangal, Karl Peggs, Emilia Lim, Neal Navani, Marco Scarci, Leah Ensell, Dhruva Biswas, Roberto Salgado, Maryam Razaq, Jerome Nicod, Stephan Beck, Saioa Lopez, Ariana Huebner, Michelle Dietzen, Thanos Mourikis, Toyin Adefila-Ideozu, Sofina Begum, Henriette Klein, Aleksander Mani, Soraia Carvalho, Daniel Kaniu, Cristina Realingo, Mpho Malima, Sarah Booth, Louise Lim, Jagan Rao, Sara Tenconi, Laura Socci, Faith Kibutu, Michael Agyemang, Robin Young, Kevin G. Blyth, Craig Dick, Alan Kirk, and Andrew Kidd. 2019. "Neoantigen-Directed Immune Escape in Lung Cancer Evolution." *Nature* 567(7749):479–85. doi:10.1038/s41586-019-1032-7.

Rossi, Sabrina, Arianna Pagliaro, Angelica Michelini, Pierina Navarria, Elena Clerici, Davide Franceschini, Luca Toschi, Giovanna Finocchiaro, Marta Scorsetti, and Armando Santoro. 2023. "The Era of Immunotherapy in Small-Cell Lung Cancer: More Shadows Than Light?" *Cancers* 15(24).

Roth, Bruce J., David H. Johnson, Lawrence H. Einhorn, Lee P. Schacter, Nehemiah C. Cherng, Harvey J. Cohen, Jeffrey Crawford, Jaqueline A. Randolph, Janis L. Goodlow, Goronwy O. Broun, George A. Omura, and F. Anthony Greco. 1992. *Randomized Study of Cyclophosphamide, Doxorubicin, and Vincristine Versus Etoposide and Cisplatin Versus Alternation of These Two Regimens in Extensive Small-Cell Lung Cancer: A Phase III Trial of the Southeastern Cancer Study Group*. Vol. 10.

Rudin, Charles M., Elisabeth Brambilla, Corinne Faivre-Finn, and Julien Sage. 2021. "Small-Cell Lung Cancer." *Nature Reviews Disease Primers* 7(1). doi:10.1038/s41572-020-00235-0.

Rudin, Charles M., John T. Poirier, Lauren Averett Byers, Caroline Dive, Afshin Dowlati, Julie George, John V Heymach, Jane E. Johnson, Jonathan M. Lehman, David Macpherson, Pierre P. Massion, John D. Minna, Trudy G. Oliver, Vito Quaranta, Julien Sage, Roman K. Thomas, Christopher R. Vakoc, and Adi F. Gazdar. 2019. "Molecular Subtypes of Small Cell Lung Cancer: A Synthesis of Human and Mouse Model Data HHS Public Access." *Nat Rev Cancer* 19(5):289–97. doi:10.1038/s41574-XXX-XXXX-8.

Sabari, Joshua K., Benjamin H. Lok, James H. Laird, John T. Poirier, and Charles M. Rudin. 2017. "Unravelling the Biology of SCLC: Implications for Therapy." *Nature Reviews Clinical Oncology* 14(9):549–61.

Sahin, Ibrahim Halil, Mehmet Akce, Olatunji Alese, Walid Shaib, Gregory B. Lesinski, Bassel El-Rayes, and Christina Wu. 2019. "Immune Checkpoint Inhibitors for the Treatment of MSI-H/MMR-D Colorectal Cancer and a Perspective on Resistance Mechanisms." *British Journal of Cancer* 121(10):809–18.

Saida, Yu, Satoshi Watanabe, and Toshiaki Kikuchi. 2023. "Extensive-Stage Small-Cell Lung Cancer: Current Landscape and Future Prospects." *OncoTargets and Therapy* 16:657–71.

Salmon, Hélène, Katarzyna Franciszkiewicz, Diane Damotte, Marie Caroline Dieu-Nosjean, Pierre Validire, Alain Trautmann, Fathia Mami-Chouaib, and Emmanuel Donnadieu. 2012. "Matrix Architecture Defines the Preferential Localization and Migration of T Cells into the Stroma of Human Lung Tumors." *Journal of Clinical Investigation* 122(3):899–910. doi:10.1172/JCI45817.

Samstein, Robert M., Chung Han Lee, Alexander N. Shoushtari, Matthew D. Hellmann, Ronglai Shen, Yelena Y. Janjigian, David A. Barron, Ahmet Zehir, Emmet J. Jordan, Antonio Omuro, Thomas J. Kaley, Sviatoslav M. Kendall, Robert J. Motzer, A. Ari Hakimi,

Martin H. Voss, Paul Russo, Jonathan Rosenberg, Gopa Iyer, Bernard H. Bochner, Dean F. Bajorin, Hikmat A. Al-Ahmadie, Jamie E. Chaft, Charles M. Rudin, Gregory J. Riely, Shrujal Baxi, Alan L. Ho, Richard J. Wong, David G. Pfister, Jedd D. Wolchok, Christopher A. Barker, Philip H. Gutin, Cameron W. Brennan, Viviane Tabar, Ingo K. Mellinghoff, Lisa M. DeAngelis, Charlotte E. Ariyan, Nancy Lee, William D. Tap, Mrinal M. Gounder, Sandra P. D'Angelo, Leonard Saltz, Zsofia K. Stadler, Howard I. Scher, Jose Baselga, Pedram Razavi, Christopher A. Klebanoff, Rona Yaeger, Neil H. Segal, Geoffrey Y. Ku, Ronald P. DeMatteo, Marc Ladanyi, Naiyer A. Rizvi, Michael F. Berger, Nadeem Riaz, David B. Solit, Timothy A. Chan, and Luc G. T. Morris. 2019. "Tumor Mutational Load Predicts Survival after Immunotherapy across Multiple Cancer Types." *Nature Genetics* 51(2):202–6.

Schaer, David A., Richard P. Beckmann, Jack A. Dempsey, Lysiane Huber, Amelie Forest, Nelusha Amaladas, Yanxia Li, Ying Cindy Wang, Erik R. Rasmussen, Darin Chin, Andrew Capen, Carmine Carpenito, Kirk A. Staschke, Linda A. Chung, Lacey M. Litchfield, Farhana F. Merzoug, Xueqian Gong, Philip W. Iversen, Sean Buchanan, Alfonso de Dios, Ruslan D. Novosiadly, and Michael Kalos. 2018. "The CDK4/6 Inhibitor Abemaciclib Induces a T Cell Inflamed Tumor Microenvironment and Enhances the Efficacy of PD-L1 Checkpoint Blockade." *Cell Reports* 22(11):2978–94. doi:10.1016/j.celrep.2018.02.053.

Schaffer, Bethany E., Kwon Sik Park, Gloria Yiu, Jamie F. Conklin, Chenwei Lin, Deborah L. Burkhart, Anthony N. Karnezis, E. Alejandro Sweet-Cordero, and Julien Sage. 2010. "Loss of P130 Accelerates Tumor Development in a Mouse Model for Human Small-Cell Lung Carcinoma." *Cancer Research* 70(10):3877–83. doi:10.1158/0008-5472.CAN-09-4228.

Schöniger, Sandra, and Josef Rüschoff. 2022. "Mismatch Repair Deficiency and Microsatellite Instability." *Encyclopedia* 2(3):1559–76. doi:10.3390/encyclopedia2030106.

Seetharam, R. N., A. Sood, and S. Goel. 2009. "Oxaliplatin: Preclinical Perspectives on the Mechanisms of Action, Response and Resistance." *Ecancermedicalscience* 3(1).

Sharonov, George V., Ekaterina O. Serebrovskaya, Diana V. Yuzhakova, Olga V. Britanova, and Dmitriy M. Chudakov. 2020. "B Cells, Plasma Cells and Antibody Repertoires in the Tumour Microenvironment." *Nature Reviews Immunology* 20(5):294–307.

Sivakumar, Smruthy, Jay A. Moore, Meagan Montesion, Radwa Sharaf, Douglas I. Lin, Caterina I. Colón, Zoe Fleishmann, Ericka M. Ebot, Justin Y. Newberg, Jennifer M. Mills, Priti S. Hegde, Quintin Pan, Afshin Dowlati, Garrett M. Frampton, Julien Sage, and Christine M. Lovly. 2023. "Integrative Analysis of a Large Real-World Cohort of Small Cell Lung Cancer Identifies Distinct Genetic Subtypes and Insights into Histologic Transformation." *Cancer Discovery* 13(7):1572–91. doi:10.1158/2159-8290.CD-22-0620.

Socinski, Mark A., Egbert F. Smit, Paul Lorigan, Kartik Konduri, Martin Reck, Aleksandra Szczesna, Johnetta Blakely, Piotr Serwatowski, Nina A. Karaseva, Tudor Ciuleanu, Jacek Jassem, Mircea Dediu, Shengyan Hong, Carla Visseren-Grul, Axel Rainer Hanauske, Coleman K. Obasaju, Susan C. Guba, and Nick Thatcher. 2009. "Phase III Study of Pemetrexed plus Carboplatin Compared with Etoposide plus Carboplatin in Chemotherapy-Naive Patients with Extensive-Stage Small-Cell Lung Cancer." *Journal of Clinical Oncology* 27(28):4787–92. doi:10.1200/JCO.2009.23.1548.

Song, Yuli, and Yi Zhang. 2022. "Research Progress of Neoantigens in Gynecologic Cancers." *International Immunopharmacology* 112.

Soularue, Emilie, Patricia Lepage, Jean Frederic Colombel, Clelia Coutzac, David Faleck, Lysiane Marthey, Michael Collins, Nathalie Chaput, Caroline Robert, and Franck Carbonnel. 2018. “Enterocolitis Due to Immune Checkpoint Inhibitors: A Systematic Review.” *Gut* 67(11):2056–67. doi:10.1136/gutjnl-2018-316948.

Spitzer, Matthew H., Yaron Carmi, Nathan E. Reticker-Flynn, Serena S. Kwek, Deepthi Madhireddy, Maria M. Martins, Pier Federico Gherardini, Tyler R. Prestwood, Jonathan Chabon, Sean C. Bendall, Lawrence Fong, Garry P. Nolan, and Edgar G. Engleman. 2017. “Systemic Immunity Is Required for Effective Cancer Immunotherapy.” *Cell* 168(3):487-502.e15. doi:10.1016/j.cell.2016.12.022.

Spranger, Stefani, Riyue Bao, and Thomas F. Gajewski. 2015. “Melanoma-Intrinsic β-Catenin Signalling Prevents Anti-Tumour Immunity.” *Nature* 523(7559):231–35. doi:10.1038/nature14404.

Strickler, John H., Brent A. Hanks, and Mustafa Khasraw. 2021. “Tumor Mutational Burden as a Predictor of Immunotherapy Response: Is More Always Better?” *Clinical Cancer Research* 27(5):1236–41.

Tanaka, Atsushi, and Shimon Sakaguchi. 2017. “Regulatory T Cells in Cancer Immunotherapy.” *Cell Research* 27(1):109–18.

Tang, Lingrong, Guangwei Tian, and Nan Li. 2024. “Current Dilemma and Future Directions over Prophylactic Cranial Irradiation in SCLC: A Systematic Review in MRI and Immunotherapy Era.” *Frontiers in Oncology* 14.

Teh, Jessica L. F., Dan A. Erkes, Phil F. Cheng, Manoela Tiago, Nicole A. Wilski, Conroy O. Field, Inna Chervoneva, Mitch P. Levesque, Xiaowei Xu, Reinhard Dummer, and Andrew E. Aplin. 2020. “Activation of CD8þ T Cells Contributes to Antitumor Effects of CDK4/6 Inhibitors plus MEK Inhibitors.” *Cancer Immunology Research* 8(9):1114–21. doi:10.1158/2326-6066.CIR-19-0743.

Thommen, Daniela S., and Ton N. Schumacher. 2018. “T Cell Dysfunction in Cancer.” *Cancer Cell* 33(4):547–62.

Togashi, Yosuke, Kohei Shitara, and Hiroyoshi Nishikawa. n.d. “Regulatory T Cells in Cancer Immunosuppression — Implications for Anticancer Therapy.” *Nature Reviews Clinical Oncology*. doi:10.1038/s41571.

Umemura. 2014. “Therapeutic Priority of the PI3K/AKT/MTOR Pathway in Small Cell Lung Cancers as Revealed by a Comprehensive Genomic Analysis.” *J. Thorac. Oncol.*

Vanharanta, Sakari, and Joan Massagué. 2013. “Origins of Metastatic Traits.” *Cancer Cell* 24(4):410–21.

Verma, Amit, Rohit Mathur, Abdullah Farooque, Vandana Kaul, Seema Gupta, and Bilikere S. Dwarakanath. 2019. “T-Regulatory Cells in Tumor Progression and Therapy.” *Cancer Management and Research* 11:10731–47.

Vesely, Matthew D., Michael H. Kershaw, Robert D. Schreiber, and Mark J. Smyth. 2011. “Natural Innate and Adaptive Immunity to Cancer.” *Annual Review of Immunology* 29:235–71. doi:10.1146/annurev-immunol-031210-101324.

Videtic, Gregory M. M., Larry W. Stitt, A. Rashid Dar, Walter I. Kocha, Anna T. Tomiak, Pauline T. Truong, Mark D. Vincent, and Edward W. Yu. 2003. “Continued Cigarette Smoking by Patients Receiving Concurrent Chemoradiotherapy for Limited-Stage Small-Cell Lung Cancer Is Associated with Decreased Survival.” *Journal of Clinical Oncology* 21(8):1544–49.

Vijver, Saskia V., Sarah Danklmaier, Lisa Pipperger, Raphael Gronauer, Gabriel Floriani, Hubert Hackl, Krishna Das, and Guido Wollmann. 2023. “Prediction and Validation of Murine MHC Class I Epitopes of the Recombinant Virus VSV-GP.” *Frontiers in Immunology* 13. doi:10.3389/fimmu.2022.1100730.

Vinay, Dass S., Elizabeth P. Ryan, Graham Pawelec, Wamidh H. Talib, John Stagg, Eyad Elkord, Terry Lichtor, William K. Decker, Richard L. Whelan, H. M. C. Shantha Kumara, Emanuela Signori, Kanya Honoki, Alexandros G. Georgakilas, Amr Amin, William G. Helferich, Chandra S. Boosani, Gunjan Guha, Maria Rosa Ciriolo, Sophie Chen, Sulma I. Mohammed, Asfar S. Azmi, W. Nicol Keith, Alan Bilsland, Dipita Bhakta, Dorota Halicka, Hiromasa Fujii, Katia Aquilano, S. Salman Ashraf, Somaira Nowsheen, Xujuan Yang, Beom K. Choi, and Byoung S. Kwon. 2015. “Immune Evasion in Cancer: Mechanistic Basis and Therapeutic Strategies.” *Seminars in Cancer Biology* 35:S185–98.

Waldner, Maximilian J., and Markus F. Neurath. 2023. “TGFβ and the Tumor Microenvironment in Colorectal Cancer.” *Cells* 12(8).

Walker, Lucy S. K., and David M. Sansom. 2011. “The Emerging Role of CTLA4 as a Cell-Extrinsic Regulator of T Cell Responses.” *Nature Reviews Immunology* 11(12):852–63.

Wander, Seth A., Neil O’brien, Lacey M. Litchfield, Declan O’dea, Claudia Morato Guimaraes, Dennis J. Slamon, and Shom Goel. 2022. “Targeting CDK4 and 6 in Cancer Therapy: Emerging Preclinical Insights Related to Abemaciclib.” *Oncologist* 27(10):811–21. doi:10.1093/oncolo/oyac138.

Wang, Qian, Zeynep H. Gümüş, Cristina Colarossi, Lorenzo Memeo, Xintong Wang, Chung Yin Kong, and Paolo Boffetta. 2023. “SCLC: Epidemiology, Risk Factors, Genetic Susceptibility, Molecular Pathology, Screening, and Early Detection.” *Journal of Thoracic Oncology* 18(1):31–46.

Wang, Shuyan, Jing An, Xueru Hu, Tingting Zeng, Ping Li, Jiangyue Qin, Yongchun Shen, Mei Chen, and Fuqiang Wen. 2024. “Single-Cell RNA Sequencing Reveals Immune Microenvironment of Small Cell Lung Cancer-Associated Malignant Pleural Effusion.” *Thoracic Cancer* 15(1):98–103. doi:10.1111/1759-7714.15145.

Weeden, Ce, B. Solomon, and M. L. Asselin-Labat. 2015. “FGFR1 Inhibition in Lung Squamous Cell Carcinoma: Questions and Controversies.” *Cell Death Discovery* 1(1).

Westcott, Peter M. K., Francesc Muyas, Haley Hauck, Olivia C. Smith, Nathan J. Sacks, Zackery A. Ely, Alex M. Jaeger, William M. Rideout, Daniel Zhang, Arjun Bhutkar, Mary C. Beytagh, David A. Canner, Grissel C. Jaramillo, Roderick T. Bronson, Santiago Naranjo, Abbey Jin, J. J. Patten, Amanda M. Cruz, Sean Luc Shanahan, Isidro Cortes-Ciriano, and Tyler Jacks. 2023a. “Mismatch Repair Deficiency Is Not Sufficient to Elicit Tumor Immunogenicity.” *Nature Genetics* 55(10):1686–95. doi:10.1038/s41588-023-01499-4.

Westcott, Peter M. K., Francesc Muyas, Haley Hauck, Olivia C. Smith, Nathan J. Sacks, Zackery A. Ely, Alex M. Jaeger, William M. Rideout, Daniel Zhang, Arjun Bhutkar, Mary C. Beytagh, David A. Canner, Grissel C. Jaramillo, Roderick T. Bronson, Santiago Naranjo, Abbey Jin, J. J. Patten, Amanda M. Cruz, Sean Luc Shanahan, Isidro Cortes-Ciriano, and Tyler Jacks. 2023b. “Mismatch Repair Deficiency Is Not Sufficient to Elicit Tumor Immunogenicity.” *Nature Genetics* 55(10):1686–95. doi:10.1038/s41588-023-01499-4.

De Wind, Niels, Marleen Dekker, Anton Berns, Miroslav Radman, and Hein Te Riele. 1995. *Inactivation of the Mouse Msh2 Gene Results in Mismatch Repair Deficiency, Methylation Tolerance, Hyperrecombination, and Predisposition to Cancer*. Vol. 82.

Wing, Kajsa, and Shimon Sakaguchi. 2010. “Regulatory T Cells Exert Checks and Balances on Self Tolerance and Autoimmunity.” *Nature Immunology* 11(1):7–13.

World Health Organization. 2023. “Lung Cancer.” https://www.who.int/news-room/fact-sheets/detail/lung-cancer.

Yang, Dian, Sarah K. Denny, Peyton G. Greenside, Andrea C. Chaikovsky, Jennifer J. Brady, Youcef Ouadah, Jeffrey M. Granja, Nadine S. Jahchan, Jing Shan Lim, Shirley Kwok, Christina S. Kong, Anna S. Berghoff, Anna Schmitt, H. Christian Reinhardt, Kwon Sik Park, Matthias Preusser, Anshul Kundaje, William J. Greenleaf, Julien Sage, and Monte M. Winslow. 2018. “Intertumoral Heterogeneity in Sclc Is Influenced by the Cell Type of Origin.” *Cancer Discovery* 8(10):1316–31. doi:10.1158/2159-8290.CD-17-0987.

Yang, Fan, Gloria Lee, and Yi Fan. 2024. “Navigating Tumor Angiogenesis: Therapeutic Perspectives and Myeloid Cell Regulation Mechanism.” *Angiogenesis* 27(3):333–49.

Yeo, Erica C. F., Michael P. Brown, Tessa Gargett, and Lisa M. Ebert. 2021. “The Role of Cytokines and Chemokines in Shaping the Immune Microenvironment of Glioblastoma: Implications for Immunotherapy.” *Cells* 10(3):1–25.

Yuan, Yuan, Jin Sun Lee, Susan E. Yost, Paul H. Frankel, Christopher Ruel, Colt A. Egelston, Weihua Guo, Simran Padam, Aileen Tang, Norma Martinez, Daniel Schmolze, Cary Presant, Behnam Ebrahimi, Christina Yeon, Mina Sedrak, Niki Patel, Jana Portnow, Peter Lee, and Joanne Mortimer. 2021. “Phase I/II Trial of Palbociclib, Pembrolizumab and Letrozole in Patients with Hormone Receptor-Positive Metastatic Breast Cancer.” *European Journal of Cancer* 154:11–20. doi:10.1016/j.ejca.2021.05.035.

Zhang, Shumeng, Qiaomai Xu, Wenjia Sun, Jianya Zhou, and Jianying Zhou. 2023. “Immunomodulatory Effects of CDK4/6 Inhibitors.” *Biochimica et Biophysica Acta - Reviews on Cancer* 1878(4).

Zhang, Tianming, Wenjun Li, Danbei Diwu, Lijun Chen, Xi Chen, and Hong Wang. 2023. “Efficacy and Safety of First-Line Immunotherapy plus Chemotherapy in Treating Patients with Extensive-Stage Small Cell Lung Cancer: A Bayesian Network Meta-Analysis.” *Frontiers in Immunology* 14.

Zhang, Zheying, Manman Lu, Yu Qin, Wuji Gao, Li Tao, Wei Su, and Jiateng Zhong. 2021. “Neoantigen: A New Breakthrough in Tumor Immunotherapy.” *Frontiers in Immunology* 12.

Zhao, Yan, Meili Shen, Liangqiang Wu, Haiqin Yang, Yixuan Yao, Qingbiao Yang, Jianshi Du, Linlin Liu, Yapeng Li, and Yuansong Bai. 2023. “Stromal Cells in the Tumor Microenvironment: Accomplices of Tumor Progression?” *Cell Death and Disease* 14(9).

Zhou, Ting, Zhonghan Zhang, Fan Luo, Yuanyuan Zhao, Xue Hou, Tingting Liu, Kai Wang, Hongyun Zhao, Yan Huang, and Li Zhang. 2020. “Comparison of First-Line Treatments for Patients With Extensive-Stage Small Cell Lung Cancer: A Systematic Review and Network Meta-Analysis.” *JAMA Network Open* 3(10). doi:10.1001/jamanetworkopen.2020.15748.

Zhu, Yu, Zi Wang, Yanan Li, Hongling Peng, Jing Liu, Ji Zhang, and Xiaojuan Xiao. 2023. “The Role of CREBBP/EP300 and Its Therapeutic Implications in Hematological Malignancies.” *Cancers* 15(4).

Appendix

Table 1. A list of definitions for the mutation types derived from WES analysis.

Mutation Type	Definition
UTR3 (3´untranslated region)	Non-coding region located at 3' end of the gene
UTR5 (5´untranslated region)	Non-coding region located at 5' end of the gene
UTR5;UTR3	Mutations impacting both 5' and 3' untranslated regions
Downstream	Mutations occurring downstream of the coding region and affecting regulatory sequences of the gene expression
Exonic;splicing	Mutations in both the exonic coding regions and splice sites, possibly affecting splicing and protein production
Intronic	Mutations within the non-coding regions between exons which may affect gene splicing or regulation
ncR0_exonic	Mutations in the exonic regions of non-coding RNA genes, which do not code for proteins but may regulate gene expression
ncR0_intronic	Mutations in the intronic regions of non-coding RNA genes
Silent	Mutations with no functional effect
Splice	Mutations at the splice junctions (intron-exon boundaries), which can cause incorrect splicing of the pre-mRNA and produce abnormal proteins
Stop	Mutations that introduce a premature stop codon, usually leading to non-functional proteins
Upstream	Mutations occurring upstream of the coding region, potentially affecting regulatory sequences of the gene expression
Upstream;downstream	Mutations occurring both upstream and downstream of a gene, potentially affecting regulatory regions
Intergenic	Mutations located between genes in non-coding regions, which may affect regulatory sequences but not protein-coding regions
Startloss	Mutations that affect the start codon, preventing the initiation of protein translation
Frameshift deletion	A deletion of nucleotides that shifts the reading frame, usually leading to non-functional proteins
Frameshift insertion	An insertion of nucleotides that shifts the reading frame, usually leading to non-functional proteins
Frameshift substitutions	Replacement of nucleotides within the reading frame, usually leading to non-functional proteins

Frameshift indels	Insertion or deletion mutations that result in a shift of the reading frame, usually leading to non-functional proteins
Nonstop	Mutations that remove the stop codon, resulting in longer, non-functional proteins
Missense	Mutations that change one amino acid in a protein
In-frame deletion	A deletion of nucleotides that does not affect the reading frame, but may still affect the protein's function
In-frame insertion	An insertion of nucleotides that does not affect the reading frame, but may still affect the protein's function
In-frame indels	An insertion or deletion that does not affect the reading frame, but may still affect the protein's function

List of abbreviations

i.p.	Intraperitoneal
ADC	Antibody-drug conjugate
Ad-CMV-Cre	Adenoviral vector containing Cre recombinase
AKT	Protein kinase B
ALK	Anaplastic lymphoma kinase
APC	Antigen-presenting cell
ASCL1	Achaete-scute homolog 1 (human)
Ascl1	Achaete-scute homolog 1 (mouse)
B7-H3	B7 homolog 3
BWA	Burrows-wheeler aligner
CAF	Cancer-associated fibroblast
CCG	Cologne center for genomics
CDK4/6	Cyclin-dependent kinase 4 and 6
CDK4/6i	CDK4/6 inhibition
CHGA	Chromogranin A
Cis/Eto	Cisplatin/Etoposide
CNA	Copy number alteration
COSMIC	Catalog of somatic mutations in cancer
CTLA-4	Cytotoxic T-lymphocyte associated protein 4
DAPI	4`,6-Diamidin-2-phenylindol
dbSNP	Database of single nucleotide polymorphism
DC	Dendritic cell
DDR	DNA damage repair
DLL3	Delta-like 3
ECM	Extracellular matrix
EGFR	Epidermal growth factor receptor
EMT	Epithelial-mesenchymal transition
ES-SCLC	Extensive-stage SCLC

FDA	U.S. food and drug administration
FFPE	Formalin-fixed paraffin-embedded
FGFR1	Fibroblast growth factor receptor 1
FOV	Field of view
GATK	Genome analysis toolkit
GEMM	Genetically engineered mouse model
H&E	Hematoxylin-Eosin
HLA-I	Human leukocyte antigen class I
ICI	Immune checkpoint inhibitor
IDO1	Indoleamine 2,3-dioxygenase 1
IEDB	Immune epitope database
IFNγ	Interferon-γ
IGV	Integrative Genomics Viewer
IL-4	Interleukin-4
IMC	Imaging mass cytometry
IVC	Individually ventilated cage
LS-SCLC	Limited-stage SCLC
Mb	megabase (1 million bases)
MDSCs	Myeloid-derived suppressor cell
MHC	Major histocompatibility complex
miRNA	microRNA
MLH1	MutL homolog 1
MMR	Mismatch repair
MMRd	MMR deficiency
MRI	Magnetic resonance imaging
MSH2	MutS homolog 2 (human)
Msh2	MutS homolog 2 (mouse)
MSH6	MutS homolog 6
MSI	Microsatellite instability
MYC	Myelocytomatosis oncogene (human)
Myc	Myelocytomatosis oncogene (mouse)
mTOR	Mammalian target of rapamycin

NCAM	Neural Adhesion Molecule
NE	Neuroendocrine
NEUROD1	Neurogenic differentiation factor 1 (human)
Neurod1	Neurogenic differentiation factor 1 (mouse)
NK cells	Natural killer cell
NSCLC	Non-small cell lung cancer
NSE	Neuron-specific enolase
OS	Overall survival
ORR	Objective response rate
PARP	Poly (ADP-ribose) polymerase
PBS	Phosphate-buffered saline
PCI	Prophylactic cranial radiotherapy
PCR	Polymerase chain reaction
PD-1	Programmed death-1
PD-L1	Programmed death-ligand 1
PDX	Patient-derived xenograft
PFS	Progression-free survival
PI3K	Phosphoinositide 3-kinase
PMS1/PMS2	Postmeiotic segregation increased 1/2
PNEC	Ppulmonary neuroendocrine cell
POU2F3	POU class 2 homeobox 3
Rb	Retinoblastoma protein
RB1	Retinoblastoma 1 (human)
Rb1	Retinoblastoma 1 (mouse)
ROI	Region of interest
RP	$Rb1^{fl/fl};Trp53^{fl/fl}$
RPM	$Rb1^{fl/fl};Trp53^{fl/fl};Msh2^{fl/f}$
RT	Room temperature
SBS	Single base substitution
SCLC	Small cell lung cancer
SNV	Single nucleotide variant
SYP	Synaptophysin

TAM	Tumor-Associated Macrophage
TE	Echo time
TGF-β	Transforming growth factor beta
Th2	T helper 2
Th17	T helper 17
TIGIT	T cell immunoreceptor with Ig and ITIM domains
TMA	Tissue Microarray
TMB	Tumor mutational burden
TME	Tumor microenvironment
TOF	Time-of-flight
TP53	Tumor protein p53 (human)
Trp53	Tumor protein p53 (mouse)
TR	Repetition time
Treg	Regulatory T cell
TSE	Turbo-spin echo
VEP	Variant Effect Predictor
WES	Whole-exome sequencing
YAP1	Yes-associated protein 1

List of figures

List of tables

Acknowledgements

I would like to express my sincere gratitude to my Ph.D. supervisor, Dr. Grit Herter-Sprie, for her guidance, scientific discussions, and proofreading of my thesis. I am also deeply thankful to Prof. Christian Reinhard for his mentorship, dedicated support, and for providing valuable tools and guidance throughout my Ph.D., especially during the publication of the findings presented in this thesis. I also thank Dr. Jan Herter for his important role as a mentor during my studies.

My sincere thanks go to Prof. Mirka Uhlirova and Prof. Björn Schumacher, my tutors in the IPMM graduate program, for their valuable scientific input and support.

I am grateful to Dr. Filippo Beleggia for his support with the WES analysis, Dr. Maria Cartolano for her help with the mutational signature analysis, Dr. Lucia Torres Fernandez for assisting with the neoantigen analysis, and Dr. France Rose for her support with the IMC quantitative analysis.

I would also like to thank Prof. Roman Thomas, Prof. Julie George, and Graziella Bosco from the SFB1399 consortium for providing an excellent research environment and platform. I am grateful to SFB1399 for funding my project.

I wish to extend my heartfelt thanks to my former lab members in AG Herter-Sprie and AG Herter, especially Martha Kiljan, Gokcen Gozum, Luca Lichius, Jiali Cai, and Li-na Niu, for their constant support and for making the lab such a joyful and collaborative place to work.

Finally, I would like to express my deepest gratitude to my parents, Diana and Lulzim Ibruli, my sister Ornela, my brother Dinald, and my nephews Aron and Roel for their unwavering love and support. Special thanks go to my best friends, Klea Lami, Norisa Meli, and Manoela Iannicelli Caiaffa, for helping me stay sane. Lastly, I am immensely thankful to my partner-in-crime, Andi Hoxha, for his tireless, unconditional encouragement and patience throughout this journey.

Lebenslauf

Name: **Olta Ibruli**
Date/ Place of birth: 30.05.1995 in Tirana, Albania
Nationality: Albanian

Education

01/2020 – 11/2025 **Ph.D.** in Cancer Research, University of Cologne
Thesis: Modeling mismatch repair deficiency in small cell lung cancer

04/2017 – 01/2020 **Master of Science** in Medical Life Sciences, University of Kiel
Thesis: The impact of the central nervous system microenvironment on the homing of pediatric B cell precursor acute lymphoblastic leukemia cells

10/2013 – 07/2016 **Bachelor of Science** in Biotechnology, University of Tirana

Research experience

03/2018 – 04/2019 **Research assistant** in preclinical imaging and oncology at Molecular Imaging North Competence Center, University of Kiel

Publications

- **Ibruli O**, et al. A novel mouse model recapitulating the MMR-defective SCLC subtype uncovers an actionable sensitivity to immune checkpoint blockade. Cancer Res. 2024.
- Sakthivelu V, Schmitt A, Odenthal F, Ndoci K, Touet M, Shaib AH, Chihab A, Wani GA, Nieper P, Hartmann GG, Pintelon I, Kisis I, Boecker M, Eckert NM, Iannicelli Caiaffa M, **Ibruli O**, et al. Functional synapses between neurons and small cell lung cancer. Nature. 2025.
- Rose F*, **Ibruli O***, et al. Imaging mass cytometry dataset of small cell lung cancer tumors and tumor microenvironments. BMC Res Notes. 2025. (*shared first authorship)
- Herter J, Kiljan M, Kunze S, Reinscheid M, **Ibruli O**, et al. Influence of chemoradiation on the immune microenvironment of cervical cancer patients. Strahlenther Onkol. 2023.
- Kiljan M, Weil S, Vásquez-Torres A, Hettich Mayer M, **Ibruli O**, et al. CyberKnife radiation therapy as a platform for translational mouse studies. Int J Radiat Biol. 2021.
- Lenk L, Carlet M, Vogiatzi F, Spory L, Winterberg D, Cousins A, Vossen-Gajcy M, **Ibruli O**, et al. CD79a promotes CNS-infiltration and leukemia engraftment in pediatric B-cell precursor acute lymphoblastic leukemia. Commun Biol. 2021.

Köln, November 2025

Erklärung zur Dissertation

Ich versichere, dass ich die von mir vorgelegte Dissertation selbstständig angefertigt, die benutzten Quellen und Hilfsmittel vollständig angegeben und die Stellen der Arbeit -einschließlich Tabellen, Karten und Abbildungen -, die anderen Werken im Wortlaut oder dem Sinn nach entnommen sind, in jedem Einzelfall als Entlehnung kenntlich gemacht habe; dass diese Dissertation noch keiner anderen Fakultät oder Universität zur Prüfung vorgelegen hat; dass sie - abgesehen von unten angegebenen Teilpublikationen -noch nicht veröffentlicht worden ist sowie, dass ich eine solche Veröffentlichung vor Abschluss des Promotionsverfahrens nicht vornehmen werde. Die Bestimmungen dieser Promotionsordnung sind mir bekannt. Die von mir vorgelegte Dissertation ist von Priv.-Doz. Dr. med. Grit Herter-Sprie betreut worden.

Köln, 10.11.2025 Olta Ibruli